Argonne NATIONAL LABORATORY

ANL/RTR/TM-17/19 Rev. 1

Review of the Technical Basis for Properties and Fuel Performance Data Used in HEU to LEU Conversion Analysis for U-10Mo Monolithic Alloy Fuel

Nuclear Science & Engineering Division

ANL/RTR/TM-17/19 Rev. 1

Review of the Technical Basis for Properties and Fuel Performance Data Used in HEU to LEU Conversion Analysis for U-10Mo Monolithic Alloy Fuel

---

prepared by

L. Jamison[1], J. Stillman[2], D. Jaluvka[2], W. Mohamed[2], Y.S. Kim[1], and E. Wilson[2]

[1]Chemical & Fuel Cycle Technologies, Argonne National Laboratory
[2]Nuclear Science & Engineering Division, Argonne National Laboratory

September 2020

(This page left intentionally blank)

Foreword

This report contains an overview of the materials properties important for analysis of the low-enriched uranium (LEU) 10 weight percent molybdenum (U-10Mo) monolithic fuel proposed to convert the U.S High Performance Research Reactors (USHPRR) currently operating with highly enriched uranium (HEU) and which cannot be converted with currently qualified LEU fuel forms. Fuel performance correlations are also included, and in order to demonstrate the degree to which behavior of the LEU fuel is similar to HEU, some key HEU fuel performance data are also included as a point of comparison. For all LEU parameters covered, comparison of the data reported in literature for the parameters useful for reactor conversion safety analyses is included in order to identify consistency and differences among the available sources. Additionally, comparisons to the recommendations given in Revision 1 of the *Preliminary Report on U-Mo Monolithic Fuel for Research Reactors* (referred to as the Preliminary UMo Report) are included.

A compilation of available data also allows an assessment of the reasonableness of the documented data inputs and property assumptions used in the conversion analysis of each of the USHPRR that have been performed to date. The five reactors classified as USHPRR are ATR (Idaho National Laboratory), HFIR (Oak Ridge National Laboratory), MITR (Massachusetts Institute of Technology), MURR (University of Missouri – Columbia), and NBSR (National Institute of Standards). It is noted that HFIR is expected to convert to LEU with a uranium-silicide dispersion fuel; the data inputs and property assumptions noted for HFIR in this report are from prior conversion analysis with U-10Mo monolithic fuel. It is further recognized that reactor-specific application of available data is expected due to the different operating regimes such as burnup, and also that the specific safety basis requirements vary with regards to assumptions required that will depend on the fuel. However, even with a range of interpretations leading to various input data parameters, this report presents a significantly consistent, and what is acknowledged as conservative, use of the available data among the USHPRR.

It is particularly important to note that all LEU data presented herein requires confirmation with the prototypic fuel fabrication process that has now been selected and that is scheduled to begin qualification irradiations. There remain several important areas where additional data should be gathered on fuel plates prototypic of the fabrication process that is currently being used to qualify the fuel. Key areas of additional experimental measurements necessary for qualification include: fresh fuel density, thermal conductivity of the fresh and irradiated U-10Mo fuel across a range of burnups (including the maximum expected for the USHPRR reactors), and additional measurements of the blister anneal temperature on a statistically significant number of plates prototypic of each USHPRR fuel element design.

Table of Contents

List of Figures

List of Tables

Terms and Definitions

Cladding: The aluminum-based alloy bonded to the fuel foil providing a barrier between the fuel foil and the coolant.

Creep: Plastic deformation (mass relocation) of the fuel or cladding induced by stresses.

Fuel: Uranium-based alloy or compound used as the source of neutrons in nuclear research and test reactors.

Fuel Core: The uranium-bearing region of each fuel plate containing fissionable material. In the case of dispersion fuels, this is also called the fuel meat.

Fuel Foil: A monolithic foil of fuel (i.e., U-10Mo) and zirconium interlayer.

Fuel Kernel: A fuel particle formed by comminution (grinding) or atomization.

Fuel Meat: The mixture of fuel kernels and matrix material that forms the fueled zone in dispersion fuel plates.

Fuel Plate: The fuel foil or fuel meat, complete with cladding.

Fuel Temperature Safety Limit: The maximum allowed fuel temperature that maintains fuel integrity.

HEU: Highly enriched uranium, defined as uranium with enrichment greater than or equal to 20 weight % U-235.

Interlayer: A thin zirconium layer applied to the surface of the monolithic fuel core.

LEU: Low-enriched uranium, defined as uranium enriched to less than 20 weight % U-235.

RTR: Research and test reactors.

Swelling: Volumetric change of the fuel induced during irradiation by solid and gaseous fission products, or other material transformations. Fuel swelling changes the overall volume of the fuel, whereas creep relocates fuel.

Target Test Value: The goal value of a design parameter to be achieved during testing, such as during an irradiation experiment.

U-Mo: A binary alloy comprised of uranium and molybdenum.

U-10Mo: A binary alloy comprised of uranium and 10 weight % molybdenum.

1 Introduction

This report provides the technical basis for properties and fuel performance data used in conversion analysis for U.S. High Performance Research Reactors (USHPRR) that will convert from highly enriched uranium (HEU) to low-enriched uranium (LEU) using a new U-10Mo monolithic alloy fuel that is being qualified. The conditions that the fuel experiences changes between an HEU and LEU fuel element design due to many causes, including the density of the fuel, the presence of U-238 resonant absorber, changes to the plate and coolant channel dimensions, and changes in fuel management due to reactivity or optimization. These types of changes have been documented in operational and safety analyses conducted for conversions over decades for over 70 reactors. These conversions have all, or almost all, required recalculation of safety-related values as well as establishing operational characteristics of the core, including power distribution, reactor core power level, and cycle length between required fuel management. An overall objective of conversion is to change the reactor core design as little as possible while maintaining the reactors' scientific, isotope production, medical, and engineering missions.

Historically, licensing of research and test reactors to operate with HEU fuel has involved a number of calculations in order to confirm that requirements specified by the regulator are satisfied. These calculations are dependent upon thermophysical properties and performance for the fuel system. As found in Revision 1 of the *Preliminary Report on U-Mo Monolithic Fuel for Research Reactors* [1] several fuel phenomena have been documented that are of interest to the reactor conversion safety bases. These properties and performance parameters are needed in order to predict quantities such as:

- minimum critical heat flux ratio for steady-state operations [fuel swelling]
- margins to onset of nucleate boiling and flow instability [fuel swelling]
- fuel centerline/maximum temperatures [thermal conductivity, fuel swelling]
- margins to the fuel temperature safety limit [blister threshold temperature, thermal conductivity]

The properties and fuel performance parameters in brackets in the above list are those which principally affect the calculated result.

From experience gained to acquire approval from regulators to convert from HEU to LEU fuel, it is apparent that for research and test reactors there is a range of conditions the fuel is required to survive, and also that this range differs substantially between reactors. Furthermore, these conditions are not directly related to the total reactor core power, but instead are directly related to the power density, arising from both the compactness of the core and the fuel assembly and plate design. The fuel assembly and fuel plate design often change, especially for conversions requiring higher-density fuel. While the compactness of the core may sometimes be changed to provide the necessary performance in a new LEU core configuration, common changes from HEU are LEU fuel management, including the sequence of positions, or path, through a reactor, residence time, and core power level. One important change is that due to the U-238 resonant absorber, or presence of other neutronic absorbers like molybdenum, LEU conversion often requires a 15-20% power increase in the core to match the scientific, materials testing, medical and other isotope production performance of the HEU reactor. Unless fuel assembly lifetime is decreased, which would consume more assemblies annually, this increases the required assembly burnup, or cumulative energy in 'MW-days' at end of life. Thus, considering all of these factors, there are many ways in which the LEU fuel assembly's performance requirements are more stringent than HEU, and require both evaluation of

changes and in many cases design optimization for successful conversion to LEU fuel. Therefore, it should be noted that any parameter (e.g. operating parameter, design limit, licensing limit, etc.) based on HEU calculations requires a new analysis in order to establish the appropriate values for a reactor fueled with LEU.

Ongoing efforts to convert research and test reactors (RTR) to operate with LEU rather than HEU fuel requires analysis for each reactor to be converted. This analysis is needed to confirm both the safety of the reactor and to ensure that the operation remains acceptable after conversion. Specifically, analysis of the reactor physics, steady-state fluid mechanics/thermal hydraulics, and transient analysis of the reactors fueled with proposed LEU fuel must be completed.

This report presents the technical basis for material properties utilized in the LEU analyses, as well as a discussion of fuel performance parameters (swelling and blister temperature). This report is focused on the components of the fuel plate. As such, structural components and other elements that are not modified from the original HEU reactor design and not otherwise analyzed are not included in this report. An initial evaluation of these properties was conducted at the time of drafting the original Preliminary UMo Report [1]. This report updates the initial evaluation and compares the results to recommendations in Revision 1 of the Preliminary UMo Report. Assumptions used in USHPRR safety analyses are discussed following the presentation of literature data. Where applicable, the Preliminary UMo Report is used as a point of comparison for the assumptions used in the USHPRR analyses that have been completed to date.

Conversion safety bases presented to regulators commonly compare the HEU and LEU results. In addition, to ensure satisfactory performance will be achieved, the LEU design must refer to the current requirements or performance of the HEU-fueled core. For this reason, in some instances data for HEU fuel are sometimes presented. These data are needed because new analyses of the HEU fuel are sometimes needed to ensure that the mission performance goals and other constraints placed on the LEU fuel can be directly compared to the HEU fuel.

Section 2 summarizes the primary properties of interest related to U-10Mo. In Section 3 the material properties of interest related to the cladding material, oxide, and zirconium interlayer are presented. The fuel performance parameters of fuel swelling and the blister anneal temperature (fuel temperature safety limit) are discussed in detail in Section 4. Section 5 provides a summary of this report and, where they exist, gaps in data that are needed for completing safety analyses for the USHPRR that will convert with U-10Mo monolithic fuel.

2 Materials Properties of U-10Mo Monolithic Fuel

This section discuss the materials properties of U-10Mo monolithic fuel critical for conversion analysis. The primary properties of interest related to U-10Mo are melting temperature, density (and how it changes with temperature and irradiation), heat capacity, thermal conductivity (and how it changes with temperature and irradiation), elastic modulus, and Poisson's ratio.

2.1 Melting Temperature of U-10Mo Monolithic Fuel

The solidus for U-10Mo fuel was extracted from [2] and found to be 1165°C. This is in agreement with the Preliminary UMo Report [1]. No specific melting temperature was discussed in reports on analyses done for HFIR [3], MURR [4], or NBSR [5]. Analyses for MITR [6] utilized a melting temperature of 1135°C, closer to the melting point of pure uranium (1132°C). Analyses for ATR [7] cited a solidus for the fuel of 828.15 K (555°C), which is closer to the alpha-gamma phase transition line than the solidus in the binary phase diagram.

The assumptions for MITR and ATR are conservative in comparison to the melting temperature recommended by the Preliminary UMo Report, so no re-analysis is needed.

2.2 Density of U-10Mo Monolithic Fuel

The density of uranium-molybdenum alloys has been investigated through several experiments [8,9,10,11,12,13,14,15] and has been found to vary with alloy composition, temperature, and enrichment. Density values can be determined from direct measurements [8,9,10] or calculated from lattice parameters derived from x-ray diffraction measurements [11,16]. The work done by Bridge, et al. [17] is often cited as a source for U-Mo lattice parameters, but that report discusses α-U only and should not be used. In this report, only gamma-phase U-Mo alloy data will be discussed, as that is the predominant phase required for fabrication of fuel plates for the UHSPRR.

X-ray diffraction measurements determine the ideal density of a material, without the inclusion of defects and pores that may be present in the non-ideal bulk system. However, since the values presented in this report will serve as the technical basis for modeling and simulation of fabricated fuel plates, density measurements that include the influence of as-fabricated defects are preferred. Consequently, for this technical basis, only those values determined from direct measurements of bulk U-10Mo are considered. Additionally, there is literature data available for atomized U-Mo alloy powder [18]. However, atomized powders have inherently lower densities than monolithic foils due to the nature of the fabrication process, which results in the formation of significant pores within the particles. Because of this porosity, density measurements from U-Mo alloy powders are not used as a technical basis in this report.

2.2.1 Dependence of U-Mo Alloy Fuel Density on Molybdenum Content

A selection of data from the literature on the density of U-Mo alloys as a function of Mo content is shown in Figure 2.1, along with a linear fit of these selected data [8,9,12].

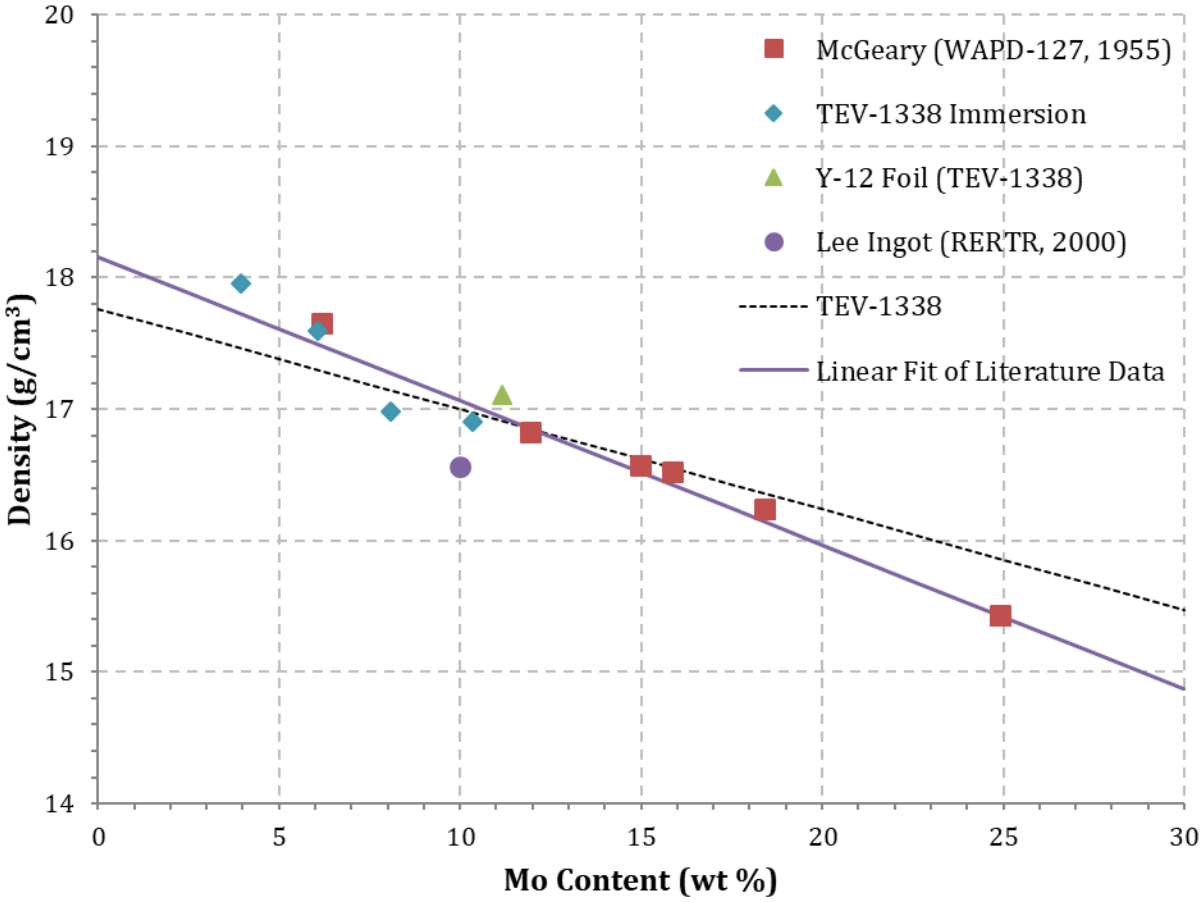

Figure 2.1. U-Mo alloy density as a function of Mo content.

A linear fit of the literature data is:

$$\rho_{U-Mo} = -0.110X_{Mo} + 18.16 \qquad (2.1)$$

where X_{Mo} is the weight percent Mo in the U-Mo alloy and the density is in g/cm³.

The Preliminary UMo Report [1] does not address the change in density due to a variation in Mo content. From Appendix C of the Preliminary UMo Report (Recommended Material Property Data Relevant to U-10Mo Fuel Plate Design), the room temperature density for U-10Mo is listed as 17.13 g/cm³, which is slightly higher than the value at 10 wt% Mo from the linear fit presented here, although still within the variation expected for the expected specifications of Mo content [19]. Both values are reasonable assumptions for the density of U-10Mo at room temperature.

2.2.1.1 Comparison to Density Values Utilized in Analyses for the USHPRR

Although 17.14 g/cm³ is listed as the assumed density in reference [3] for HFIR, 17.02 is more commonly used [20,21]. Analyses for the ATR [7] use 17.0 g/cm³, while those for NBSR [5] selected a density of 17.2 g/cm³, and MURR [4] and MITR [6] both use 17.02 g/cm³ for the room temperature density of unirradiated U-10Mo. All of these values are within 1.2% of the value proposed in the Preliminary UMo report, an acceptable variation.

The assumptions for density used by the five USHPRRs to be converted (ATR, HFIR, MITR, MURR, and NBSR) are compared to the linear fit given by equation 2.1 and the recommended value from the Preliminary UMo Report [1] (17.13 g/cm³ from Appendix C) in Figure 2.2. The density used for MITR [6] and MURR [4] ascribes approximately 1% porosity to the fuel analysis, which allows for the uncertainty given the lack of density data on prototypic foils. Confirmation of the density during prototypic fuel fabrication is required since there is a degree of uncertainty in the "fully-dense" or ideal density, and there may be some measureable level of porosity despite the nearly fully dense U-10Mo fuel foil that is expected after rolling the cast material. This is required at a macroscopic level to understand fuel loading in the plates, rather than at the lattice level, so techniques such as immersion density of bare rolled fuel cores may be the ideal starting point for the next data measurements.

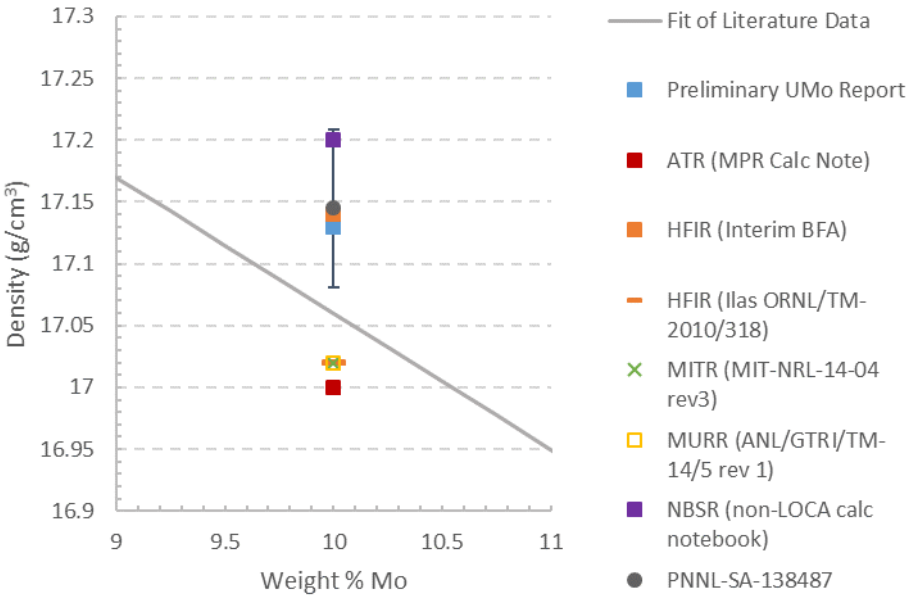

Figure 2.2. Comparison of density data of unirradiated U-10Mo fuel as used in USHPRR analyses.

PNNL has reported [22] on density measurements of U-10Mo at room temperature collected at both PNNL and LANL, which was fabricated using the prototypic processes. The average of all of the density values measured in the report (on both 8.5 mil and 25 mil thick samples) is 17.14 ± 0.05 g/cm³, as shown in Figure 2.2. The room temperature density for U-10Mo is listed in the Preliminary UMo Report as 17.13 g/cm³, in reasonable agreement with the PNNL report that evaluated U-10Mo fabricated with the prototypic processes. Re-evaluation of analyses that have already been completed is not required, but it is recommended to use 17.13 g/cm³ for room temperature density for future calculations.

2.2.2 Temperature Dependence of U-Mo Density

There are limited studies examining the temperature dependence of the density of U-10Mo. One study was published in 1957 by Del Grosso [13] and another was conducted more recently by Burkes, et al. [10,14]. Klein [23] also listed density versus temperature data for U-10Mo, citing a personal communication with Atomic Power Development Associates (APDA). However, this data is likely based on the data reported by Del Grosso, as it falls precisely along the faired average line provided in the Del Grosso report, as can be seen in Figure 2.3, and whom worked for APDA. Therefore, this reference cannot be considered as an independent determination of the effect of temperature on the density of U-10Mo.

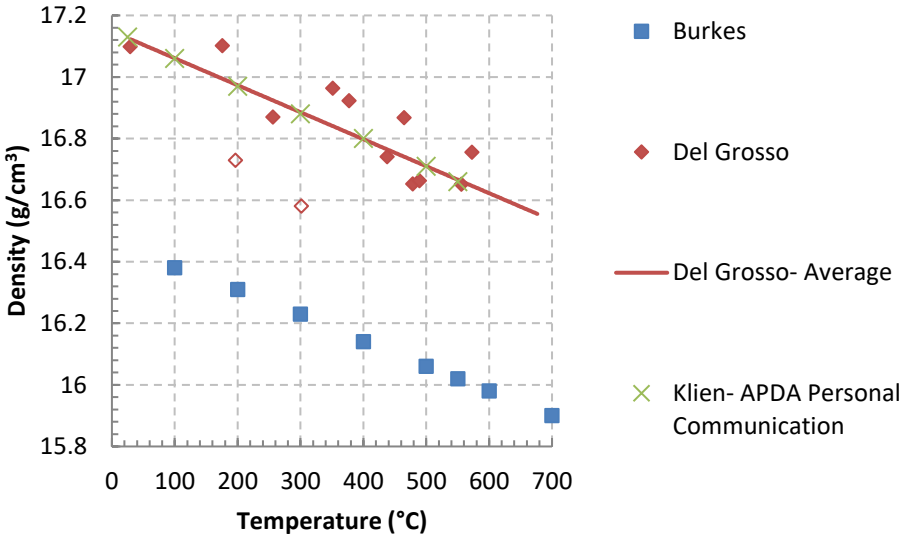

Figure 2.3. U-10Mo density as a function of temperature.

The average line of the data from Del Grosso [13], shown in equation 2.2 excludes data outliers (marked by an open symbol), as determined by a running average calculation in [13].

$$\rho_{U-10Mo} = 17.15 - 8.766 \times 10^{-4}(T) \tag{2.2}$$

A significant observation that can be made from Figure 2.3 is that the Burkes data [14] is substantially lower than the Del Grosso data [13]. From a discussion in the Burkes paper, this is likely due to extensive porosity in the samples (up to 3.8%) analyzed in that work. Although the density values are significantly different, the rate of change in the density with temperature between the two data sets is comparable. The agreement in slope between Del Grosso and Burkes indicates that the density change in the UMo alloy itself is not affected by the presence of porosity. In Burkes [10], this relation was used to develop an equation for the dependence of the density of U-10Mo on temperature, extrapolated from the rule-of-mixtures density at room temperature, shown in equation 2.3.

$$\rho_{U-10Mo} = \rho_{RT,U-10Mo} - (8.63 \times 10^{-4} \pm 2.76 \times 10^{-5})T \tag{2.3}$$

As a note, this equation should be modified by replacing (T) with (T-20) for the correct fit, as the equation should evaluate to 17.15 at T=20 based on the development discussed in the report. Additionally, in reference [10], the units for density are listed as kg m^{-3}, but they should be g cm^{-3} for

the numerical values to agree (or the slope should be a factor of 1000 higher), as was shown in Figure 6 of reference [10]. Equation 2.3 was formulated by taking the average of three data sets, two of which were not independent, and the error in this equation is from the standard deviation of the average, and is not a reflection of the variance in the experimental measurement.

2.2.2.1 Comparison of the Temperature Dependence of Density to Preliminary UMo Report

The Preliminary UMo Report [1] does not include a specific correlation recommendation for the density variation with temperature, although tabulated values are included in the recommendations of Appendix C. These tabulated values are in good agreement with the Del Grosso [13] correlation recommended in this report (equation 2.2), as shown in Figure 2.4.

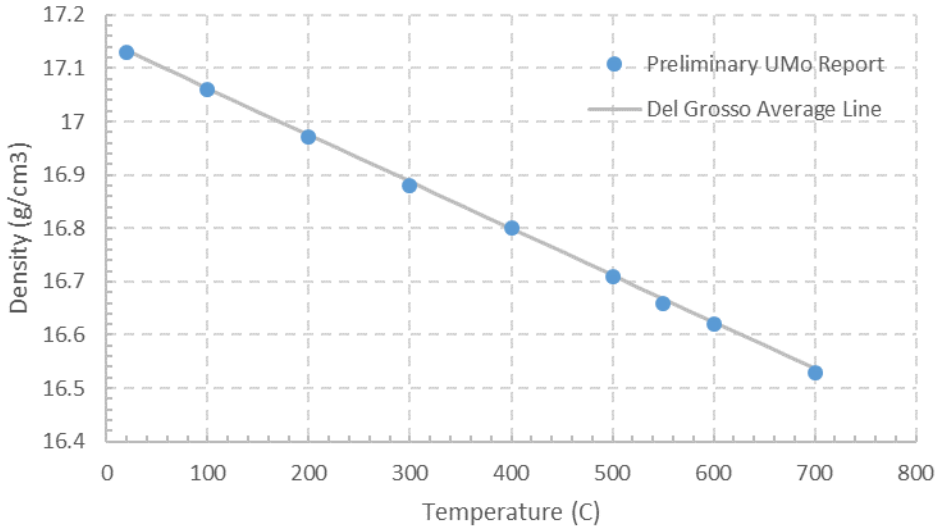

Figure 2.4. Comparison of the values recommended in Appendix C of the Preliminary UMo Report [1] and the Del Grosso [13] average line.

2.2.2.2 Comparison of the Temperature Dependence of the Density of U-10Mo Fuel to the Correlations Used for Analyses of the USHPRR

As discussed previously, it is recommended to use the Del Grosso average line, equation 2.2, to determine the temperature dependence of U-10Mo density. HFIR [3] uses equation 2.4, which is in close agreement with the recommended fit.

$$\rho_{U10Mo} = 17.14 - 8.68x10^{-4}(T) \qquad (2.4)$$

where T is the temperature in °C.

It has been proposed for ATR to use equation 2.5 which includes approximately 1% porosity, but a comparable slope to the Del Grosso faired average line.

$$\rho_{U10Mo} = \left(17.0 - 8.63x10^{-4} \times \left(\left(\frac{T-32}{1.8}\right) - 20.0\right) \times (2.54^3)\right) \times \left(\frac{0.00220462}{\frac{t_{swell}}{t_0} + 1}\right)\frac{lbm}{in^3} \qquad (2.5)$$

where T is the temperature in °F, and t_{swell} is the fuel thickness after irradiation, set to zero for this comparison. The density values were also converted to units of g/cm³ for comparison.

In Figure 2.5, the correlations used for analyses of HFIR and ATR, including the uncertainty of ±0.08 g/cm³ utilized in the HFIR analyses (indicated by the dashed lines) and the standard deviation of ±1.037 g/cm³ utilized in the analyses for ATR (indicated by the dotted lines), are compared to the recommended tabulated values from Appendix C of the Preliminary UMo Report. The correlations and tabulated values discussed here are in reasonable agreement (taking into account that the ATR correlation includes additional as-fabricated porosity). However, because these fits are all based on a single set of measurements, it is strongly recommended, and considered imperative, to collect a set of density values on samples with comparable porosity to prototypic as-fabricated foils to establish the accurate values.

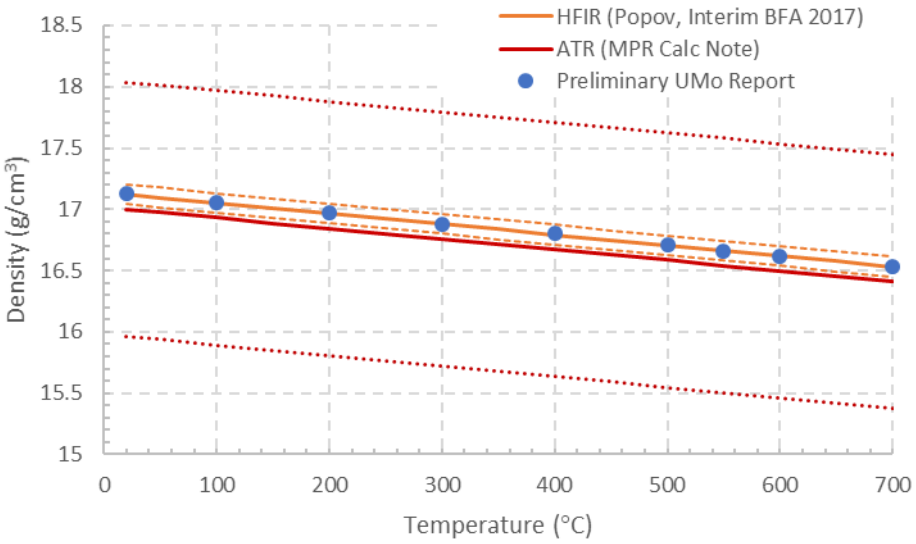

Figure 2.5. Comparison of correlations used for HFIR [3] and ATR [7] to the tabulated values in Appendix C of the Preliminary UMo Report [1].

Lastly, NBSR [24], MURR [4], and MITR [25] do not explicitly address the temperature-dependence of density in their safety analyses because they neglect the thermal expansion of the fuel. Therefore, to conserve mass, temperature dependence of the density is also neglected in the analyses.

2.2.3 Enrichment Dependence of the Density of U-Mo Fuel

The density of U-10Mo is also dependent upon the enrichment of the uranium. The rule of mixtures, shown in equation 2.6, can be used to calculate the room temperature theoretical density of a U-10Mo alloy. This equation should be used with caution, however, as it does not account for volume contraction that may occur during alloying, or porosity present in the sample. It is used here to illustrate the magnitude of the effect of enrichment on density. It is recommended, instead, to utilize available experimental data or a correlation based on experimental data for the density of the U-Mo alloy.

$$\rho_{UMo} = X_{Mo}\rho_{Mo} + (1 - X_{Mo})\rho_{U} \quad (2.6)$$

where X_{Mo} is the mole fraction of molybdenum in the alloy and ρ_{UMo}, ρ_{Mo}, and ρ_U are the densities (g/cm^3) of the alloy, elemental molybdenum, and elemental uranium, respectively.

For natural uranium, assuming ρ_{Mo} = 10.22 g/cm^3 [26] and ρ_U = 18.89 g/cm^3 [11] (gamma uranium), equation 2.6 evaluates to ρ_{UMo} = 17.02 g/cm^3. Enriched uranium has substantially more U-235, resulting in a lower molecular weight than natural uranium. Assuming that the U-234 content remains the same, the alloy is enriched to 19.75% U-235, and the number of uranium atoms/unit volume remains the same between natural and enriched uranium, the LEU-10Mo density is calculated to be 16.98. The dependence of density on the enrichment of the U-10Mo fuel was examined in reference [15]. U-10Mo alloys with two different enrichments (11.54% U-235 and 19.35%U-235) were examined, and the densities were found to be 17.15±0.050 g/cm^3 and 16.95±0.088 g/cm^3, respectively. The measured densities were lower than those calculated from the rule of mixtures. This is potentially due to as-fabricated porosity in the fuel, unaccounted for in the rule of mixtures calculation. Additionally, volume contraction due to alloying is not taken into account, which is why the rule of mixtures is not recommended for use. This exercise does show that the variation in density due to enrichment is minor, so data collected from natural or depleted uranium alloy samples can be utilized for enriched applications.

2.2.4 Irradiation Dependence of the Density of U-Mo Fuel

In addition to composition, temperature, and enrichment, irradiation also influences the fuel density. Fuel density decreases with burnup primarily due to fuel swelling by fission product accumulation. A model developed by Kim et al. [27] to assess fuel swelling of U-10Mo as a function of fission density (or burnup) is available as follows:

$$\frac{\Delta V}{V_{f.0}} = 0.05 f_d, \quad for\ f_d \le 3 \times 10^{21} \frac{fissions}{cm^3}$$

$$\frac{\Delta V}{V_{f,0}} = 0.15 + 0.063(f_d - 3) + 0.0033\,(f_d - 3)^2, \qquad for\ \ f_d > 3 \times 10^{21} \frac{fissions}{cm^3} \tag{2.7}$$

where $\left(\Delta V / V_{f,0}\right)$ is fuel swelling given in volume fraction, ΔV is the change in fuel volume due to irradiation, $V_{f,0}$ is the pre-irradiation U-Mo volume, and f_d is fission density in 10^{21} f/cm^3.

The irradiation-induced change in the density of U-Mo is expressed by [27]:

$$\rho_f = R_{irr}\rho_{f,0} \tag{2.8}$$

where $\rho_{f,0}$ is the density of unirradiated U-10Mo and R_{irr} is a reduction factor for degradation in density by irradiation defined by [27]:

$$R_{irr} = \frac{1}{1 + \frac{\Delta V}{V_{f,0}}} \tag{2.9}$$

Although there may appear to be a scarcity of measurement data available in the literature for density reduction during irradiation, this is attributable mainly to the effect of irradiation typically being correlated to the change in dimension or volume. Burkes and co-authors have reported a few data points for density reduction versus fission density [28,29]. They performed measurements on

samples from a plate originally produced at INL. Using the recommended unirradiated density value from the Preliminary UMo Report (17.13 g/cm^3), the density data of the irradiated samples from reports by Burkes were used to determine the reduction factor.

It can be observed from Figure 2.6 that the density reduction calculated by applying equation 2.9 and utilizing the fuel swelling correlations given in equation 2.7 is generally higher than the measured data points, although it should be noted that if the data are plotted using revised fission density values calculated by Robinson [30] then there is closer agreement between the correlation and the measured data. The correlation results are slightly higher than the measured data because the model prediction does not consider additional volume expansion from pore formation at the interface of the U-Mo foil and the AA6061 cladding, which is part of the measured data.

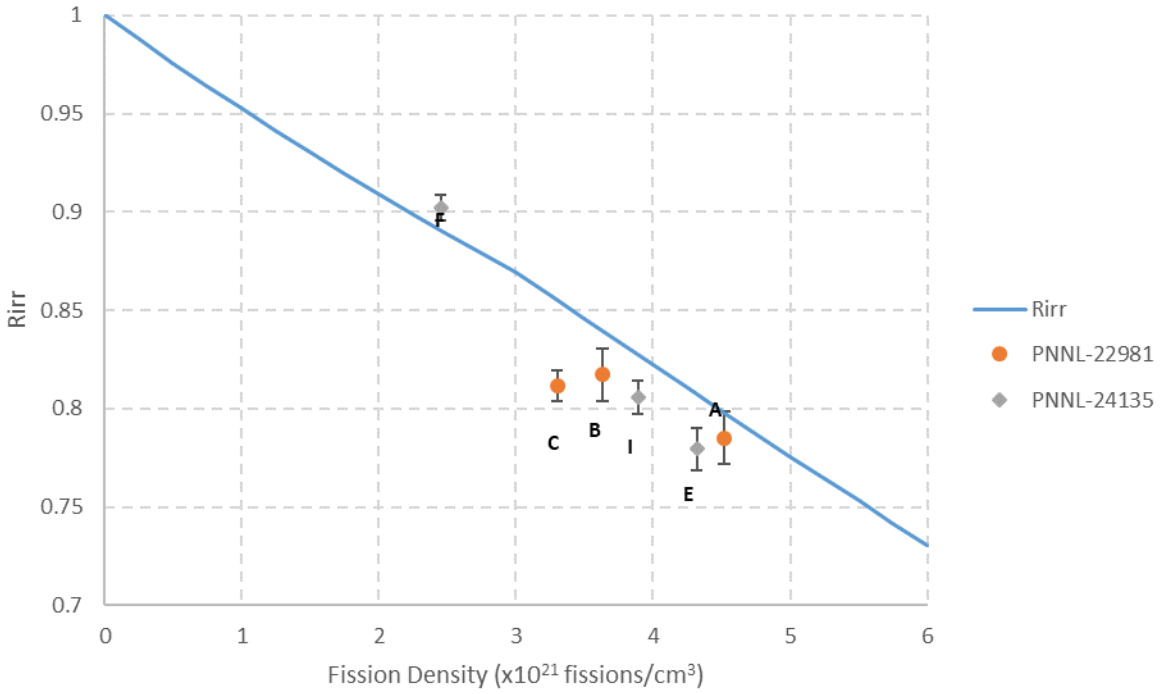

Figure 2.6. Reduction in density of U-10Mo during irradiation. The data were evaluated from the density data reported in Burkes [28] and Burkes [29] collected at room temperature.

2.2.4.1 Comparison of the Irradiation Dependence of Density to the Preliminary UMo Report

The Preliminary UMo Report [1] does not recommend a specific correlation for the reduction of density of U-Mo fuel with irradiation. Recommended density values from reference [31] are included in Section 5.2.3 of the Preliminary UMo Report, while Appendix C of the same report recommends tabulated values of density estimated based on total swelling, without a reference to the swelling correlation that was used. Fuel Swelling will be discussed in section 4.1 of this report. A comparison of the tabulated density values from Section 5.2.3 of the Preliminary UMo Report and the fit described in section 2.2.4 (equations 2.7 to 2.9) is shown in Figure 2.7. The correlation is based on the unirradiated density value of 17.13 g/cm^3, as listed in Appendix C of the Preliminary UMo Report. It can be seen that the correlation yields moderately higher density values than the tabulated data.

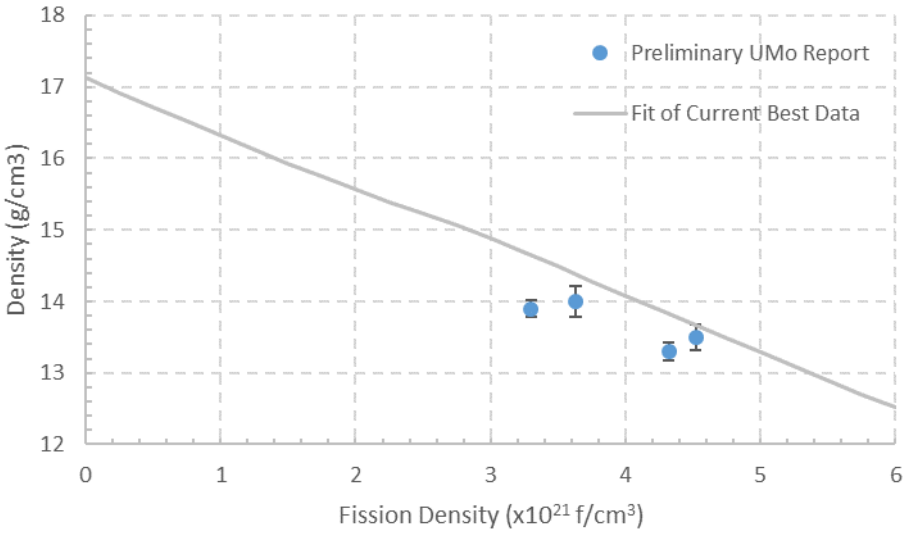

Figure 2.7. Comparison of the proposed correlation for the reduction in density of U-10Mo fuel at room temperature with irradiation and the values tabulated in Appendix C of the Preliminary UMo Report [1].

Like the Preliminary UMo Report, this report does not recommend a correlation for the reduction in density. It is almost always fuel swelling (Section 4.1) that is directly used for USHPRR safety basis analyses.

2.2.4.2 Comparison to the Correlations Used in Analyses for the USHPRR for the Impact of Irradiation on the Density of U-10Mo Fuel

MITR, MURR, and NBSR do not directly address the reduction in density of the U-10Mo with irradiation. Since irradiation does not change the mass of the fuel, the fuel core dimensions and fuel density are typically modeled as constant throughout the fuel lifetime. It should be noted, however, that MITR [6], MURR [4], and NBSR [5] incorporate assumptions for the change of the thickness of the coolant channel gap as a function of burnup in the analyses models. The coolant channel gap reduction is assumed to include the effect of fuel swelling as well as fuel creep and oxide formation on the surface of the fuel plate.

The Interim BFA (Basis for Analysis) for HFIR [3] discusses the change in density due to irradiation, but addresses this change through the swelling correlation, rather than through a direct measurement or calculation of the reduced fuel density. Calculations done for ATR [7] incorporate fuel swelling into the overall density equation, which also includes the effect of temperature, which are shown in equations 2.5 and 2.10. In these equations, t_{swell} is the thickness of the irradiated fuel, t_0 is the unirradiated thickness, and T is the temperature in °F. As a note, the "x10^{21}" following F_d in equation 2.10 should be discarded, as the fission density (F_d) is in fissions/cm^3. Additionally, t_0 should be in the numerator of equation 2.10. A comparison of the ATR correlation [7] and the tabulated values from the body of the Preliminary UMo Report [1] at room temperature (20°C / 68°F) are shown in Figure 2.8.

$$t_{swell} = \frac{5.9957 \times 10^{-43} \times (F_d \times 10^{21})^2 + 4.30015 \times 10^{-21} \times F_d \times 10^{21}}{100 \times t_0} \quad (2.10)$$

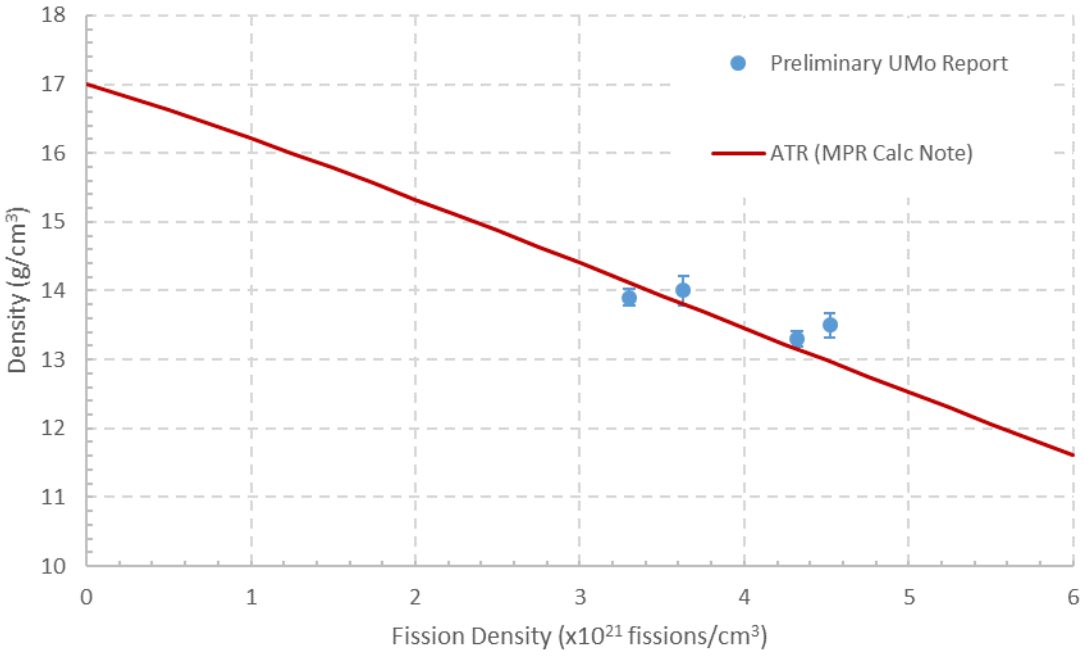

Figure 2.8. The correlation utilized for analyses for the ATR [7], and the values tabulated in Appendix C of the Preliminary UMo Report [1].

2.3 Heat Capacity of U-10Mo Monolithic Fuel

Burkes et al. [14] recommended a correlation for the heat capacity of U-10Mo based on their own data and data available in the literature [32,33]. This correlation is shown in equation 2.11,

$$c_p = (0.137 \pm 3.31 \times 10^{-3}) + (5.12 \times 10^{-5} \pm 1.41 \times 10^{-5})T + (1.99 \times 10^{-8} \pm 1.29 \times 10^{-8})T^2 \quad (2.11)$$

where c_p is the heat capacity in J/(g K) and T is the temperature in °C from 100 to 1000 °C. The data presented by Fackelmann [33] is a reproduction of the data collected by Farkas [32], so utilizing both sets of data in a fit is not recommended. Instead, a linear fit of the Burkes [14] and Farkas [32] data is proposed, as shown in equation 2.12, where c_p is in J/(g °C) and T is in °C.

$$c_p = 0.133 + 6.99 \times 10^{-5}T \quad (2.12)$$

Measurements of the specific heat capacity, density, and thermal diffusivity of composite samples were used as the basis for calculating the U-10Mo thermal conductivity. As a result of this methodology, the uncertainty in the specific heat capacity measurements are included in the uncertainty of the thermal conductivity. Therefore, no additional sampling from a distribution is recommended for specific heat capacity.

2.3.1 Comparison to the Correlation for the Heat Capacity of UMo Fuel in the Preliminary UMo Report

The Preliminary UMo Report recommends a correlation for the specific heat capacity, which is reproduced in equation 2.13,

$$c_p(U-10Mo) = (0.113 \times 10^3 \pm 4.28) + (7.05x10^{-2} \pm 5.20 \times 10^{-3}) \times T \qquad (2.13)$$

where T is in K and c_p is in J/kg-K.

Equations 2.12 and 2.13 are compared in Figure 2.9. The results of equation 2.12 are labeled as "Fit of Current Best Data." It should be noted that the units for c_p from equation 2.13 were converted to J/g-K for comparison to the correlation given in equation 2.12. Although the exact formulation of the correlations differ, the values are in agreement to three significant figures in the valid temperature ranges of the correlations. For future calculations requiring the heat capacity of U-10Mo fuel, equation 2.13 is recommended.

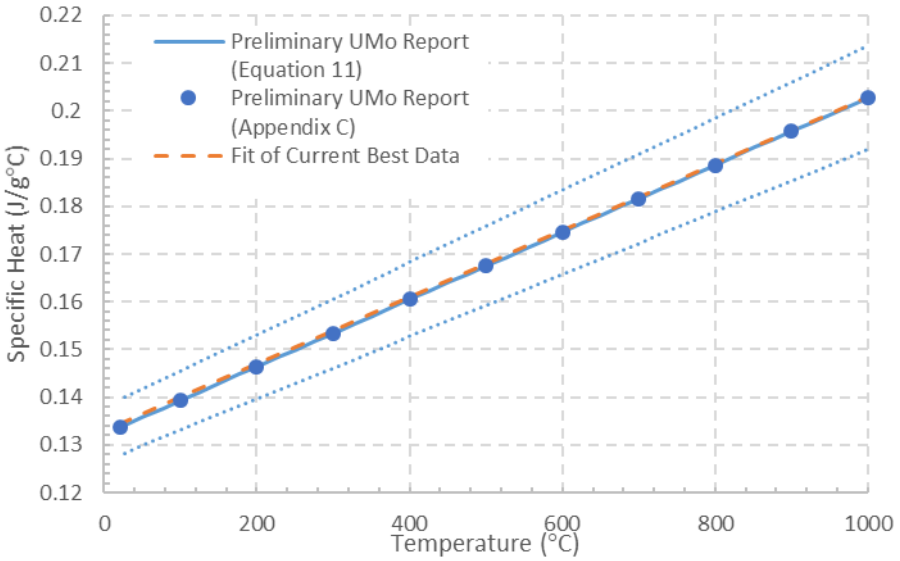

Figure 2.9. Comparison of the correlations for the specific heat of U-10Mo from the Preliminary UMo Report [1] and the Fit of Current Best Data (equation 2.12), where the dotted lines indicate the upper and lower bounds for the correlation in the Preliminary UMo Report.

2.3.2 Comparison to Correlations for the Heat Capacity of U-10Mo Fuel Utilized in Analyses of the USHPRR

The MURR report [4] formulates the volumetric heat capacity of U-10Mo as shown in equation 2.14, where the specific heat capacity and density are treated as a single variable. The combined parameter ρc_p is typically utilized in safety analysis models, rather than addressing density and heat capacity separately, so this form is more convenient for modeling.

$$\rho c_p = 1.923 \times 10^6 + 1199.9(T + 273.15) \qquad (2.14)$$

where ρc_p is given in J/(m^3 °C) and T in °C.

Assuming the density of unirradiated U-10Mo is 17.02 g/cm^3, as given in the report for MURR [4], equation 2.14 was modified to determine c_p, as shown in equation 2.15. This derived equation is identical to that given in reference [10].

$$c_p = 0.113 + 7.05 \times 10^{-5}(T + 273.15) \quad (2.15)$$

where c_p is given in J/(g K) and T in °C. The heat capacity data used in the MURR analysis [4] were taken from [10] (which is the same as equation 2.13) because those values were lower (and, hence, more conservative) than those found by equation 2.11.

For properties not explicitly discussed in Reference [6], MITR refers to MURR [4], and therefore uses the same formulation for heat capacity.

The HFIR report [3] adopted a slightly different correlation, which was based on that given in [34], and is shown in equation 2.16 below.

$$c_p = 0.114 + 7.23 \times 10^{-5}T \quad (2.16)$$

where heat capacity is in J/(g K) and T is in K. The valid temperature range for this correlation is 298 – 1073 K. The same constant term, but a slightly different temperature coefficient, was used when compared to the correlation given in [34]. It is not clear if this difference is by intention or due to a typographical error. Nonetheless, the differing coefficients yield a maximum difference for the specific heat capacity of 1.2% at room temperature.

Analyses for ATR utilized equation 2.17 below, which is in agreement with the correlation recommended in the Preliminary UMo Report when the values are converted to metric units.

$$c_{U-10Mo} = \left(113 + \left(\frac{T + 459.67}{1.8}\right) \times 0.0705\right) \times 5.266 \times \frac{10^{-7}}{0.00220462} \frac{BTU}{lbm°\mathrm{F}} \quad (2.17)$$

NBSR [24] uses equation 2.18 for the specific heat capacity.

$$c_p^{UMo} = 29.84 - 8.9 \times 10^{-3}T + 4.32 \times 10^{-5}T^2 - 2.06 \times 10^{-8}T^3 \quad (2.18)$$

However, a discrepancy exists when comparing the tabulated values for specific heat capacity in the LOCA [35] and non-LOCA [5] calculation notebooks for NBSR. Although it is stated that the same equation (equation 2.18) was utilized to produce both tables, it appears an incorrect conversion from J/mol-K to kJ/m^{3}K was used in the LOCA calculation notebook. This resulted in incorrect values for the specific heat capacity that are ~2.5 times larger than those used in the non-LOCA analysis. It is recommended that the NBSR LOCA analysis be reviewed to assess the impact of using the incorrect specific heat capacity.

As shown in Figure 2.10, the correlations utilized in analyses for the USHPRR, with the exception of NBSR, are in close agreement with the Preliminary UMo Report, as all fall within the reported uncertainty band for the Preliminary UMo Report correlation. It is noted that the NBSR non-LOCA calculation notebook utilized higher values for specific heat capacity, although these values remain within 11% of the values proposed by the Preliminary UMo Report. The NBSR LOCA calculation notebook values have been excluded from this comparison, as they are considered erroneous, as

discussed above. For future calculations requiring the heat capacity of U-10Mo fuel, equation 2.13 is recommended.

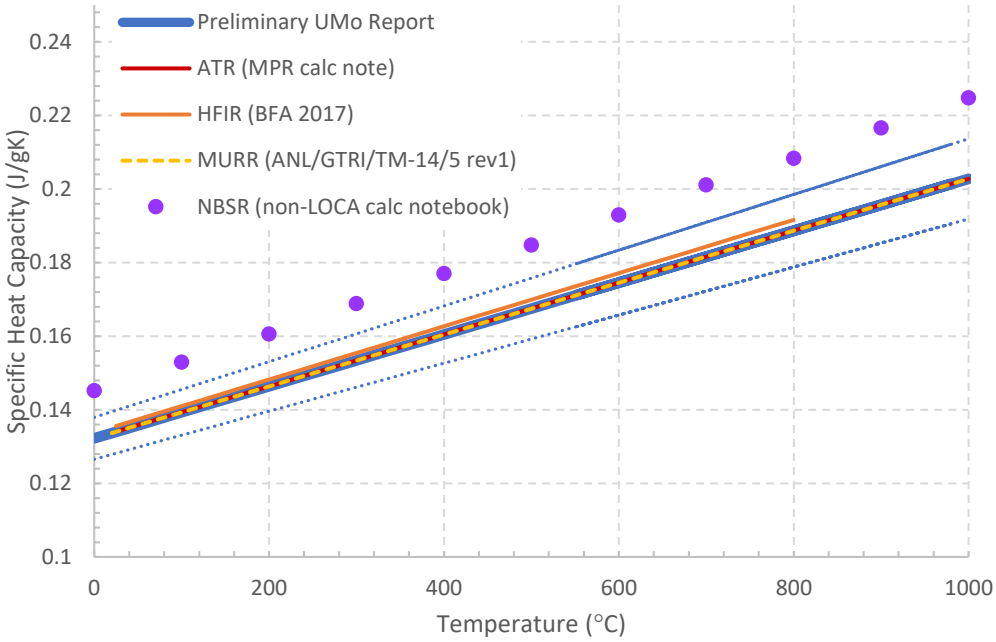

Figure 2.10. Comparison of the specific heat capacity correlations and values used for analyses of the USHPRR to the Preliminary UMo Report [1]. The dotted blue lines are the high and low confidence intervals for the Preliminary UMo Report equation.

2.4 Thermal Diffusivity of U-10Mo Monolithic Fuel

The Preliminary UMo Report [1] includes a correlation and tabulated values for the thermal diffusivity of U-10Mo fuel, based on a single data set [10]. The thermal diffusivity is measured and incorporated, along with measurements of density and heat capacity, into the calculation of thermal conductivity. The HFIR Preliminary BFA [3] includes the same correlation, but none of the other USHPRRs explicitly utilize the thermal diffusivity.

2.5 Thermal Conductivity of U-10Mo Monolithic Fuel

Thermal conductivity of U-Mo alloys has been studied since the early fuel development era dating back to the 1940s. The data utilized in this discussion is limited to gamma-phase U-Mo alloys, with thermal conductivity data in the applicable temperature range (~100-400C).

2.5.1 Unirradiated Thermal Conductivity of U-Mo alloys

Data for unirradiated U-Mo alloys are available for U-5Mo [36], U-8Mo [37,38], U-9Mo [39,40], U-10Mo [12,14,23,41,42], and U-12Mo [37], all of which are shown in Figure 2.11below. The tabulated data values can be found in Appendix B: The UMo handbook [43] had done an analysis and fit of this data, but errors were found in the data set used to develop the fit, so re-analysis was needed.

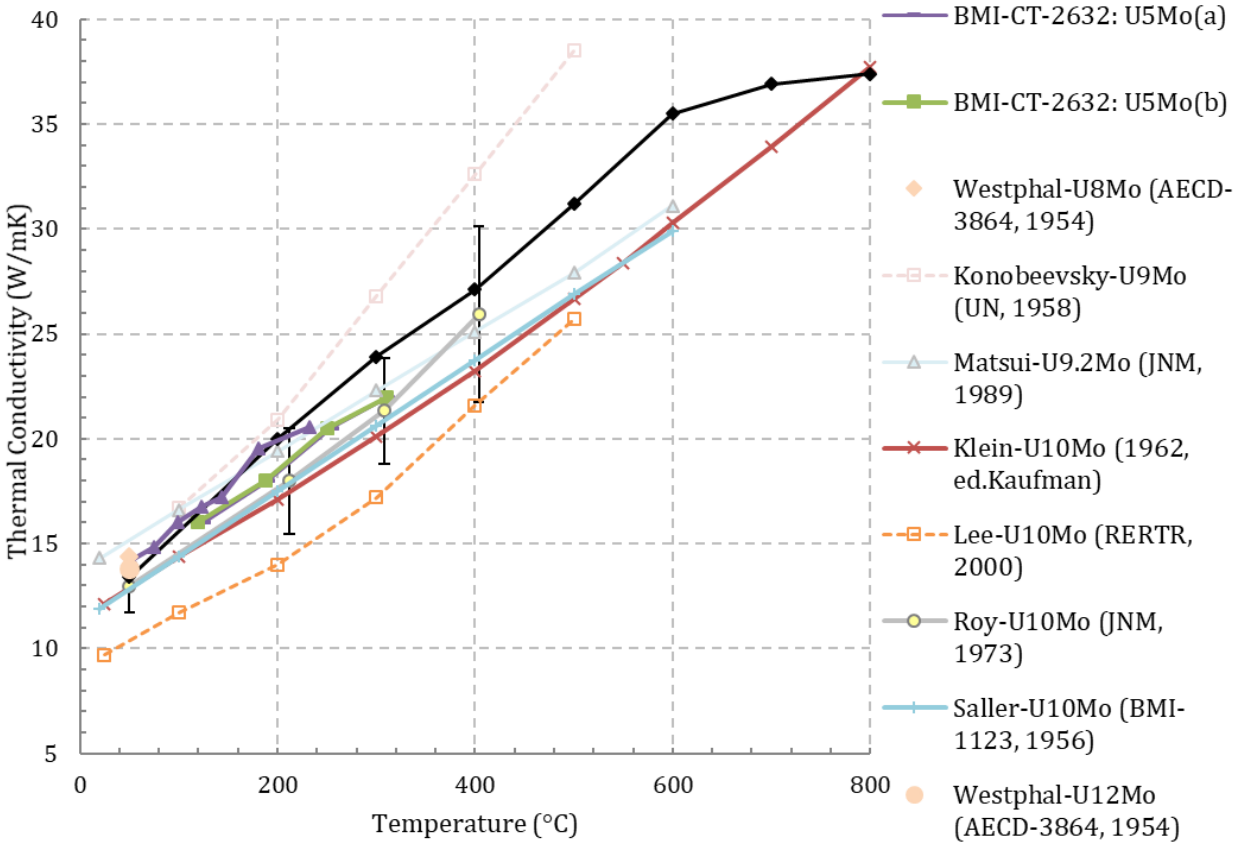

Figure 2.11. Thermal conductivity dependence on temperature for selected data sets [12,14,23,29,36,37,38,39,40,41,42,43].

As an additional note, an error was found in Touloukian [44] in the data for the U-5Mo from BMI [36], listed as curves 3-5 in Touloukian. Touloukian [44] listed curves 3 (thermal conductivity values 0.16-0.220 W/cm-°C) and 5 (thermal conductivity values 0.205-0.250 W/cm-°C) as gamma phase. However, when comparing the tabulated data (data table number 228 in [44]) to the data plotted in BMI Figure 152 (the cited work [36]), it is apparent that curves 3 and 4 are gamma-phase (as received and water quenched from 700°C), and curve 5 is alpha phase (annealed at 520°C for 40 hours). Figure 2.12 shows the figure from BMI [36] with the curve numbers as identified in Touloukian. Although the work by Touloukian [44] is a review and not an independent data set, it is included for discussion here because it is frequently referenced in literature.

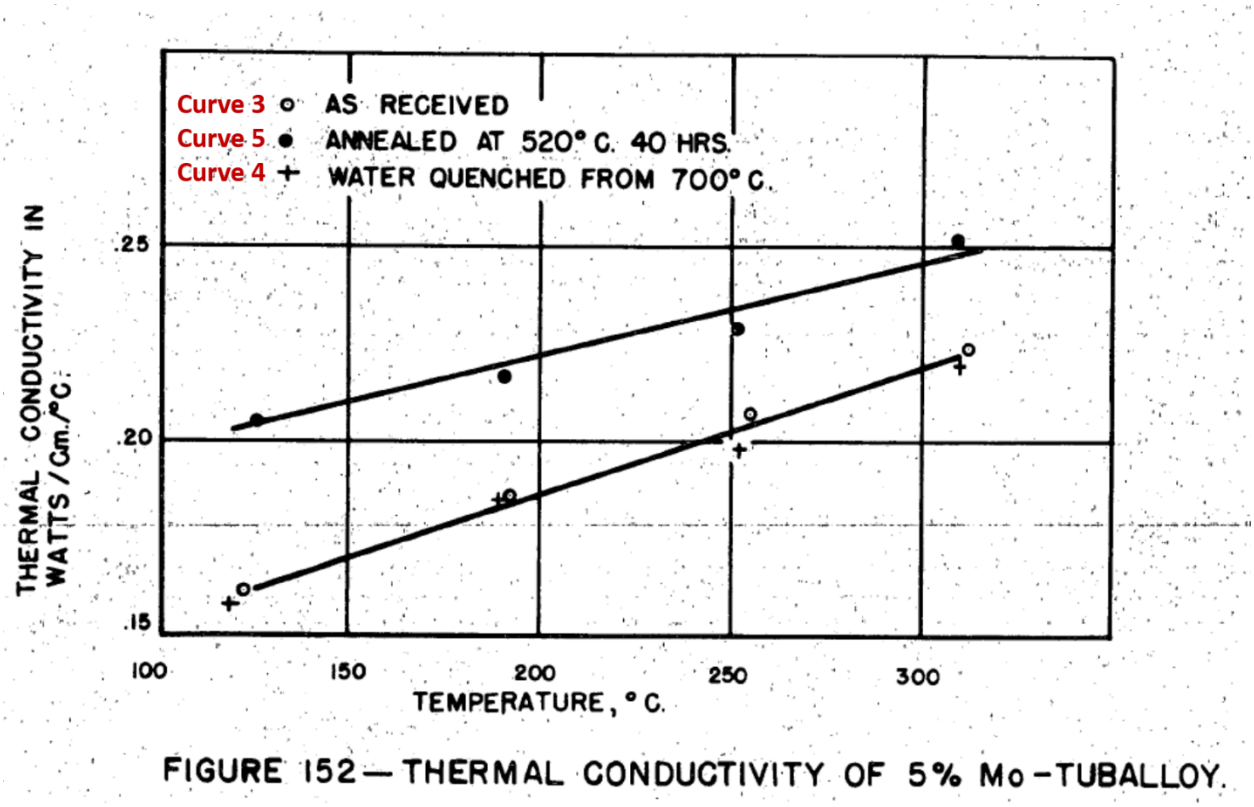

Figure 2.12. Comparison of a) Data table reproduced from Touloukian [44] and b) Plot from BMI CT-2632 [36].

The UMo Handbook [43] developed an equation for the thermal conductivity of U-Mo fuel using a modified mixture rule that takes into account the alloying effect, shown in equation 2.19. This method is based off with a modified mixture rule developed for UZr alloys [45] and is assumed to be applicable to U-Mo alloys due to the similarities of Zr and Mo.

$$k^0_{U-Mo} = \left(1 - \sqrt{1 - x_{Mo}}\right)k_{Mo} + \sqrt{1 - x_{Mo}}\left\{(1 - x_{Mo})k_U + x_{Mo}k_{c,Mo}\right\} \quad (2.19)$$

Where k^0_{U-Mo} is the U-Mo alloy thermal conductivity, x_{Mo} is the Mo content in weight fraction, k_U is the thermal conductivity of uranium, k_{Mo} is the thermal conductivity of molybdenum, and $k_{c,Mo}$ is the alloying effect term. k_U is defined in equation 2.20 [45,46], k_{Mo} is defined in equation 2.21, and $k_{c,Mo}$ is defined in equation 2.22. The thermal conductivities are in W/(m °C), and T is in °C. The $k_{c,Mo}$ term is valid for Mo content between 5 and 12 weight percent, and temperatures from 25 to 600°C (equation 2.22 is in K).

$$k_U = 21.73 + 1.591 \times 10^{-2}(T + 273.15) + 5.907 \times 10^{-6}(T + 273.15)^2 \quad (2.20)$$

$$k_{Mo} = 150.0 - 4.0 \times 10^{-2}(T + 273.15) \quad (2.21)$$

$$k_{c,Mo} = -274.4 + 985.2x_{Mo} - 1.941 \times 10^3 {x_{Mo}}^2 + 3.640 \times 10^{-2}T + 7.365 \times 10^{-5}T^2 + 5.793 \times 10^{-2}x_{Mo}T \quad (2.22)$$

This same method was utilized to develop a correlation for the data displayed in Figure 2.11, excluding Konobeevsky [39] and the two highest temperature data points from Burkes [14] as

outliers. Additionally, the Lee [12] data was adjusted to correct for the higher than typical porosity in the sample. Furthermore, the k_{Mo} equation was modified to match that given by Touloukian [44], given in equation 2.23. The new correlation is shown in equation 2.24.

$$k_{Mo} = 152.2 - 4.92 \times 10^{-2}(T + 237.15) + 8.76 \times 10^{-6}(T + 273.15)^2 \quad (2.23)$$

$$k_{c,Mo} = -313.13 + 1382.9x_{Mo} - 1993.3{x_{Mo}}^2 + 0.31203T - 3.5455 \times 10^{-5}T^2 - 1.2068x_{Mo}T \quad (2.24)$$

This correlation (recommended in the initial evaluation) combines the effect of both temperature and Mo content on the thermal conductivity of U-Mo alloys, and is primarily based on thermal conductivity values based on electrical conductivity measurements and converted using the Wiederman-Franz law.

Because a data set measured by Burkes [14] using the current best technique on close to prototypic U-10Mo is available, it is instead suggested to utilize a linear fit of the current best data. The recommended correlation for fresh fuel is shown in equation 2.25, and is based on tabulated data [14] and an additional data point that is presented at 50°C in Figure 11 of reference [31], digitized as 13.35 W/m K. A combined correlation for the dependence of thermal conductivity on temperature and fission density is recommended in the following section.

$$k_{U-10Mo} = 0.0335 \times T + 13.29 \quad (2.25)$$

where $k_{U\text{-}10Mo}$ is the thermal conductivity in W/(m °C) and T is the temperature in °C from 50 to 800°C.

2.5.1.1 Comparison to the Preliminary UMo Report of the Correlation for the Dependence of Thermal Conductivity of U-10Mo Fuel on Temperature

Figure 2.13 compares the correlations recommended by the Preliminary UMo Report [1], the initial evaluation recommendation, and the fit of current best data (equation 2.25). The correlations from both the Preliminary UMo Report and initial evaluations include data collected using the older technique, which excludes the phonon contribution to thermal conductivity. As a result, the thermal conductivity determined from these two correlations is lower than from the fit of the current best data for some (initial evaluations) or all (Preliminary UMo Report) temperatures in the range of interest. Additionally, the correlation recommended in the initial evaluation incorporates data available for other U-Mo alloys, resulting in a substantially different slope. It is recommended to use the combined correlation in the following section that includes the impact of both temperature and irradiation on thermal conductivity of U-10Mo.

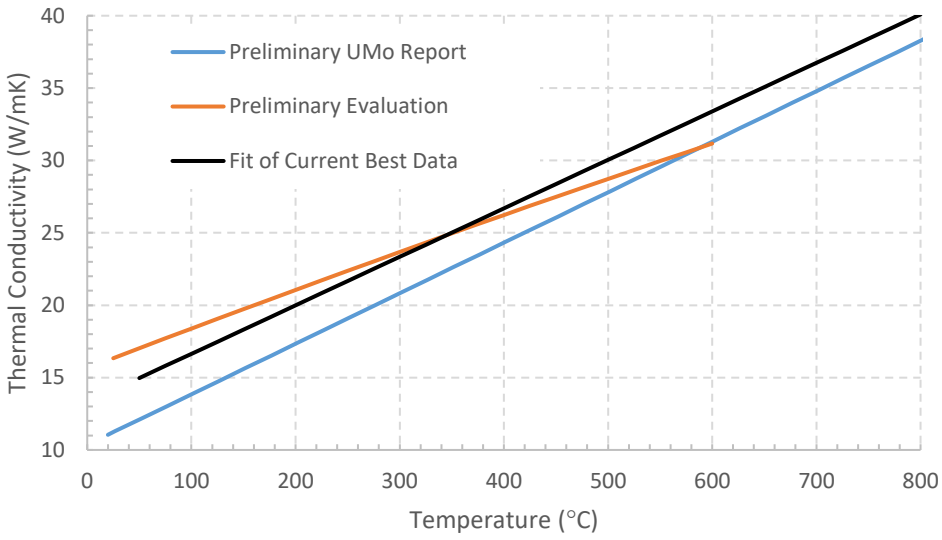

Figure 2.13. Comparison of correlations recommended by the Preliminary UMo Report [1], the recommendation from the initial evaluation, and the fit of current best data (equation 2.25**).**

2.5.1.2 Comparison to the Correlations Utilized in Analyses for the USHPRR for the Temperature Dependence of the Thermal Conductivity of Unirradiated U-10Mo Fuel

Analyses for MURR [4] utilize a linear fit of the data from Burkes [14] to describe the thermal conductivity of unirradiated U-10Mo as a function of temperature, shown in equation 2.26.

$$k = 14.821 + 0.0309 \times T \tag{2.26}$$

A report for HFIR [3] predicts the thermal conductivity with a linear fit of data from Matsui [40] and Burkes [14,18], described in equation 2.27.

$$k = 13.07 + 0.033 \times T \tag{2.27}$$

A report for NBSR [24] cites two sources for the thermal conductivity as a function of temperature, the UMo Handbook [43] and Burkes [14]. From the calculation notebooks [5,35], the UMo Handbook formulation was utilized (equations 2.19 to 2.22). Analyses for ATR [7] and MITR [6] use correlations that include the effects of both temperature and irradiation on the thermal conductivity of the U-10Mo fuel, as shown in equations 2.28 and 2.29, respectively.

$$k_{U-10Mo} = \left(0.8087 + 0.03487 \times \left(\frac{T + 459.67}{1.8}\right) + 0.6718 \times F_d - 0.0046 \times \left(\frac{T + 459.67}{1.8}\right) \times F_d\right) \times \frac{0.57779}{12 \times (60 \times 60)} \frac{BTU}{s - in - °F} \tag{2.28}$$

$$k = 12.57 + 0.04T - F_d \times (1.322 + 0.00278T) - T^2(2.351 \times 10^{-5} + 4.996 \times 10^{-6} F_d) \tag{2.29}$$

The temperature for all of the above equations is in °C, the thermal conductivity is in W/(m K), and the fission density (where applicable) is in fissions/cm^3 x 10^{21}. Analyses for ATR [7] are conducted in imperial units, so the temperature is in °F and the thermal conductivity is in BTU/(s in °F), which were converted to metric units for comparison to the rest of the USHPRR.

The correlations for the thermal conductivity of U-10Mo as a function of temperature for the analyses of the USHPRR are compared in Figure 2.14, alongside the correlation recommended by the Preliminary UMo Report [1] and the fit of current best data. With the exception of those for MURR [4], all correlations are conservative when compared to the fit of current best data. For MURR, the deviation is less than 10% at 50°C, and is less than 5% at temperatures relevant for MURR safety analysis. The MURR correlation is well within the assumed 95% confidence interval (CI) of 20% (indicated by thin grey lines in the plot).

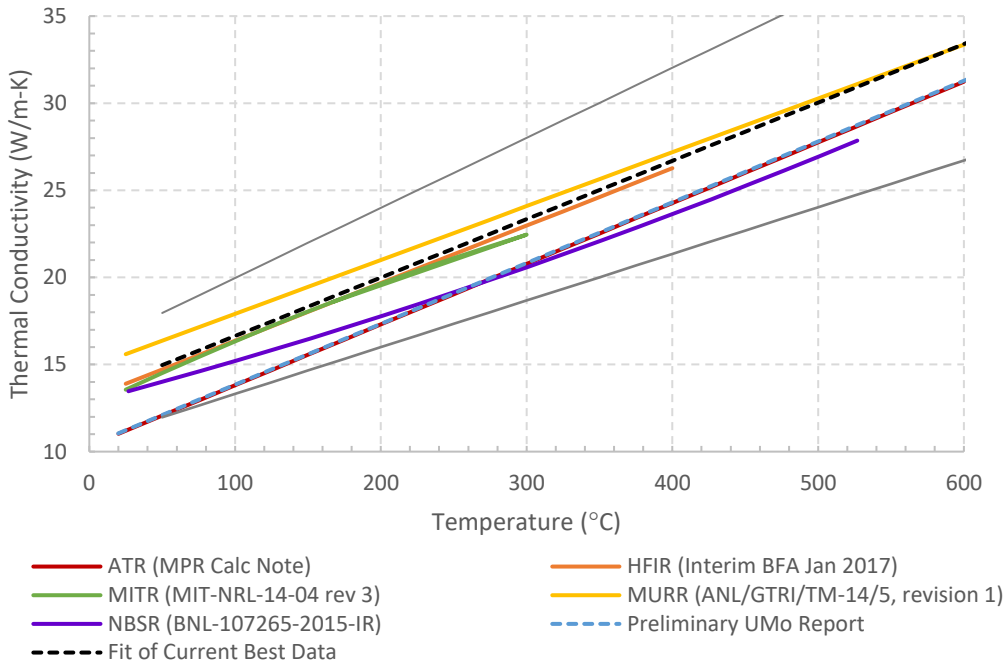

Figure 2.14. Comparison of the correlations used for analyses of the USHPRR, the correlation recommended by the Preliminary UMo Report, and the fit of current best data at 200°C.

Additional data for the thermal conductivity of prototypic U-10Mo is necessary to determine the proper formulation. In practice for reactor analysis, a single combined correlation for thermal conductivity that encompasses a range of fission densities from fresh fuel through end of life is ordinarily used. See Section 2.5.2 for a discussion of the currently best available data for fresh and irradiated U-10Mo. See Section 2.6.1 for recommendations regarding data gaps and expected future data requirements.

2.5.2 Irradiated Thermal Conductivity of U-10Mo Fuel

During irradiation, the thermal conductivity of the U-Mo fuel alloy decreases, primarily as an effect of porosity formation due to fission gas accumulation. Two models, one developed by Bruggeman [47] and the other by Peddicord [48], have traditionally been utilized to predict the effect of porosity on thermal conductivity. However, as shown in Figure 2.15, these models substantially overestimate the thermal conductivity when compared to the limited experimental data that are available [13,28,49].

This is an indication that the models do not fully capture the physics leading to changes in thermal conductivity with irradiation in this fuel system. Additionally, the Bruggeman [47] and Peddicord [48] correlations likely only account for porosity visible by optical microscopy and scanning electron microscopy, missing the substantial amount of fission gasses trapped in nanobubbles, as has been observed via TEM [50], or in solution with the alloy. The under prediction of the reduction in thermal conductivity with irradiation could also be caused by the influence of solid fission products incorporated into the fuel system, as well as the formation of large pores aligned along the interface (rather than the assumed homogeneous distribution).

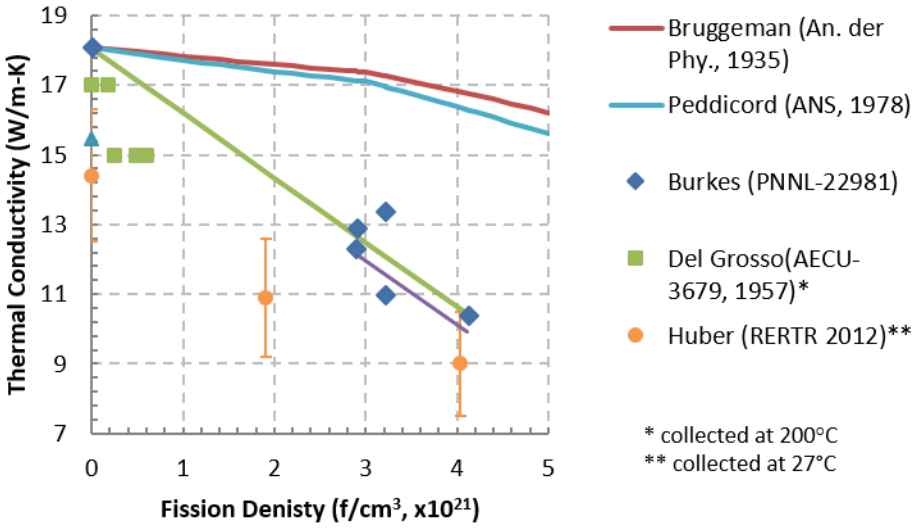

Figure 2.15. Thermal Conductivity as a Function of Fission Density at 150°C. Del Grosso data tabulated by [32].

Recently provided data values for thermal conductivity of irradiated U-10Mo from the AFIP-2, -3, and -6 experiments [31,51] are under evaluation. A fit of this data as a function of temperature and fission density was developed following the same process used to develop equation 2.29, excluding the AFIP-6 data, which demonstrated a substantial amount of scatter. The AFIP-6MkI plate blistered during the test and is considered unsuitable for use. Likewise, AFIP6MkII had a sizeable proportion of a secondary phase (likely α-phase uranium) and these data are also considered unsuitable for U-10Mo fuel used in the program which is specified to be greater than 90 wt% γ-phase uranium [19]. This indicates that the AFIP-6 data are not based on prototypic behavior or fuel. A new correlation, which is based on the AFIP-2 and AFIP-3 data measurements provided in [51], is shown in equation 2.30, where T is the temperature from 50 to 350 C and f_d is the fission density in x10^{21}f/cm^3 from 0 to 4.5.

$$k = 9.807 + T \times 0.06021 - f_d \times (0.7382 + 0.004734 \times T) - T^2 \times (7.700 \times 10^{-5} + 3.452 \times 10^{-7} \times f_d) \quad (2.30)$$

The root-mean-square (RMS) discrepancy of evaluations of equation 2.30 relative to the dataset provided in [51] is 8.3%. This represents a modest improvement compared to the RMS discrepancy of 9.2% for evaluations of equation 2.29 relative to the same dataset. Because of the second-order dependence with temperature in equations 2.29 and 2.30, extrapolation to temperatures exceeding 350 C is not recommended as there are no measured data available to assess the correlation results.

Equation 2.30 (recommended in the initial evaluation) has recently been re-evaluated with a linear dependence on T and to incorporate data for unirradiated U-10Mo in the fit [14,31,51]. The resulting fit of current best data is shown in equation 2.31, the recommended correlation, valid for temperatures of 50-350°C and fission densities up to 5 ($x10^{21}$) fissions/cm^3. The RMS discrepancy of evaluations of equation 2.31 relative to the dataset provided in in [51] is 5.2%.

$$k = 11.33 + T \times 0.04175 - F_d \times (0.7908 + 0.00611 \times T) \quad (2.31)$$

2.5.2.1 Comparison to the Values Recommended for the Degradation of Thermal Conductivity with Irradiation in the Preliminary UMo Report

The Preliminary UMo Report [1] does not recommend a specific correlation, and instead suggests using tabulated data. A comparison of the data recommended in the Preliminary UMo Report, the correlation recommended during initial evaluations, and the fit of current best data at 200 °C is shown in Figure 2.16. The fit of current best data and the tabulated data from the Preliminary UMo Report are in good agreement, but as will be discussed in detail in section 2.5.3, significant data gaps exist.

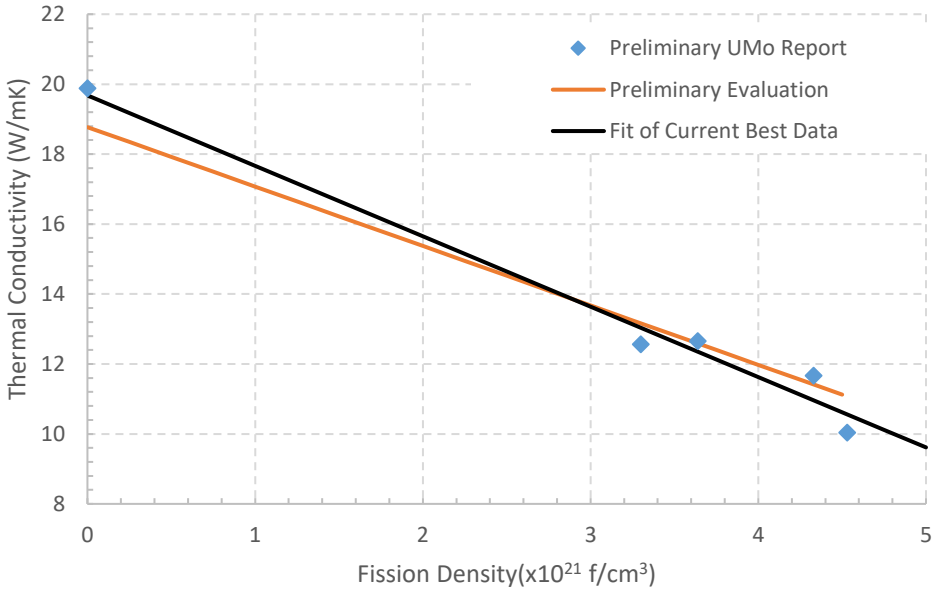

Figure 2.16. Comparison of the data recommended by the Preliminary UMo Report [1], recommendation in the initial evaluation, and the fit of current best data at 200°C for the reduction in thermal conductivity of U-10Mo fuel with irradiation

2.5.2.2 Comparison of the Values and Correlations Utilized in Analyses of the USHPRR for the Degradation of U-10Mo Thermal Conductivity with Irradiation

A comparison of the correlations or values used for analyses of the USHPRR compared to the values recommended by the Preliminary UMo Report [1] are shown in Figure 2.17.

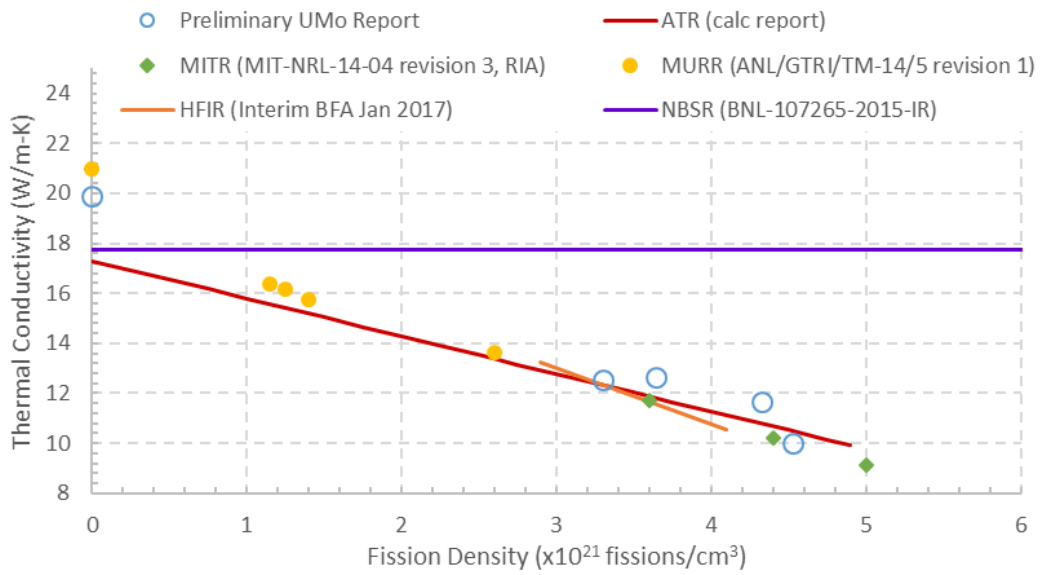

Figure 2.17. Comparison of the values or correlations used for analyses of the USHPRR [6] and the values recommended by the Preliminary UMo Report [1] at 200°C.

Analyses for MURR [4] used the correlation of the unirradiated U-10Mo thermal conductivity shown in equation 2.26 coupled with a fit for irradiated U-10Mo derived from data presented by Burkes [28], which is dependent upon temperature and fission density, as shown in equation 2.32,

$$k = 12.57 + 0.04T - f_d(1.322 + 0.00278T) - T^2(2.351 \times 10^{-5} + 4.996 \times 10^{-6} f_d) \qquad (2.32)$$

where T is the temperature in °C from 50-300 °C and f_d is the fission density in x10^{21} f/cm^3 from 0-4.1x10^{21} f/cm^3. For a given fission density, equation 2.32 is evaluated at several temperatures over the range of 50-300 °C and then compared with the thermal conductivity from equation 2.26 at the same temperature values. The minimum ratio of the irradiated/unirradiated thermal conductivity over this temperature range is then used as a conservative multiplier on equation 2.26 to derive the thermal conductivity for safety analyses, as shown in Table 2.2 of reference [4].

MITR [6] uses this same methodology for Reactivity Insertion Analysis (RIA), which is illustrated in Table 2.1 at 200 °C and fission densities relevant for the safety analysis performed for MITR.

Table 2.1. Values used in analyses for MITR [6] at 200 °C.

Fission Density (x10^{21} fissions/cm^3)	Ratio of Irradiated to Unirradiated Thermal Conductivity	Thermal Conductivity (W/m°C)
5.00	0.434	9.11
4.40	0.487	10.23
3.60	0.559	11.74
0.00	1	21.00

It should be noted that this methodology, and equation 2.32 in particular, should not be used beyond the recommended ranges of the temperature or fission density, as the quadratic dependence on temperature can lead to erroneous predictions for the thermal conductivity and the resulting fuel temperature for both steady-state and accident analyses.

A report for HFIR [3] defines the thermal conductivity for irradiated U-10Mo, as a function of temperature for two different fission densities, shown in equations 2.33 and 2.34, and suggests interpolating for intermediate fission densities.

$$k = 8.83 + 0.022T, for\ fd = 2.9 \times 10^{21} \frac{f}{cm^2} \quad (2.33)$$

$$k = 8.02 + 0.0127T, for\ fd = 4.11 \times 10^{21} \frac{f}{cm^3} \quad (2.34)$$

Analyses for NBSR [24,35] do not consider the reduction in thermal conductivity with irradiation in safety analysis because of the negligible impact on the results for the limiting LOCA. Instead, NBSR utilizes the fresh fuel thermal conductivity, regardless of the fuel burnup.

Analyses for ATR [7] utilized the correlation in equation 2.28, which has been converted to W/(m °C) for comparison. All suggested correlations are within the range of the experimental data available, and are thus considered reasonable. However, these equations are based on limited experimental data, and additional measurements would substantially improve the accuracy of the correlations

2.6 Thermal Expansion of U-10Mo Fuel

A correlation for thermal expansion of U-10Mo is included in the Preliminary UMo Report [1], and a different correlation is included in the Interim BFA for HFIR [3], but is not explicitly included in the reports for the other USHPRR. As such, a detailed discussion of this material property is not included in this report.

2.6.1 Data Gaps and Expected Future Data Needs

The data for the thermal conductivity of irradiated U-10Mo presented in reference [28] and used to prepare the correlation used by MURR [4] and MITR [6], equation 2.32, covered a measured burnup range between 2.9x10^{21} and 4.1x10^{21} f/cm^3, and a temperature range from 50 to 300 ^{o}C. The more recent data provided in references [29] and [51] for some of the same samples from the AFIP-2 experiment, plus an additional sample from AFIP-3, cover a calculated burnup range from 3.3x10^{21} to 4.5x10^{21} f/cm^3, and a temperature range from 50 to 350 ^{o}C. It is noted that the calculated burnups of the samples are 10% to 14% higher than the measured burnup values. Clarification of the source of this discrepancy is needed. The thermal conductivity of a sample from the AFIP-6MkI experiment with a calculated burnup of 2.45x10^{21} f/cm^3 was also measured and reported, but the results for that sample are not considered reliable because the experiment blistered in-pile during irradiation, as discussed in Section 2.5.2. Additionally, thermal conductivity measurements for unirradiated U-10Mo for temperatures ranging from room temperature to more than 600 ^{o}C have been collected, although the measurements conducted by Burkes and used to prepare equation 2.26 were for material that is not prototypic.

Figure 2.18 shows the range of available thermal conductivity data (blue boxes in the figure) alongside the results of the calculated peak U-10Mo fuel temperature from accident analyses for MITR [52], MURR [4], and NBSR [24]. It can be seen that, for a significant number of cases for these reactors, the peak fuel temperature occurs at fuel burnups that are outside the range of data which have been collected to date for U-10Mo. Additionally, a recent characterization of available thermal conductivity data conducted in reference [53] concluded that the limiting cases for ATR-LEU safety analyses will likely be for U-10Mo fuel in two burnup regions of interest: from $2.0x10^{21}$ to $2.5x10^{21}$ f/cm^3 (for a so-called high-power case) and > $5.0x10^{21}$ f/cm^3 (for a so-called low-power case). These burnup ranges also fall outside of the range of currently available data for thermal conductivity of U-10Mo. It is noted that the analysis performed in reference [53] utilized a correlation for thermal conductivity that is based on the data in reference [51], but the correlation itself is not included in reference [53].

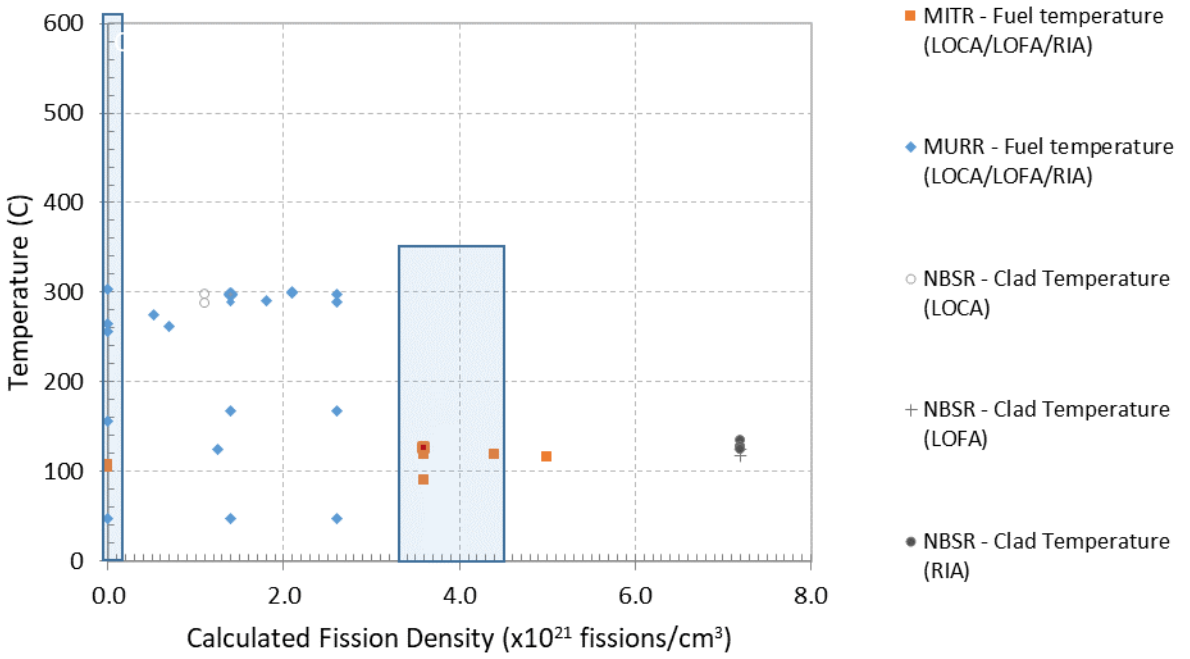

Figure 2.18. Range of Data Measurements for U-10Mo Thermal Conductivity Displayed with Results of Accident Analyses for MITR, MURR, and NBSR.

Consequently, data measurements of the thermal conductivity for fresh prototypic material, and prototypic material at intermediate burnups ($1.4x10^{21}$ to $3.3x10^{21}$ f/cm^3) and higher burnups ($4.5x10^{21}$ to $7.2x10^{21}$ f/cm^3) are needed. The intermediate burnup data will be particularly useful for evaluating the safety of all end-of-life fuel in MURR and middle-of-life fuel in all reactors. The higher burnup data are needed for evaluating end-of-life ATR and NBSR elements. It is imperative that these new thermal conductivity measurements be taken from prototypic material. Furthermore, measurements for fresh and irradiated material made with the same measurement techniques and equipment would be extremely valuable in developing a single combined correlation for thermal conductivity that encompasses a range of fission densities from fresh fuel through end of life. Lastly, improved consistency between the calculated and measured fission densities of irradiated samples, or clarification of any differences between the calculated and measured fission density, is needed.

2.7 Yield Strength of U-10Mo Fuel

A correlation for yield strength is given in the Preliminary UMo Report [1] for both fresh and irradiated fuel, but of all the USHPRR, only HFIR [3] mentions yield strength, and only a value for a single temperature for fresh fuel is given. Therefore, a discussion of this material property is not included in this report.

2.8 Elastic Modulus of U-10Mo Monolithic Fuel

Two groups of data for elastic modulus of U-10Mo exist in the literature. The early group before 1974 [54,55,56], and a more recent group [57,58]. Factors affecting the elastic modulus include the specimen preparation process, heat treatment, test temperature, carbon content, and strain rate. At room temperature, elastic modulus for U-10Mo found in the literature ranges from 70 – 91 GPa. The lowest value is by Burkes (70 GPa), which is the latest measurement and using specimens representative of the real fuel of interest.

2.8.1 Temperature Dependence of U-10Mo Elastic Modulus

The temperature dependence of elastic modulus is recorded by Schulthess [58], as shown in Table 2.2.

Table 2.2. Temperature dependence of elastic modulus of U-10Mo.

Temperature (°C)	Modulus (GPa)	± Standard Deviation (GPa)
20	88.421	1.3150
200-250	41.763	1.6810
350	42.225	1.4750
400-450	32.043	1.7880
550	19.929	2.4410

Using these data, but excluding the data set at 200-250°C as an outlier and using 425°C as a temperature for the 400-450°C data set, a data fit was obtained as follows:

$$E_{U10Mo} = 90.0 - 0.13T \quad (2.35)$$

where E is in GPa and T is in °C. This equation is recommended for use with caution, as it is based on a single set of data.

The elastic modulus of U-10Mo has been dealt with only in the HFIR report [3], where a single data point is used at operating temperature.

The Preliminary UMo Report bases a recommended correlation, shown in equation 2.36, on the same set of data as was used to develop equation 2.35.

$$\mathrm{E} = 91.2 - 0.140 \times \mathrm{T}, \mathrm{T} = 21 - 550\text{°C} \quad (2.36)$$

However, due to uncertainties in how the data should be interpreted, there is a difference in the linear fit recommended in the Preliminary UMo Report compared to equation 2.35. As shown in Table 2.2, one of the data points used for the fits was listed as a range of temperatures, rather than being collected at a single temperature value. In Figure 2.19, the recommended correlation from the Preliminary UMo Report is plotted with the original data set, equation 2.35, and the value used in HFIR analyses (the only USHPRR to explicitly discuss the Young's Modulus of the fuel) for an operation temperature of 140°C.

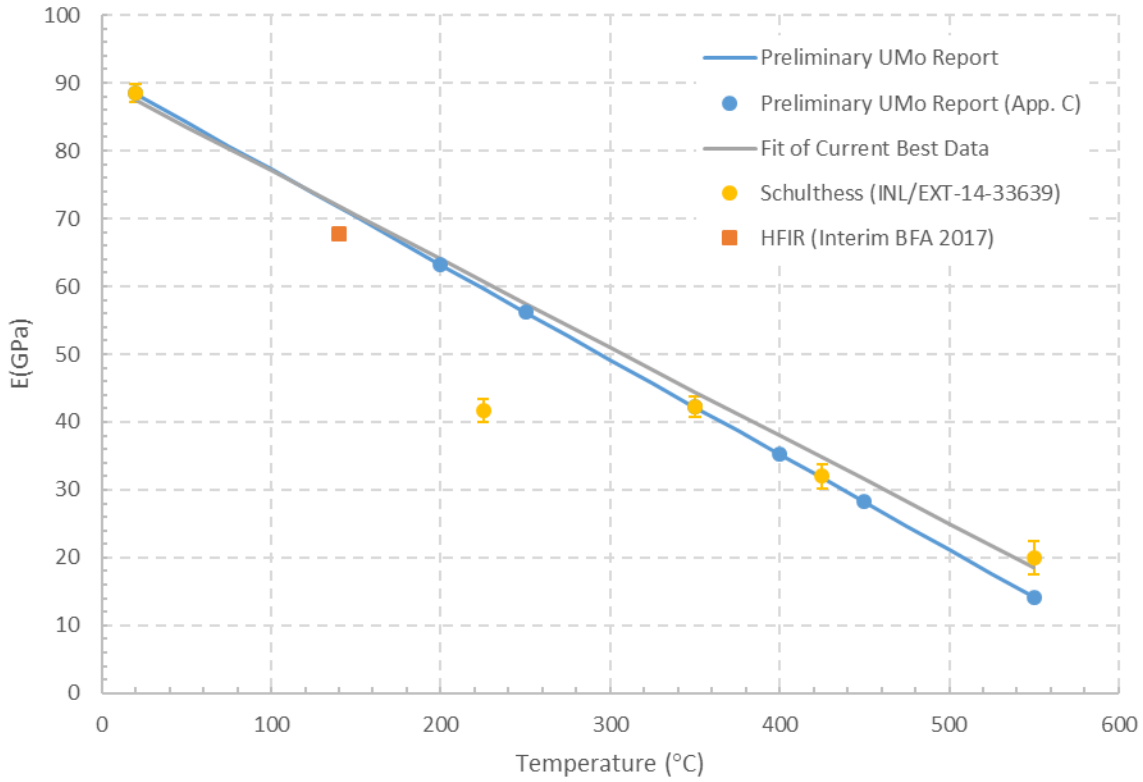

Figure 2.19. Comparison of the Preliminary UMo Report [1], fit of current best data (equation 2.35), the current best data set [58], and the value utilized for HFIR analyses [3] for U-10Mo Young's Modulus.

2.8.2 Irradiation Dependence of U-10Mo Elastic Modulus

Irradiation causes the elastic modulus to decrease, as has been reported in literature [59,60] and tabulated in Appendix C. Both of the literature references report data from the same set of samples, with [59] reporting slightly higher values. As [60] is available in the open literature, the data reported there were used to develop a linear fit, as follows.

$$E_{U10Mo} = 89.8 - 5.2 f_d \qquad (2.37)$$

where E is in GPa and f_d is fission density in $x10^{21}$ f/cm^3. The exact temperature of the irradiated bend test samples is difficult to quantify, as discussed in [59]. They are at least 30°C (the ambient temperature of the hot cell), and are likely 10-40°C higher than that due to gamma heating. This equation should be used with caution, as it is based on a single set of data. It is recommended to collect additional data on the mechanical behavior of U-10Mo fuel, in particular the yield strength and Young's modulus, on both as-fabricated and irradiated prototypic fuel.

The Preliminary UMo Report recommends a set of equations (equation 2.38), where the irradiation dependence of the Young's Modulus at elevated temperatures are approximated from the unirradiated trend. Data on the Young's Modulus of irradiated U-10Mo has only been collected at ambient temperature.

$$\mathrm{E} = \begin{Bmatrix} 78.469 - 4.076 \times f_d & at\ 21°C \\ 56.108 - 2.914 \times f_d & at\ 200°C \\ 49.897 - 2.592 \times f_d & at\ 250°C \\ 37.474 - 1.947 \times f_d & at\ 350°C \\ 31.263 - 1.624 \times f_d & at\ 400°C \\ 25.052 - 1.301 \times f_d & at\ 450°C \\ 12.629 - 0.656 \times f_d & at\ 550°C \end{Bmatrix} \quad (2.38)$$

HFIR is the only USHPRR to directly discuss the degradation of the Modulus of U-10Mo fuel with irradiation. It is recommended in the Interim BFA [3] to reduce the Modulus by 5.4 GPa per 10^{21} fissions/cm^3, starting from a fresh fuel Modulus of 67.75 GPa. This assumption is compared to equations 2.37 and 2.38, as well as the recommended fresh fuel values from Table C11 of the Preliminary UMo report, in Figure 2.20. Although not explicitly stated, the correlation is not plotted lower than 0.5 x10^{21} f/cm^3 in the Preliminary UMo Report, so it is assumed that the correlation is not to be extended to lower fission densities. The correlation for HFIR is reasonably consistent with the correlation from the Preliminary UMo Report in the applicable temperature range (21°C - 200°C).

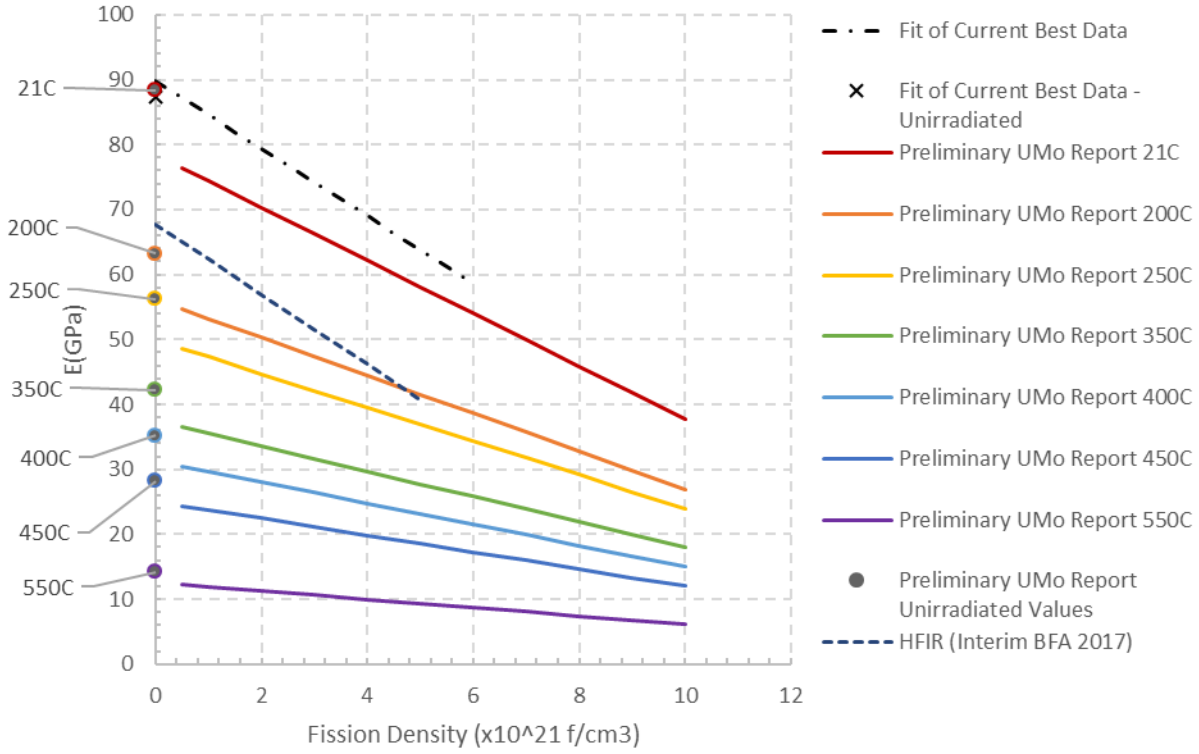

Figure 2.20. Comparison of the degradation of Elastic Modulus with irradiation recommended by HFIR, the Preliminary UMo Report, and the fit of current best data (equation 2.37). The temperatures at which the unirradiated moduli were determined are marked along the y-axis.

The values for the irradiated correlations (equations 2.38 and 2.39) have discontinuities between the irradiated correlation and the calculated unirradiated value at the same temperature, although that discontinuity is larger for equation 2.39. A combined correlation unifying the irradiated and unirradiated correlations is currently being developed by the US Fuel Qualification Pillar. Additionally, because the data on which the correlations in this section were based were collected on material from a single experiment, it is recommended to collect an additional set of confirmatory data.

2.8.3 Discussion of the Assumptions of the U-10Mo Modulus for the USHPRR

As the MURR LEU fuel element design contains the thinnest and widest plates amongst the USHPRR, it serves as an important case for assessing mechanical stability under flow conditions. In work on plate deformation for the MURR fuel element, an aluminum system was studied through experiments and modeling [61]. In this study, the AA6061 modulus was used to simulate the experiments, and likewise for assessing whether a MURR LEU fuel plate would significantly deform under flow conditions as described in Section 3.1.4 (the AA6061 modulus was used for the fuel as well). Noting that the effect of irradiation on mechanical properties is to degrade the U-10Mo modulus, for MURR, where fission densities peak at 3.4×10^{21} f/cm^3, equation 2.37 evaluates to 72.2 GPa. This is substantially higher than the aluminum modulus used in the MURR modeling, discussed in Section 3.1.4, and so it would remain conservative and reasonable to assume AA6061 properties in lieu of fresh or irradiated U-10Mo properties. Even if the modulus of the fuel were to degrade substantially, the impact on the fuel plate is expected to remain small. A simulation carried out using the methodology employed for the MURR model showed a small plate deflection of about 10%. Thus, a 0.5 μm increase vs. the 5 μm original deflection was found when the modulus was artificially lowered by a factor of 100. The quite small impact is expected since the moment of inertia of the plate is dominated by the AA6061 cladding, and the fuel inside the plate is not as consequential. This is similar to the structural benefits of an I-beam.

2.9 Poisson's Ratio of U-10Mo Fuel

A Poisson's ratio for U-10Mo of 0.35 was utilized by Ozaltun [62], based on data from Waldron [56]. The Preliminary UMo Report [1] recommends a Poisson's ratio of 0.41 based on a report by Reese [63]. A Poisson's ratio of 0.3 has been used in mechanical modeling of the fuel [59], so it is recommended to continue to use 0.35 for analyses, as was done for HFIR [3] (the only USHPRR to explicitly discuss the Poisson's Ratio of the fuel).

3 Material Properties of the AA6061, Oxide Layer, and Zr Interlayer

This section discusses the material properties of the cladding, aluminum-oxide layer, and zirconium interlayer. The material properties of interest related to the AA6061 cladding material are: density, thermal expansion, heat capacity, thermal conductivity, Young's modulus, and Poisson's ratio. The properties of interest related to the oxide are: density, heat capacity, and thermal conductivity. The zirconium interlayer properties of interest are: density, thermal expansion, heat capacity, and thermal conductivity. The Preliminary UMo Report is used as a reference point for the assumptions used in the USHPRR analyses, where applicable.

3.1 AA6061 Cladding

The cladding material selected for U-10Mo monolithic fuel plates is AA6061, for which the nominal composition is: Si (0.4 - 0.8 wt%), Fe (0.7 wt% max.), Cu (0.15 - 0.4 wt%), Mn (0.15 wt% max), Mg (0.8 – 1.2 wt%), Cr (0.04 – 0.35 wt%), Zn (0.25 wt% max.), Ti (0.15 wt% max.), unspecified other elements (0.05 wt% max. each and 0.15 wt% total max.), with Al as the remainder [64].

The as-received cladding for the fabrication of the U-10Mo fuel plates is AA6061-T6, but the hot isostatic press (HIP) fabrication step results in properties closer to the AA6061-O temper [65]. Neutron irradiation causes radiation hardening of the cladding, which may be non-uniform due to the neutron flux profile. AA6061-T6 properties will be utilized in this report, where the temper is specified. There is ongoing work to evaluate the effect of the variation in physical, thermal, and mechanical properties of the AA6061 cladding on the thermo-mechanical behavior of U-10Mo monolithic fuel plates via numerical simulations.

3.1.1 Density and Thermal Expansion of AA6061

The density of AA6061 alloy at 20°C is ρ_0=2.70 g/cm^3 [66]. The density at temperatures other than room temperature is estimated by applying the thermal expansion data as shown in equation 3.1 [67].

$$\rho = \frac{1}{(1 + \Delta T \overline{\alpha}_l)^3} \rho_0 \tag{3.1}$$

where $\Delta T = T\text{-}T_0$ where 0 stands for room temperature, $\overline{\alpha}_l$ is the mean linear thermal expansion coefficient, as defined in equation 3.1, ρ_0 is the density of Al at room temperature, and T is in K.

$$\overline{\alpha}_l = \frac{1}{T - T_0} \int_{T_0}^{T} \alpha_l \, dT \tag{3.2}$$

Using equation 3.2 and the data obtained from MIL-HDBK-5H [70], the mean coefficient of linear thermal expansion (CTE) of AA6061 at several temperatures were obtained and provided in Table 3.1, where the instantaneous coefficient of linear thermal expansion for pure Al is also listed for reference.

Table 3.1. Instantaneous and mean linear thermal expansion coefficient of AA6061 based on data from [70].

T (°C)	α_l (x10^{-6}K^{-1}) for pure Al [44]	α_l (x10^{-6}K^{-1})	$\bar{\alpha}_l$ (x10^{-6}K^{-1})
25	23.1	22.7	22.7
127	25.1	23.7	23.2
227	26.4	24.7	23.7
327	28.4	25.7	24.2
427	30.9	26.6	24.7
527	34	27.6	25.2
627	37.4	28.6	25.7

For convenience, a linear fit of the data for instantaneous coefficient of thermal expansion obtained from MIL-HDBK-5H [70], as developed in [67] is as follows:

$$CTE_{AA6061} = 1.99 \times 10^{-5} + 9.6 \times 10^{-9}T \qquad (3.3)$$

where temperature (T) is in °C.

For the entire temperature range in Table 3.1 (298 – 900K), the variation in density is only 4.5%. Hence, the reduction of density at elevated temperatures may not need to be considered.

3.1.1.1 Comparison of the AA6061 CTE to the Preliminary UMo Report

The Preliminary UMo Report [1] utilizes the density of pure aluminum (2.702 g/cm^3), as it is essentially the same as the density of AA6061. The Preliminary UMo Report also states to use the coefficient of thermal expansion (CTE) to calculate the density at temperatures greater than room temperature, and although several correlations and data sets of AA6061 CTE were introduced in the body of the report, there was no specific recommendation given. A set of tabulated data is recommended in Appendix C, which, from a comparison to the references in the body of the report, is from [69]. A comparison of the values recommended in Appendix C of the Preliminary UMo Report and the correlation recommended here (equation 3.3) is shown in Figure 3.1. Although different references are cited, there is excellent agreement.

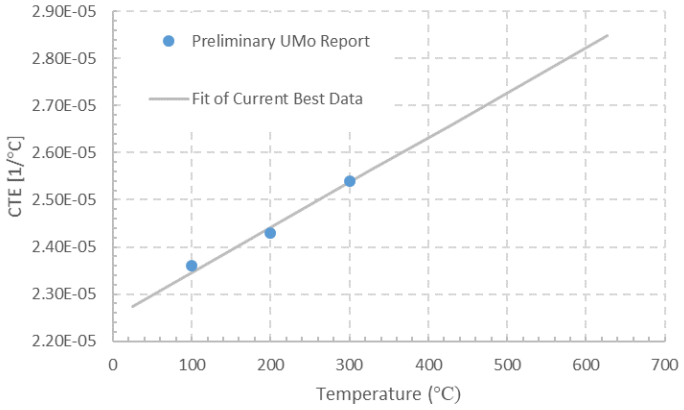

Figure 3.1. Comparison of the coefficient of thermal expansion (CTE) of AA6061 recommended by the Preliminary UMo Report [1] and the fit of current best data (equation 3.3).

3.1.1.2 Comparison of AA6061 Densities Used for Analyses for the USHPRR

Reports for MURR [4], MITR [6], and NBSR [35] use ρ_0=2.7 g/cm^3 for the density of AA6061 for all temperatures. Analyses for ATR also do not take the thermal expansion effects into account, and used an aluminum density of 2.647 g/cm^3, which is conservative relative to the recommended density of 2.7 g/cm^3. Because of the minimal change in density over the temperature range examined, disregarding the impact of temperature on density is reasonable. The report for HFIR [3] does consider the temperature effect, and uses thermal expansion to estimate density at temperatures other than room temperature using equation 3.1. The average thermal expansion coefficient of 24.2x10^{-6} K^{-1} is used for this calculation, which is the average of the instantaneous coefficient of linear thermal expansion of pure Al between 293 and 400K. This is a higher value than recommended by the Preliminary UMo Report [1] or determined by the fit of current best data, as shown in Figure 3.2. However, this difference in CTE has a minimal impact on the calculated density, so it is considered to be a reasonable assumption.

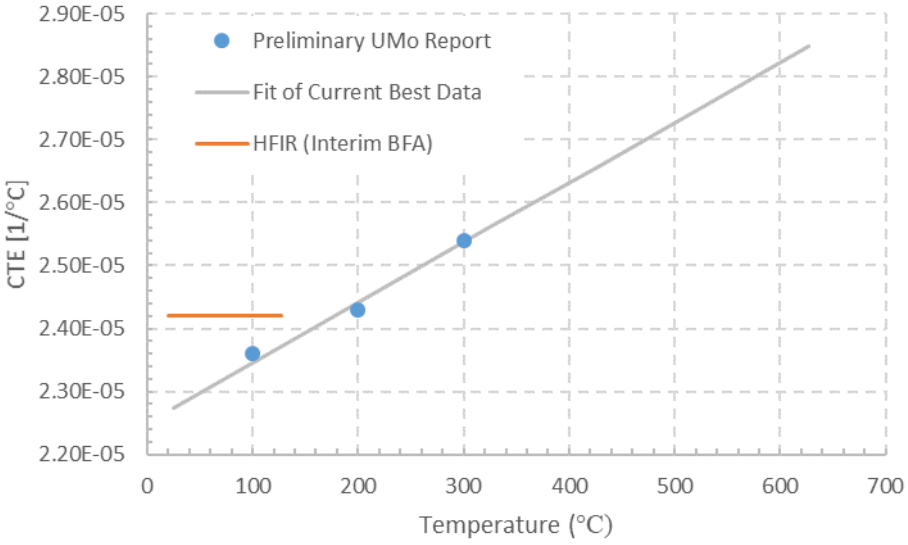

Figure 3.2. Comparison of the CTE assumed by analyses for HFIR [3], the Preliminary UMo Report [1], and the fit of current best data (equation 3.3)

3.1.2 Melting Temperature of AA6061

The solidus of AA6061 is 582°C and the liquidus is 652°C [66]. The same values are recommended by the Preliminary UMo Report in Appendix C [1] and used for analyses of the ATR [7]. It is worth noting that ATR is the only USHPRR to explicitly discuss the melting temperature of the cladding.

3.1.3 Heat Capacity of AA6061

A correlation of the heat capacity of AA6061 is found in the report [67] and is shown in equation 3.4, which was developed using data from [70].

$$c_p = 0.324 + 2.93 \times 10^{-3}T - 4.34 \times 10^{-6}T^2 + 2.42 \times 10^{-9}T^3 \quad (3.4)$$

where c_p is in J/(g K) and T is in K in the range of 298 ≤ T ≤ 811 K.

3.1.3.1 Comparison to the AA6061 Heat Capacity Recommended in the Preliminary UMo Report

The Preliminary UMo Report [1] recommends a data set from Polkinghorne in Appendix C. These values are compared to the fit of current best data (equation 3.4) in Figure 3.3. The Preliminary UMo Report [1] includes data up to, and beyond, the solidus temperature of AA6061 (582°C) and beyond the recommended temperature regime for equation 3.4.

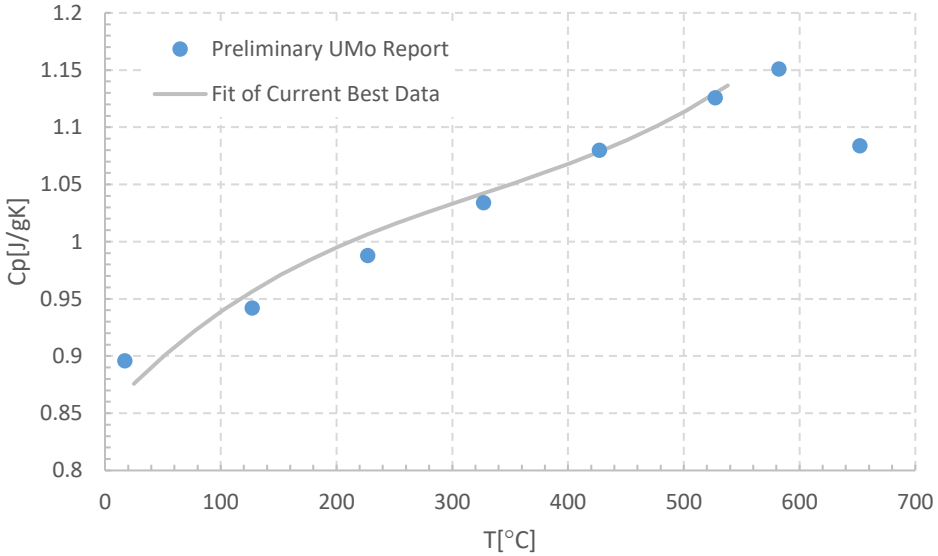

Figure 3.3. Comparison of the data set recommended by the Preliminary UMo Report and the fit of current best data (equation 3.4) for the specific heat of AA6061.

3.1.3.2 Comparison to the AA6061 Heat Capacity Recommended in Analyses for the USHPRR

Heat capacity is presented analyses for MURR [4] as follows:

$$\rho c_p = 4.252 \times 10^6 - 2.685 \times 10^3 (T + 273.15) + 2.214 (T + 273.15)^2 - 3.774 \times 10^8 (T + 273.15)^{-1} \quad (3.5)$$

where the unit of the correlation is in J/(m^3 K) and T is temperature in ^{o}C. The same correlation is recommended for analyses of MITR [6].

The HFIR report [3] uses the following expression for the heat capacity of AA6061, using the data from [70].

$$c_p = 0.324 + 2.93 \times 10^{-3} T - 4.34 \times 10^{-6} T^2 + 2.42 \times 10^{-9} T^3 \quad (3.6)$$

where T is the temperature in K in the range of 298–811 K, c_p in J/(g K).

Analyses for ATR uses tabulated data from Polkinghorne [69] with an assumed standard deviation of ±3%. There is a discrepancy between the data values used for the analyses for ATR and the Preliminary UMo Report, although the same data source is cited. Reference [7] listed the values in BTU/in^{3}F, so conversion to J/gK for comparison was needed. The density value used for this

conversion was 2.647g/cc, as used in the analyses for ATR [7]. If a density of 2.7 g/cc is used for this conversion, one obtains the same values as reported in the Preliminary UMo Report. Analyses for NBSR [5,35] assume a constant specific heat (0.896 J/(g K)), approximately equal to the 50°C value from the other correlations and tabulated values. The correlations and values used for analyses are compared to the recommendation by the Preliminary UMo report [1] in Figure 3.4. The correlation used for analyses of MURR [4] was converted from a ρc_p term to c_p assuming a density of 2.7 g/cm^3 to allow direct comparison.

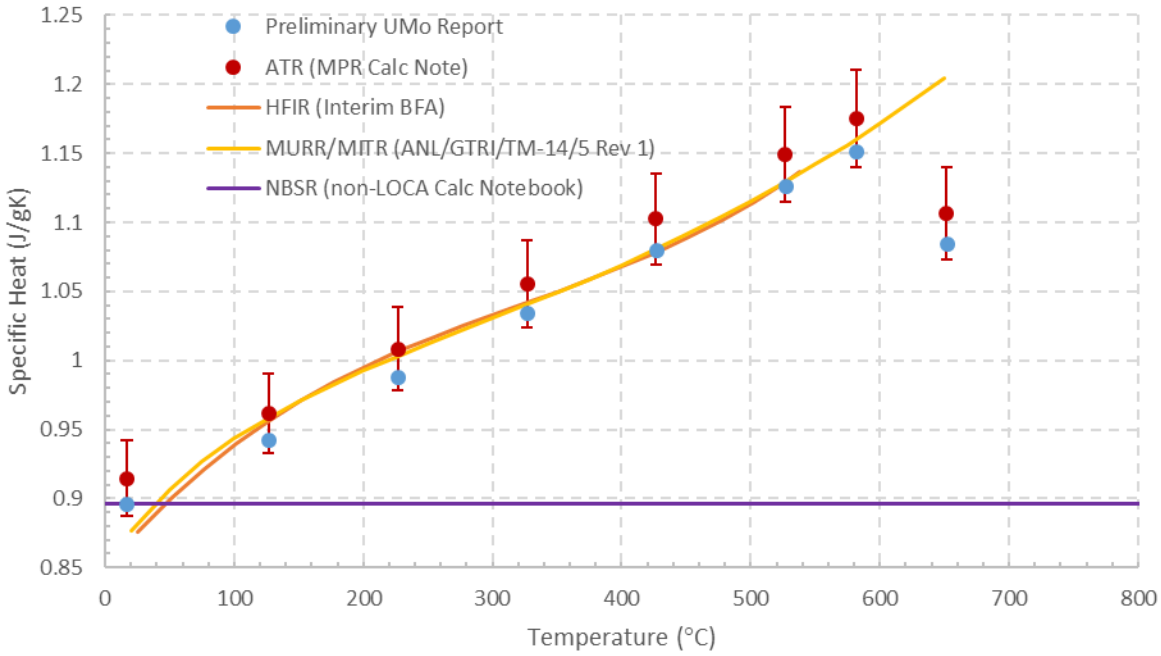

Figure 3.4. Comparison of the specific heat capacities used for analyses of the USHPRR and the recommended values from the Preliminary UMo Report [1].

All correlations and values are approximately consistent, with the exception of NBSR [5], which is conservative compared to the correlations and data used by the other USHPRR, as well as the recommended correlation, equation 3.4.

3.1.4 Thermal Conductivity of AA6061

The thermal conductivity of AA6061 is found in a report [67], which is a fit based on the data from [70], as found below:

$$k = 106 + 0.149T + 8.47 \times 10^{-5}T^2 - 2.14 \times 10^{-7}T^3 \qquad (3.7)$$

where k is in W/(m K) and T is in K in the range of 298 ≤ T ≤ 800 K.

3.1.4.1 Comparison of the Recommended Thermal Conductivity of AA6061

The Preliminary UMo Report [1] recommends tabulated data from [69] in Appendix C. This data is compared to the recommended correlation (equation 3.7) in Figure 3.5.

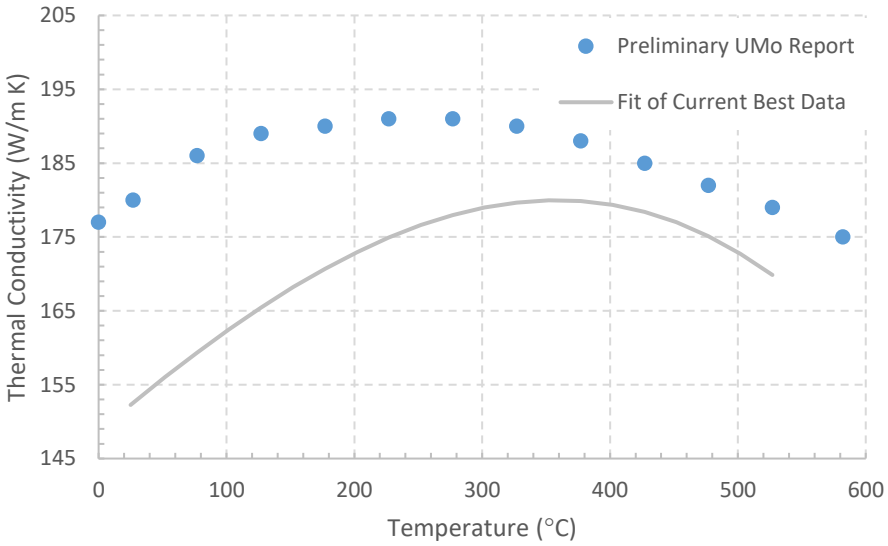

Figure 3.5. Comparison of the recommended values for AA6061 thermal conductivity in Appendix C of the Preliminary UMo Report [1] to the fit of current best data (equation 3.7).

The recommended correlation is significantly lower than the values recommended by the Preliminary UMo Report [1]. The Preliminary UMo Report data is from reference [69], where the O temper of AA6061 is recommended, compared to AA6061-T6 in reference [68]. The impact of the difference in thermal conductivity of AA6061 is minimal because the temperature change across the cladding is minimal with thermal conductivities in this range.

3.1.4.2 Comparison of Correlations Used by the USHPRR for the Thermal Conductivity of AA6061

Analyses for MURR [4] and MITR [6] use the same correlation for the thermal conductivity of AA6061, shown in equation 3.8.

$$k = 147.8 + 0.1792T - 2.616 \times 10^{-4}T^2 \qquad (3.8)$$

where T is in °C.

The correlation used in the HFIR report [3] is identical to equation 3.7. Tabulated values were used for analyses for ATR, and a constant thermal conductivity of 180 W/(m K) was assumed for analyses of NBSR. A comparison of these correlations and values, in addition to the recommended values from the Preliminary UMo Report is shown in Figure 3.6.

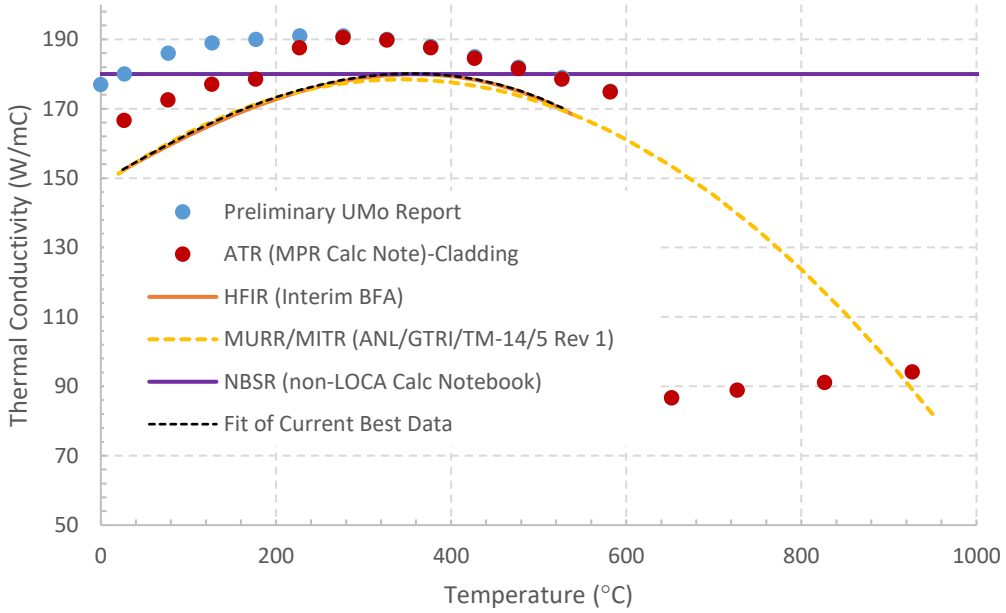

Figure 3.6. Comparison of correlations and values used for the thermal conductivity of AA6062 in analyses of the USHPRR the values recommended by the Preliminary UMo Report, and the recommended fit of current best data (equation 3.7).

All assumptions by the USHPRR in the temperature ranges for steady-state and accident analyses that are relevant for each reactor are equal to or conservative compared to the recommended values from the Preliminary UMo Report. It is noted that for NBSR a constant value for the thermal conductivity of AA6061 is assumed, which is non-conservative relative to the Preliminary UMo Report for temperatures above ~525 C. However, in no case is the calculated cladding temperature greater than ~300C.

3.1.5 Young's Modulus and Poisson's Ratio of AA6061

Data for tensile properties of AA6061 are found in the literature [70,71,72]. A fit of the data from [70], [71] and the data measured with the static method from [72], a correlation for the Young's Modulus of AA6061 is obtained as:

$$E_{AA6061} = 54.9 + 1.07 \times 10^{-1}T - 2.03 \times 10^{-4}T^2 \qquad (3.9)$$

where the temperature, T, is in K, as developed in [67].

Poisson's ratio of AA6061 is 0.33 [68].

3.1.5.1 Comparison to the Young's Modulus of AA6061 Recommended by the Preliminary UMo Report

The Preliminary UMo Report recommends tabulated values for the Young's Modulus of AA6061, rather than a correlation. The tabulated values recommended by the Preliminary UMo Report are compared to the recommended correlation discussed here (equation 3.9) in Figure 3.7.

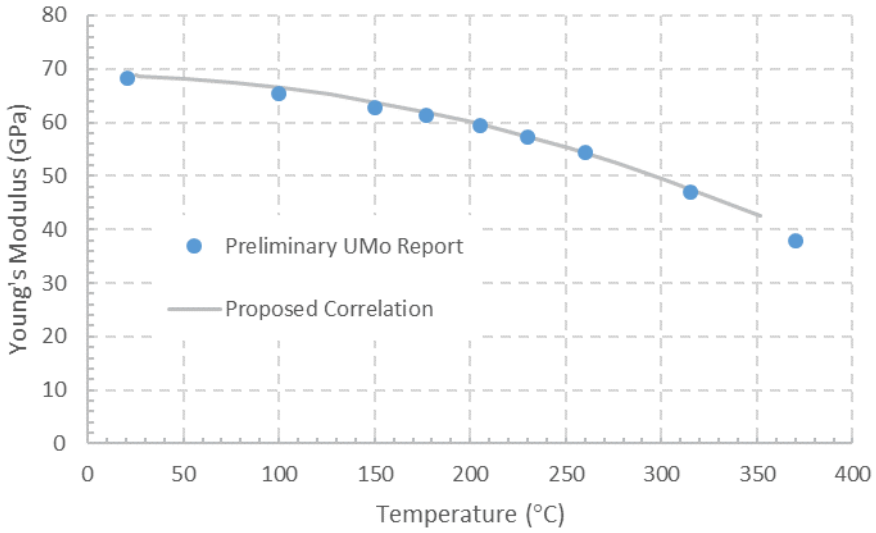

Figure 3.7. Comparison of the recommendations for the Young's Modulus of AA6061 in the Preliminary UMo Report and equation 3.9**.**

The recommended correlation (equation 3.9) is in good agreement with the data set recommended in Appendix C of the Preliminary UMo Report.

3.1.5.2 Comparison to the Poisson's Ratio of AA6061 Recommended by the Preliminary UMo Report

The Preliminary UMo Report recommends a tabulated set of data for the Poisson's ratio in Appendix C, shown in Table 3.2. There is no reference for this data set.

Table 3.2. Recommended Poisson's Ratio Values from Appendix C (Table C-31) of the Preliminary UMo Report.

Temperature (°C)	Poisson's Ratio
21	0.33
25	0.33
100	0.33
149	0.34
204	0.34
260	0.34
316	0.36
371	0.4

The values recommended in the Preliminary UMo Report are in reasonable agreement with the constant value of 0.33 recommended here, up to temperatures of ~300°C.

3.1.5.3 Comparison of the Young's Modulus of AA6061 Used for Analyses of the USHPRR

Significant mechanical deflection analysis has been done regarding MURR. Analysis has investigated the fuel plate deformation under differential hydraulic pressures arising from flow channel differences [61]. The assumed mechanical properties AA6061 were a Young's Modulus of 68.0 GPa and a Poisson's Ratio of 0.33 [61]. This is in agreement with an evaluation of equation 3.9 at 60 °C. Given available literature data, the property values used for MURR are reasonable. In this report [61]

MURR LEU plates are thinner than the HEU plates, and are, at 44 mil thick, the thinnest among the USHPRR reactors. As the MURR LEU fuel element design contains the thinnest and widest plates amongst the USHPRR, it serves as an important case for mechanical stability under flow conditions. Despite thinner plates, the predicted maximum plate deflection is very small at approximately 5 μm, so sensitivity to assumptions of the mechanical properties is not consequential.

A report for the analyses of HFIR [3] uses the correlation shown in equation 3.9, the only USHPRR to explicitly discuss the Young's Modulus of AA6061 within the reports on the safety analyses conducted.

3.1.6 Yield Strength of AA6061

Tabulated data [65,73] for the yield strength of HIP-processed AA6061 cladding was presented in the Preliminary UMo Report [1]. Because this data is limited to room temperature evaluation, it is recommended to use O-temper AA6061 as a reasonable approximation for HIP-processed AA6061 [1,73]. Of the USHPRR, a report for HFIR [3] is the only one that explicitly addresses the yield strength of unirradiated AA6061 at room temperature, which is in agreement with the Preliminary UMo Report [1].

Limited data for the yield strength of irradiated AA6061 is available [74], and in addition to the Preliminary UMo Report [1], only a report for HFIR [3] explicitly discusses the yield strength of irradiated AA6061.

3.1.7 Creep Behavior of AA6061

Data for irradiation-induced creep of AA6061 are available in the literature. Jeong et al. [75] estimated that the fission-induced creep rate of aluminum was an order of magnitude lower than that of U-10Mo. However, because the thickness of the Zr interlayer is much larger than the recoil ranges of fission fragments, no fission-induced creep is possible in the cladding. Neutron-induced creep is typically an order of magnitude lower than that by fission [76]. Therefore, the irradiation-induced creep of AA6061 cladding is considered negligible.

Thermal creep of AA6061 need not be considered because it is negligible at the low reactor operation temperatures [77]. The Preliminary UMo Report includes tabulated data for thermal creep from ASM [66] in Appendix C.

3.1.8 Swelling of AA6061

Swelling of AA6061 under irradiation is minimal for the neutron fluences relevant to the USHPRR [74], as shown by the data recommended in the Preliminary UMo Report [1] and discussed by a report for HFIR [3]. The other USHPRR do not explicitly address the irradiation swelling of AA6061.

3.1.9 Irradiation Hardening of AA6061

Limited data on the irradiation hardening of AA6061 is avaialble from Farrell [74,78]. In [74], data is presented on the hardening of AA6061-O temper due to irradiation, representative of the as-fabricated state of the cladding, as discussed in [65]. A linear fit of the data was presented in Figure 6 of [74], and the line was digitally extracted and determined to be:

$$UTS = 4.18 \ln(f) - 211.56 \quad (3.10)$$

Where UTS is the ultimate tensile strength in ksi, the fast neutron (E > 0.1 MeV) fluence (f) is in n/m^2, and the temperature is 50°C.

The Preliminary UMo Report displays figures from [74], and extracts the yield strength at 3 fluences, rather than reporting a correlation. Stress-strain curves from [78] were also presented in the Preliminary UMo Report, including a recommended data set in Appendix C, without recommending a specific yield strength or UTS. If the UTS is required for analysis, it is recommended to use the correlation presented in equation 3.10.

3.2 Oxide Layer

Aluminum alloys undergo oxidation in air even at room temperature, producing a protective oxide (Al_2O_3). The protective oxide, however, degrades in water by the formation of various oxide-hydrates at the outer surface over time, leaving only a thin (~0.01 μm) protective Al_2O_3 layer on the substrate. The most frequently found oxide-hydrates in typical conditions are boehmite ($Al_2O_3.H_2O$) and bayerite ($Al_2O_3.3H_2O$) [79]. The dominant between these two is boehmite, with bayerite found on the outer surface of the boehmite layer. The term "oxide thickness" generally refers to the total thickness of the layers of the protective oxide (Al_2O_3) and hydrated oxides ($Al_2O_3.H_2O$ and $Al_2O_3.3H_2O$). However, because boehmite dominates the oxide layer, the properties of boehmite are the most representative of the oxide layer.

3.2.1 Oxide Density

The density of the oxide (boehmite) is available in the literature as 3.02 g/cm^3 [80], as was accepted by Griess [81], a common reference for the density of boehmite. However, the measured data range is was more reccently reported to be 3.02-3.05 g/cm^3, with a theoretical density of 3.08 g/cm^3 [82].

The average of the measured data range, 3.03 g/cm^3, is recommended.

The Preliminary UMo Report [1] recommends a density of 3.01 g/cm^3 [83], based on an older reference [84], while analyses for HFIR [3] reference a range of oxide densities (3.0-3.07 g/cm^3), as compared in Figure 3.8. The other USHPRR do not explicitly discuss the oxide density.

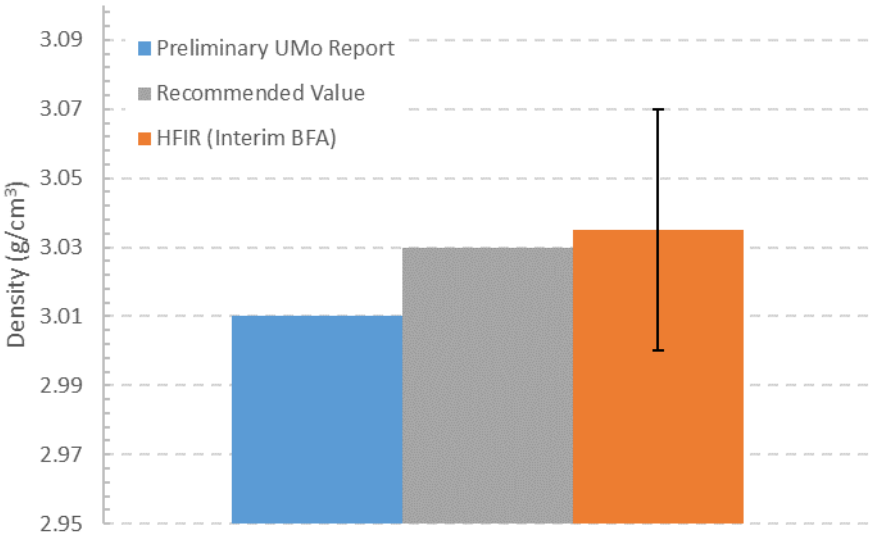

Figure 3.8. Comparison of the oxide densities recommended by the Preliminary UMo Report [1], the HFIR Interim BFA [3], and this report

The values recommended by the Preliminary UMo Report [1] and the value recommended by this report fall within the general experimental range for density of the oxide, so either value would be reasonable for use.

3.2.2 Oxide Heat Capacity

Heat capacity of boehmite is reported by Hemingway et al. [85]. A fit to his data results in:

$$c_p = 3.4043 \times 10^{-3} + 3.83 \times 10^{-3} T - 2.694 \times 10^{-6} T^2 \quad (3.11)$$

where c_p is in J/(g K) and T is in K.

3.2.2.1 Comparison of the Heat Capacity of the Oxide to the Preliminary UMo Report

The Preliminary UMo Report [1] recommends the equation below in the body of the report, from Polkinghorne [69]

$$c_p = 937.3 + 1.382 \times T - \frac{2.267 \times 10^7}{T^2} \quad (3.12)$$

where c_p is in J/kg-K and T is the temperature up to 600K. The appendix recommends values extrapolated from this equation up to temperatures of 1200K.

A comparison of the correlation recommended by the Preliminary UMo Report [1], the values recommended in Appendix C of the Preliminary UMo Report, and the correlation recommended here is shown in Figure 3.9.

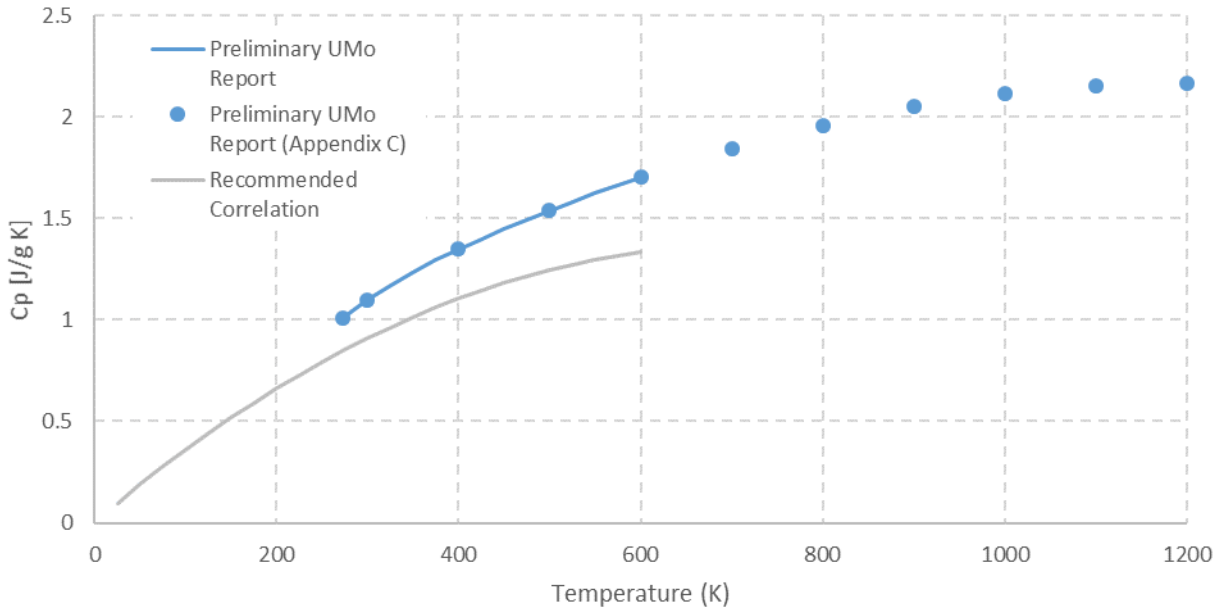

Figure 3.9. Comparison of the recommended correlation and values from the Preliminary UMo Report [1] and the correlation recommended here (equation 3.11).

The c_p recommended by the Preliminary UMo Report [1] is consistently higher than that from equation 3.11. The citation for the c_p equation in the Preliminary UMo Report is Polkinghorne [69], which sources [83]. Wefers produced the sample measured in the more recent Hemingway report [85]. Differences in the heat capacity could be due to slight differences in the composition, which can impact the thermophysical properties of the aluminum oxide, as discussed in [85]. Because both are significantly higher than the value used for analyses of the USHPRR (discussed in the next section), either correlation is acceptable if re-analysis is required, although equation 3.11 is recommended. The exact composition of the oxide layer can vary due to differences in the reactor conditions (such as coolant pH), so the more conservative equation 3.11 is recommended.

3.2.2.2 Comparison of the Oxide Specific Heat Used for USHPRR Analyses

A report for MURR [4] uses a value of $\rho \cdot c_p = 1.0$ J/(m^3 K) for boehmite. When this number is converted to c_p, 0.33×10^{-6} J/(g K) is obtained. This value is six orders of magnitude lower than the 0.905 J/(g K) value at 25 °C computed using equation 3.11. However, this value was justified because it is more conservative, and the effect of the presence of oxide in the safety analysis was negligible. It has been suggested that MITR [6] use the same value for heat capacity. The specific heat capacity was not explicitly discussed in analyses for the rest of the USHPRR.

3.2.3 Oxide Thermal Conductivity

Thermal conductivity of boehmite was reported in [86] as 2.25 W/(m K), in agreement with [69], cited in the Preliminary UMo Report. The thermal conductivity measurements were done on wet boehmite samples, which includes inherent porosity. As these measurements were done on samples generated in an out-of-pile test, the porosity may have been lower than in-pile materials. A discussion on the impact of porosity on the properties of the oxide layer will be incorporated in the next revision of this report.

Reports for MURR [4], MITR [6], and ATR [7] all use this value for the thermal conductivity of boehmite. The thermal conductivity of boehmite utilized by NBSR was not explicitly discussed [5,35]. HFIR [3] introduces a correlation for the thermal conductivity of the oxide that is dependent upon the oxide thickness:

$$k_{oxide} = 2.25, \qquad x < 0.001"(25\mu m)$$
$$k_{oxide} = 2.25 - 0.016(x - 25), \quad 0.001 \leq x \leq 0.004 \tag{3.13}$$

where x is the oxide thickness in μm. A comparison of the HFIR correlation to the value used by the Preliminary UMo Report [1] and the rest of the USHPRR is shown in Figure 3.10.

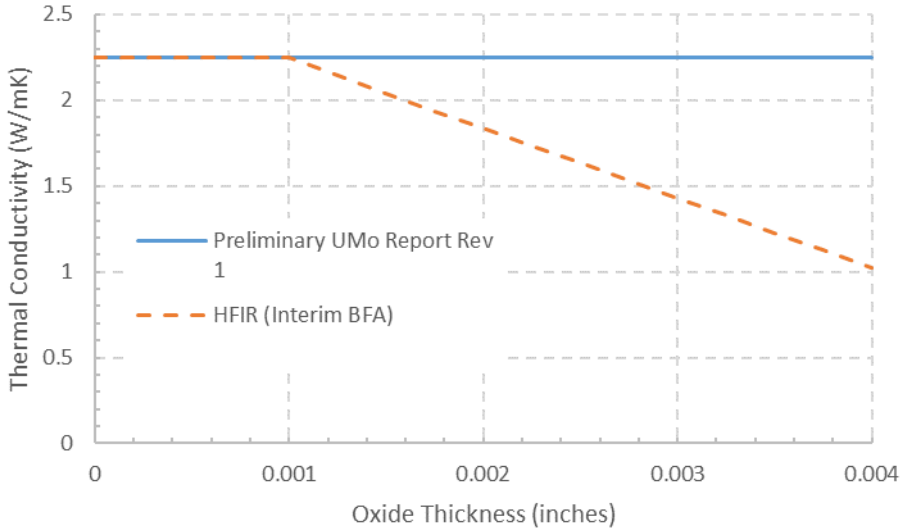

Figure 3.10. Comparison of the correlation used for analyses of HFIR [3] to the oxide thermal conductivity recommended by the Preliminary UMo Report [1].

The recommended value for oxide thermal conductivity is 2.25 W/mK, in agreement with the Preliminary UMo Report. As the HFIR correlation is more conservative than the recommended value, it is not considered to be necessary to re-do the analyses.

3.2.4 Oxide growth

Oxide growth on the aluminum cladding is a reactor-specific correlation. Therefore, this report does not recommend a particular correlation, although the Griess [81] correlation in equation 3.14, developed from out-of-core test data, is a general correlation that can be used.

$$t = A \times \theta^{0.778} \times e^{-\frac{4600}{T}} \tag{3.14}$$

where t is the thickness in mils (0.001 inch), θ is the time in hours, T is the temperature, and A is a constant dependent upon the water pH. For pH of 4.7-5, A is 443. For pH of 5.7-7, A is 1200.

The Preliminary UMo Report [1] recommends the Griess correlation multiplied by a factor of 0.7 for use in the ATR (multiplied by 25.4 to calculate the thickness in μm instead of mils). Analyses for HFIR [3] use the Griess correlation unmodified, and calculations for the ATR [7] assumed an oxide thickness of 0.001 inch with a 1 sigma of 14.2%. Analyses for MITR [6], MURR [4], and NBSR [5,35]

do not explicitly discuss a correlation for the oxide thickness, although MURR [4] mentions that a modified Griess correlation is used. Reference [25] argues that oxide growth, like the channel reduction caused by fuel swelling, increases the margin to onset of nucleate boiling, which occurs in fresh elements, and thus, is not directly treated. Again, no single correlation is recommended for the USHPRR since oxide growth is reactor dependent.

3.3 Zirconium Interlayer

Two types of pure zirconium are available in the industry: sponge and iodide crystal bar zirconium. There is little difference in the impurity content between them. The sponge Zr is > 99.6% in purity with impurities in ppm: O_2 1300, N_2 80, H_2 20, Hf 400, and Ni 40 while the iodide crystal bar is > 99.9% in purity with impurities in ppm: O_2 65, N_2 15, H_2 12, Hf 35, and Ni 20. The iodide crystal bar is softer with lower oxygen content, usually less than 100 ppm. Because of the lower fabrication cost, however, the sponge Zr is more frequently used, and is considered as pure Zr. Sponge Zr is produced by the process known as the Kroll process and is porous, hence the term sponge. In this section, pure zirconium and zirconium both refer to sponge zirconium.

3.3.1 Density and Thermal Expansion of Zirconium

The density of pure Zr as a function of temperature can be converted from the fractional linear thermal expansion using equation 3.15, shown below.

$$\rho = \frac{1}{(1 + \Delta T \bar{\alpha}_l)^3} \rho_0 \tag{3.15}$$

where the density at room temperature, ρ_0 =6.57 g/cm^3 [44] and $\bar{\alpha}_l$ is the mean linear thermal expansion coefficient. $\bar{\alpha}_l$ was calculated from integration of a second-order polynomial fit (equation 3.16) of the instantaneous thermal expansion (α') data from Touloukian [44], shown in equation 3.17.

$$\alpha' = 3.4556 + 0.0080087 \times T - 3.2231 \times 10^{-6} \times T^2 \tag{3.16}$$

$$\bar{\alpha}_l = 3.4556 + 0.00400435 \times (T + T_0) - 1.07437 \times 10^{-6} \times \left(T^2 + T \times T_0 + {T_0}^2\right) \tag{3.17}$$

where T is the temperature in K, T_0 is the reference temperature set to 293K, and α'and $\bar{\alpha}_l$ are in units of x10^{-6} K^{-1}.

Values for α', $\bar{\alpha}_l$, and the corresponding density values as a function of temperature are shown in Table 3.3.

Table 3.3. Instantaneous and Mean Linear Thermal Expansion Coefficients and Density of Zirconium [46].

T (K)	α' (x10^{-6}K^{-1}) [44]	$\overline{\alpha}_l$ (x10^{-6}K^{-1})	ρ (g/cm^3)
293	5.7	5.5	6.57
400	5.9	5.8	6.56
500	6.6	6.1	6.55
600	7.1	6.4	6.53
700	7.6	6.6	6.52
800	7.9	6.8	6.50
900	8	7.0	6.49
1000	8.2	7.2	6.47

For the temperature range 293–800 K, the variation in density is only 1%. Hence, using $\rho_0 = 6.57 g/cm^3$ at $T_0 = 293K$ for other temperatures is considered to be reasonable.

3.3.1.1 Comparison to the Density and Thermal Expansion of Zirconium Recommended by the Preliminary UMo Report

The temperature dependence of density of Zr in the Preliminary UMo Report is from [46], and is in agreement with the density values presented in Table 3.3.

The Preliminary UMo Report introduces a correlation by Touloukian [44] and a plot from the ASM handbook [64] within the body of the report for the coefficient of thermal expansion (CTE) of Zr. In Appendix C, a digitization of the ASM handbook is recommended. A comparison of the data recommended in Appendix C of the Preliminary UMo Report and the fit of current best data is shown in Figure 3.11.

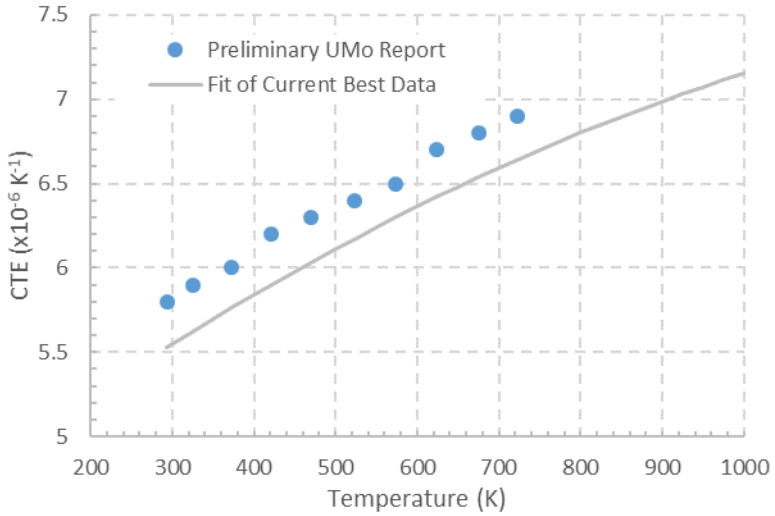

Figure 3.11. Comparison of the CTE of Zr recommended by the Preliminary UMo Report [1] and the fit of current best data (equation 3.17)

The data recommended by the Preliminary UMo Report [1] are consistently higher than the fit of current best data. The correlations presented in this report (equations 3.16 and 3.17) are based on more recent data than the reference for the ASM plot [87]. Additionally, the temperature dependence of density recommended by the Preliminary UMo Report was calculated using equations 3.15 and 3.17 in the referenced report [46], so the data in Table 3.3 and the correlations in equations 3.16 and 3.17 are recommended.

3.3.1.2 Comparison to the Density and Thermal Expansion of Zirconium Used for Analyses of the USHPRR

The density of Zr is assumed to be approximately constant in the temperature range of interest in analyses for ATR [7], MITR [6], MURR [4], and NBSR [5]. Analyses for HFIR [3] have suggested equation 3.18 for COMSOL finite element modeling, suggesting equation 3.19 as an alternative, where LTE is linear thermal expansion, as shown in equation 3.20. However, some analyses [20] assumed a constant density of 6.52g/cm^3.

$$\rho_{Zr} = 6.518 - 0.0827 \times 10^{-3}T - 4.803 \times 10^{-8}T^2 + 7.322 \times 10^{-12}T^3 \quad (3.18)$$

$$\rho_{Zr} = \frac{6.57}{(LTE)^3} \quad (3.19)$$

$$LTE = -1.11 \times 10^{-3} + 2.325 \times 10^{-6}T + 5.595 \times 10^{-9}T^2 - 1.768 \times 10^{-12}T^3 \quad (3.20)$$

A comparison of the assumed density values for the USHPRR and the Preliminary UMo Report [1] is shown in Figure 3.12. The values assumed for analyses of the USHPRR are either in agreement, or more conservative than the data recommended in the Preliminary UMo Report.

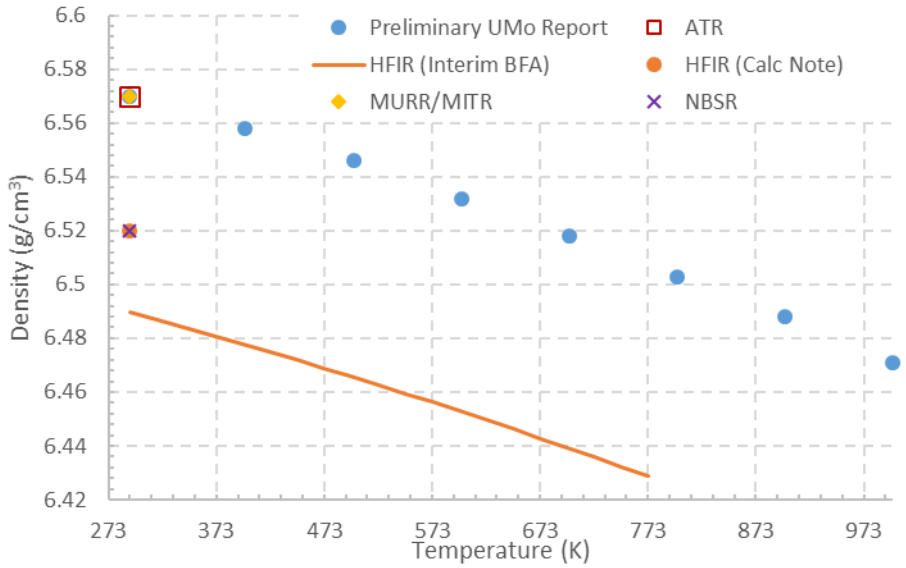

Figure 3.12. Comparison of Zr density values used by analyses for the USHPRR and recommended by the Preliminary UMo Report

3.3.2 Heat Capacity of Zirconium

Heat capacity data of Zr have been reviewed and compiled by Kim [46]. He proposed a correlation as a function of temperature, which was taken from Reference [67], as follows:

$$c_p = 22.839 + 9.091 \times 10^{-3}T - 2.132 \times 10^{4}T^{-2} \quad (3.21)$$

where c_p is in J/(mol K) and T is in K in the range of 293 ≤ T ≤ 1135 K. Equation 3.21 was also adopted in [34]. Because inverse square temperature dependence cannot be incorporated into safety analysis, equation 3.21 was refit for a linear dependence. The refit correlation is given in equation 3.22.

$$c_p = 0.2476 + 1.023 \times 10^{-4}T \quad (3.22)$$

where c_p is in J/(g K) and T is in K for temperatures 293 ≤ T ≤ 1135 K. The two correlations are compared in Figure 3.13, where equation 3.21 is the correlation discussed in the Preliminary UMo Report and equation 3.22 is the linear fit of current best data.

3.3.2.1 Comparison to the Heat Capacity of Zirconium from the Preliminary UMo Report

Within the body of the Preliminary UMo Report [1] both an equation for the specific heat of Zr (equation 3.21) and a figure from the ASM Handbook [64] are introduced, although no specific recommendation is given. From the tabulated values in Appendix C, the ASM Handbook values are recommended by the Preliminary UMo Report. A comparison of the fit of current best data (equation 3.22), the equation discussed in the body of the Preliminary UMo Report (equation 3.21), and the recommended values from Appendix C of the Preliminary UMo Report are shown in Figure 3.13.

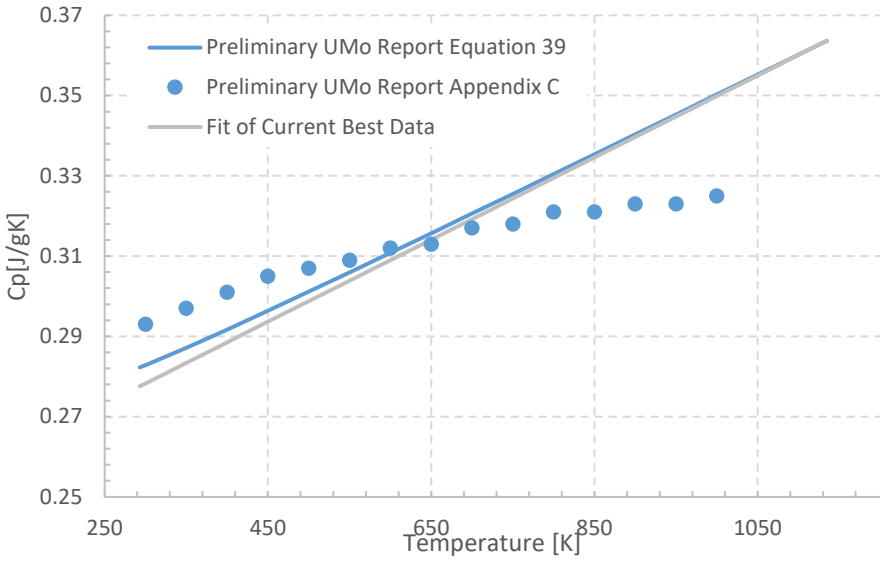

Figure 3.13. Comparison of the correlation given in the Preliminary UMo Report [1], the values recommended in Appendix C of the Preliminary UMo Report, and the linear fit of current best data for the specific heat of zirconium.

The fit of current best data and the equation given in the body of the Preliminary UMo Report [1] are in close agreement. However, the recommended data from Appendix C of the Preliminary UMo Report diverges from these equations, particularly at temperatures greater than ~725K. Because the two equations discussed here (equations 3.21 and 3.22) are based on several data sets collected more recently than the data given in the ASM Handbook, either of these equations are recommended, depending on the restrictions of the analyses being conducted. If an inverse temperature is allowed, equation 3.21 is recommended. If only a linear relationship is allowed, equation 3.22 is recommended.

3.3.2.2 Zirconium Heat Capacity for Analyses of the USHPRR

The correlation used for analyses of MURR [4], and recommended for analyses for MITR [6] is given in a form that heat capacity is coupled with density using the data from [88], and is shown in equation 3.23.

$$\rho c_p = 1.859 \times 10^6 + 739.2T \qquad (3.23)$$

where the correlation calculates values in J/(m^3 K) and T is temperature in ^{o}C. The report [4] says that a constant density of 6.57 g/cm^3 for all temperatures is recommended, and was used to calculate the heat capacity for comparison to the correlations used by the rest of the USHPRR. The main reason for using this form rather than that shown in equation 3.21 was that the square inverse multiplication of temperature in the last term of equation 3.21 could not be accommodated by the computer program used for the safety analysis.

Analyses for ATR [7] use equation 3.24, which was converted from units of BTU/(lbm °F) to J/(g °C) for comparison to the rest of the USHPRR. As a note, the brackets in the equation below were missing in the documentation.

$$c_{Zr} = \left[24.1618 + 8.7558 \times 10^{-3} \times \frac{(T + 459.67)}{1.8} - 6.9942 \times \frac{10^4}{\left(\frac{(T + 459.67)}{1.8}\right)^2}\right] \times 5.266 \times 10^{-4} \times \frac{1}{91.224 * 0.00220462} \quad (3.24)$$

A report for HFIR [3] uses:

$$c_{Zr} = 187.38 + 0.583T - 0.001258T^2 + 1.0155 \times 10^{-6}T^3 \quad (3.25)$$

where c_{Zr} is the heat capacity of Zr in J/(kg K) and T is in K, valid for temperatures between 298 and 1073K.

Analyses for NBSR [5] assume a constant heat capacity for Zr (0.27 J/ (g K)) valid for temperatures between 260K and 1367K. As a note, the units in the documentation were listed as W/(m³ K), and it was assumed they should be J/ (m³ K) for conversion to J/ (g K) for comparison to the rest of the USHPRR. The density used to convert the heat capacity to specific heat capacity was 6.52g/cm³.

A comparison of correlations used for analyses of the USHPRR compared to the correlation discussed in the Preliminary UMo Report [1] is shown in Figure 3.14.

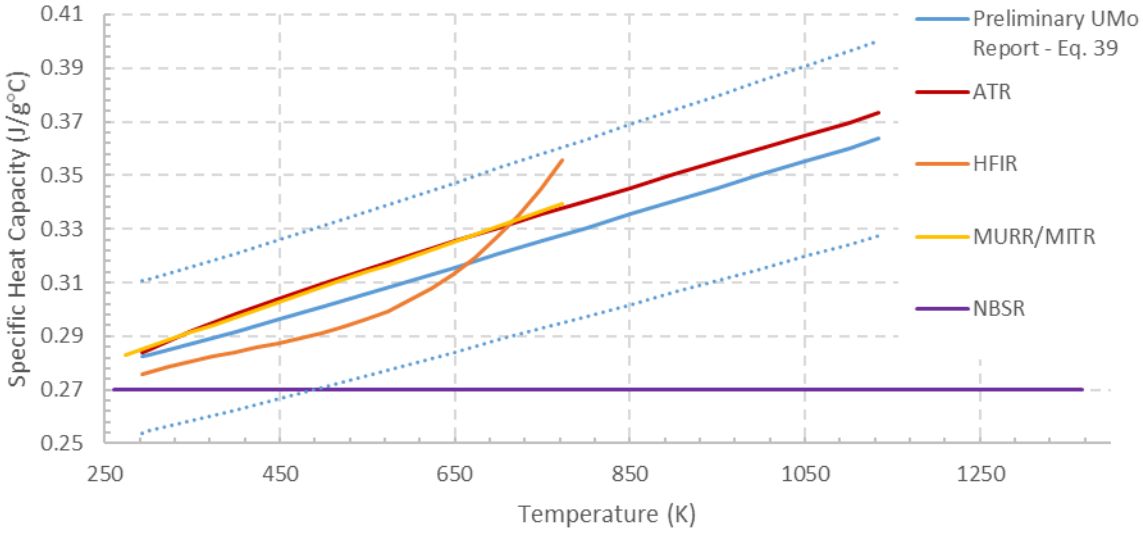

Figure 3.14. Comparison of Zr heat capacity correlations, where the dotted lines indicate a variation of the Preliminary UMo Report correlation of ±10%.

The maximum difference between the correlations and the Preliminary UMo Report (with the exception of NBSR [5]) occurs at 500°C (the maximum temperature for which the correlation used for analyses of HFIR [3] is applicable). This difference is within a 10% variance of the correlation discussed in the Preliminary UMo Report, as marked by dotted lines in Figure 3.14. This is well within the 50% variance investigated in reference [89], which had minimal impact in the overall fuel plate behavior. The value assumed for NBSR is substantially lower than the correlations, but is still within the 50% variance investigated. All assumptions made for analyses of the USHPRR are still considered

valid. If additional analyses are needed, equation 3.21 is recommended if a nonlinear relationship is allowed. If only a linear relationship is allowed, equation 3.22 is recommended.

3.3.3 Thermal Conductivity of Zirconium

The measured thermal conductivities of sponge Zr that were available before 1970 were reviewed and the recommended values were tabulated based on the data assessment by Touloukian [44]. Fink [88] produced a correlation based on the Touloukian data, with the addition of data available after 1970, as:

$$k_{Zr}(T) = 8.8527 + 7.0820 \times 10^{-3}T + 2.532910^{-6}T^2 + 2.9918 \times 10^{3}T^{-1} \quad (3.26)$$

where T is in K in the range of 293 ≤ T ≤ 2000 K. Fink declared that the uncertainty (+1σ) in equation 3.26 is between 8.4% and 9.9% in the temperature range 298 ≤ T ≤ 1000K.

3.3.3.1 Comparison to the Thermal Conductivity of Zirconium in the Preliminary UMo Report

There is no specific recommendation within the body of the Preliminary UMo Report [1]. Instead, both the Fink correlation (equation 3.26) and a figure from the ASM Handbook [64] were presented. In Appendix C, tabulated data extracted from the ASM Handbook was recommended. These values are compared to the Fink correlation in Figure 3.15.

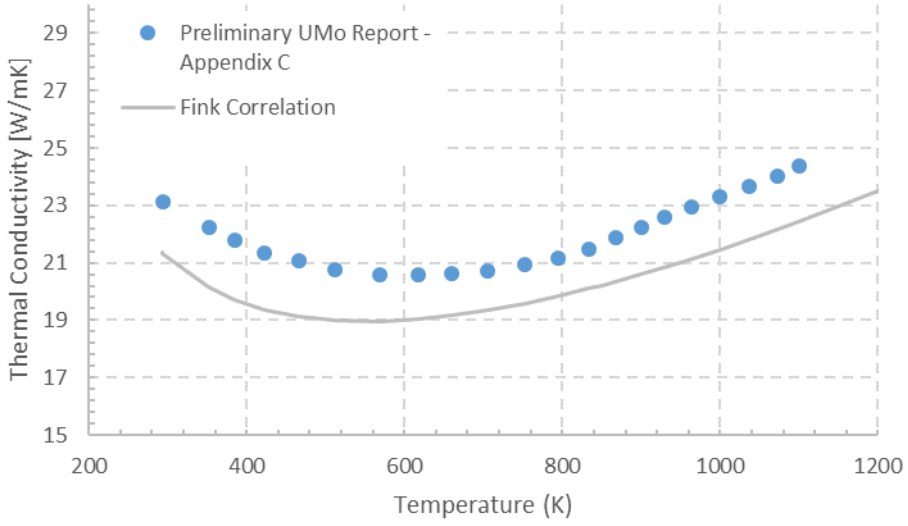

Figure 3.15. Comparison of the Fink correlation (equation 3.26) to the tabulated values recommended in Appendix C of the Preliminary UMo Report for the thermal conductivity of Zr.

The values in Appendix C of the Preliminary UMo Report [1] are consistently higher than the values calculated from the Fink correlation. It is recommended to use the Fink correlation rather than the values from the ASM Handbook as it is a more recent analysis of the available data for the thermal conductivity of Zr and has smaller uncertainty than the curve proposed in the ASM Handbook. The Fink correlation has a 1σ ranging from 5 to 9.5%, depending on temperature. The reference from the ASM Handbook states that the uncertainty in thermal conductivity is ±10% at temperatures below 800K, but increases to as much as ±20 or ±25% at higher temperatures.

3.3.3.2 Comparison to the Thermal Conductivity of Zirconium Used for Analyses of the USHPRR

The Fink correlation was used for analyses of MURR [4], ATR [7], and MITR [6] for the thermal conductivity of Zr. Analyses for NBSR [5] uses a constant thermal conductivity (22.7 W/(m K)) for temperatures between 260 and 1367K. Analyses for HFIR [3] use equation 3.27, valid for temperatures between room temperature (assumed to be 20°C) and 500°C. Note that the exponent for the T^5 term was miss-typed as 10^{15} instead of 10^{-15}.

$$k_{Zr} = 36.84 - 0.077T + 1.259 \times 10^{-4}T^2 - 8.966 \times 10^{-8}T^3 + 3.168 \times 10^{-11}T^4 - 4.413 \times 10^{-15}T^5 \quad (3.27)$$

k_{Zr} is the thermal conductivity of Zr in W/(m K) and T is the temperature in K. A comparison of the values and correlations used for analyses of the USHPRR and the values recommended in Appendix C of the Preliminary UMo Report are shown in Figure 3.16.

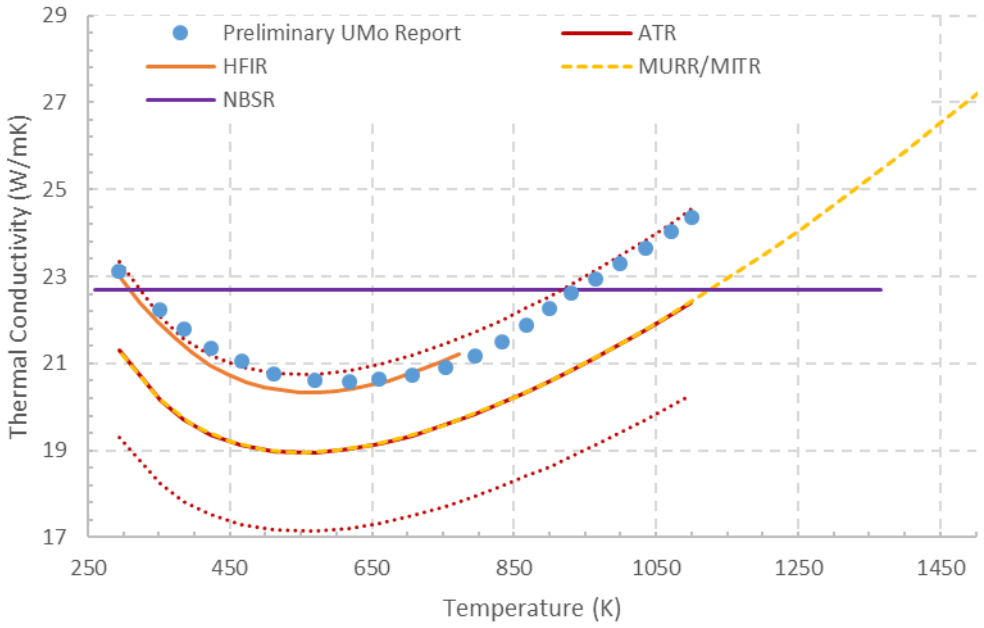

Figure 3.16. Comparison of the values and correlations used for the thermal conductivity of Zr in analyses of the USHPRR and the values recommended in Appendix C of the Preliminary UMo Report. The dotted lines indicate the ±9.5% standard deviation assumed by analyses for the ATR.

The correlations, and values recommended in Appendix C of the Preliminary UMo Report, all fall within the standard deviation of ±9.5% used in analyses for the ATR, as indicated by dotted lines in Figure 3.16. The exception to this is the NBSR, where the assumed thermal conductivity is greater than the correlations in the intermediate temperature range (~450-850K). Reference [89] investigated the impact of a variation in thermal conductivity of zirconium ±50% from nominal, and found only minimal impact on the stresses and temperatures in the fuel plate. The greatest difference between the ATR correlation and the NBSR constant value assumption is ~20%, well within the 50% variation investigated. Therefore, the assumption of a constant thermal conductivity for Zr is reasonable.

3.3.4 Mechanical Properties of Zirconium

The Preliminary UMo Report includes information and recommendations for the Young's modulus, Poisson's ratio, yield strength, ultimate strength, and thermal creep strain rate of zirconium. However, these properties were not used in the analyses of the USHPRR, so a detailed discussion is not included here. Finite element analyses [89] have been conducted to determine the impact of changes in the Young's modulus and yield stress of the Zr layer. Although changing these parameters showed some effect on the stresses at the interfaces between the Zr interlayer and the fuel core and cladding, effect on the overall thermo-mechanical behavior of the fuel plate was found to be minimal.

4 Fuel Performance Parameters

The two primary fuel performance parameters that limit the conditions in which the fuel can be used are the swelling of the fuel (in relation to the channel gap closure) and the blister anneal temperature, which serves as a fuel temperature safety limit. These parameters will be discussed in the following sections, as well as the impact of creep of the U-10Mo fuel.

4.1 U-10Mo Monolithic Fuel Swelling

Fission-induced swelling of monolithic U-10Mo is isotropic. Because of dimensional restrictions in the axial and width directions, only the foil thickness increases as a result of fuel swelling due to mechanical constraint of the fuel in the width and length directions. On this basis, fuel swelling can be simply computed by the equation shown below.

$$\Delta t_p = \left(\frac{\Delta V}{V_0}\right)_f t_{0,f} \tag{4.1}$$

where Δt_p is plate thickness change in fraction after irradiation, and $t_{0,f}$ is the as-fabricated foil thickness. Here $t_{0,f}$ is known from the fabrication record, with some uncertainty, as minor variations in thickness will occur across the plate (within the specified tolerances).

An empirical correlation for U-10Mo swelling based on monolithic fuel irradiation test data [27] is shown in equation 4.2, the equation recommended for use.

$$\left(\frac{\Delta V}{V_0}\right)_f = 0.05 f_d, \qquad f_d \le 3 \times 10^{21} \frac{fissions}{cm^3}$$
$$\left(\frac{\Delta V}{V_0}\right)_f = 0.15 + 0.063(f_d - 3) + 0.0033(f_d - 3)^2, \quad f_d > 3 \times 10^{21} \frac{fissions}{cm^3} \tag{4.2}$$

where fuel swelling is in fraction and f_d is the fission density in 10^{21} f/cm^3, including fissions by actinides bred during irradiation. The data used to develop the correlation was based on a single data point from the middle of the fuel plate, where effects of creep are assumed to be minimal. However, because the maximum fission density in most experimental plates are achieved at the plate edge, this reduces the data availability at higher fission densities.

4.1.1 Fuel Swelling Comparison to the Preliminary UMo Report

The Preliminary UMo Report [1] developed two swelling correlations based on a binning method of data available across the fuel plate, which expands the set of available data, particularly at higher fission densities. The correlation recommended in the Preliminary UMo Report, reproduced as equation 4.3, includes data from the AFIP-6MkII test. A second correlation presented in the Preliminary UMo Report, and reproduced as equation 4.4, excludes this data, for the reasons discussed in section 2.5.2.

$$\%Swelling = 6.13 \times 10^{-43} {f_d}^2 + 4.00 \times 10^{-21} f_d \tag{4.3}$$
$$\%Swelling = 3.83 \times 10^{-43} {f_d}^2 + 4.54 \times 10^{-21} f_d \tag{4.4}$$

These two correlations, as well as the recommended best-estimate correlation from this report (equation 4.2), are compared in Figure 4.1. Although there is agreement at lower fission densities, the correlations diverge at higher fission densities due to the use of different data sets.

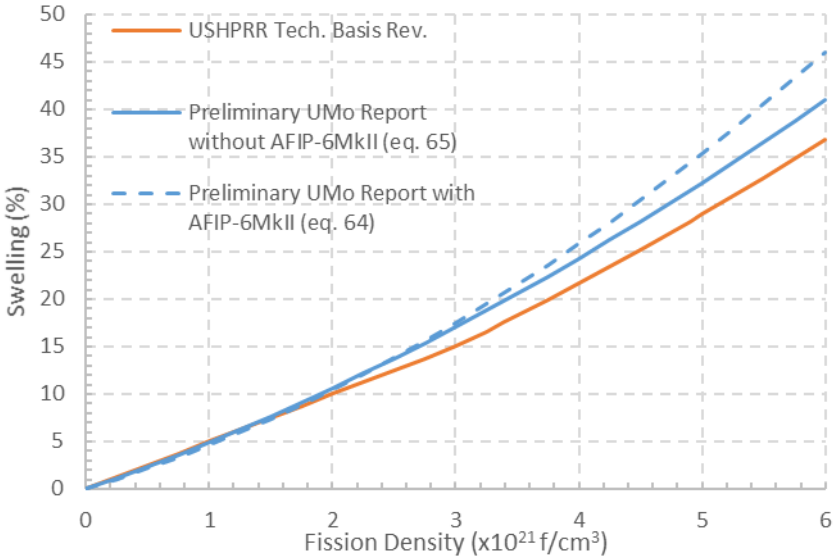

Figure 4.1. Comparison of the swelling correlations from the Preliminary UMo Report and the fit of current best data.

4.1.2 Fuel Swelling Comparison of the Correlations Utilized in Analyses for the USHPRR

U-10Mo swelling due to irradiation given in equation 4.2 is considered in the HFIR [3] and MITR [6] reports. Fuel swelling is also discussed in work for MURR [4,90] that considers channel restriction at end of life of 8 mil from all sources, which was derived based on the same equation. Analyses for ATR [7] utilized equation 4.5, based on a draft version of the correlation from the Preliminary UMo Report [1].

$$t_{swell} = \frac{(5.69957 \times 10^{-43}(f_d \times 10^{21})^2 + 4.30015 \times 10^{-21} \times f_d \times 10^{21})t_0}{100} \; in \qquad (4.5)$$

As a note, the "x10^{21}" term should be discarded, as the fission densities are in fissions/cm^3. t_{swell} is the fuel meat thickness after swelling, t_0 is the as-fabricated fuel meat thickness, and t_{swell}/t_0 (% thickness change) was used for comparison to the other USHPRR.

NBSR [91] has recently begun using equation 4.6 in their analyses.

$$\frac{\Delta t}{t_0}(\%) = 0.5700{f_d}^2 + 4.300f_d \qquad (4.6)$$

The correlations used for analyses of the USHPRR are shown in Figure 4.2. NBSR and ATR are in alignment with the recommendation of the Preliminary UMo Report which includes AFIP-6MKII data, while analyses for HFIR, MITR, and MURR use the correlation recommended by this report. A

comparison of the swelling values for each of the USHPRR at the maximum fission density calculated by each of the equations is shown in Table 4.1.

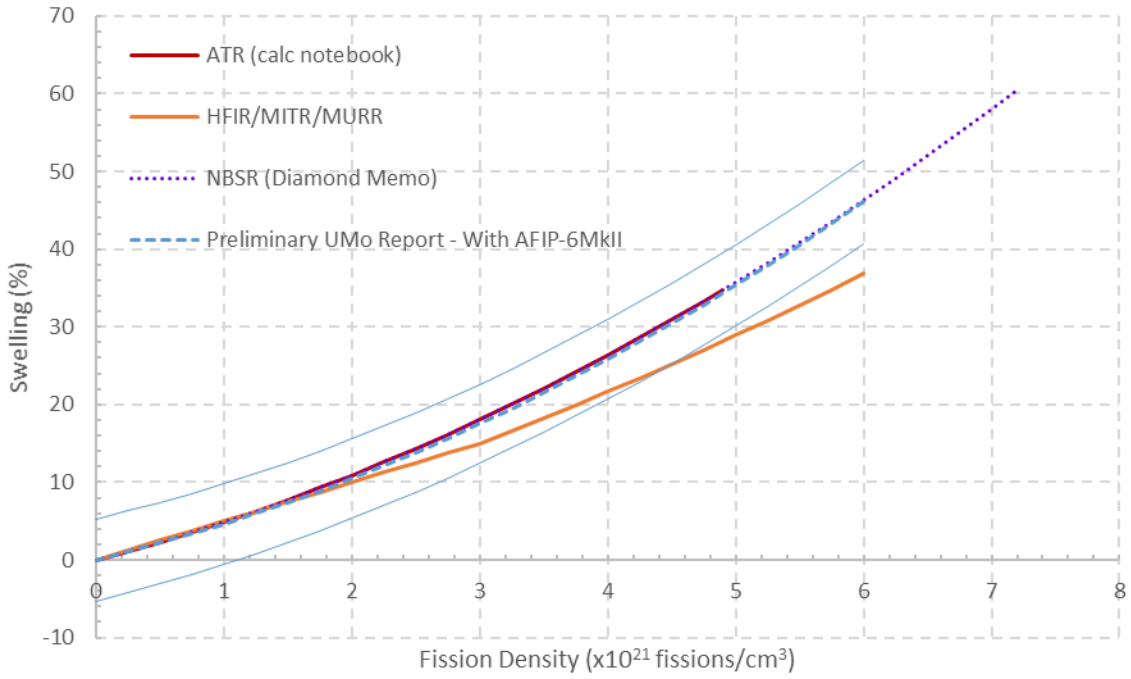

Figure 4.2. Comparison of the correlations used for analyses of the USHPRR and the Preliminary UMo Report (the thin blue lines represent the 95% confidence interval for the Preliminary UMo recommended correlation).

Table 4.1. Comparison of the calculated swelling values for each of the USHPRR using the recommended correlations from this report and the Preliminary UMo Report

Reactor	Fission Density ($x10^{21}$ fissions/cm^3)	Swelling (%)		
		Recommended (equation 4.2)	Preliminary UMo Report without AFIP-6MkII (equation 4.4)	Preliminary UMo Report with AFIP-6MkII (equation 4.3)
ATR	4.9	28	31	35
HFIR	6	37	41	46
MITR	5.0	29	32	36
MURR	3.4 (plate 1)	18	20	21
	2.6 (plate 23)	13	14	15
NBSR	7.2	47	53	61

As discussed in Section 4.1.1, there is reasonable agreement among all correlations at lower fission densities (< $2x10^{21}$ fissions/cm^3), but there is a significant disparity at higher fission densities.

4.2 Irradiation Creep of U-10Mo Fuel

Irradiation creep of U-10Mo has been reported [92]. Creep affects fuel swelling most significantly in the foil peripheral regions. As shown in Figure 4.3, the measured fuel swelling at the foil edges is lower than the prediction, while away from the edge of the fuel the measured swelling is larger than the prediction. The areas marked as A (blue) and B (green), compared in Table 4.2, are similar, suggesting that mass relocation by creep from region A to region B occurs. The data fit for equation 4.2, the recommended fuel swelling correlation, was based on the measured fuel swelling at the foil center to minimize the influence of creep. Depending upon the node size, it has not been considered necessary to address creep separately. If regions A and B are in the same node, and that node is on the order of one-half centimeter or larger, these regions balance out, and a swelling equation alone can be used rather than addressing the effects of creep as well, as long as the average fission density for the node is utilized.

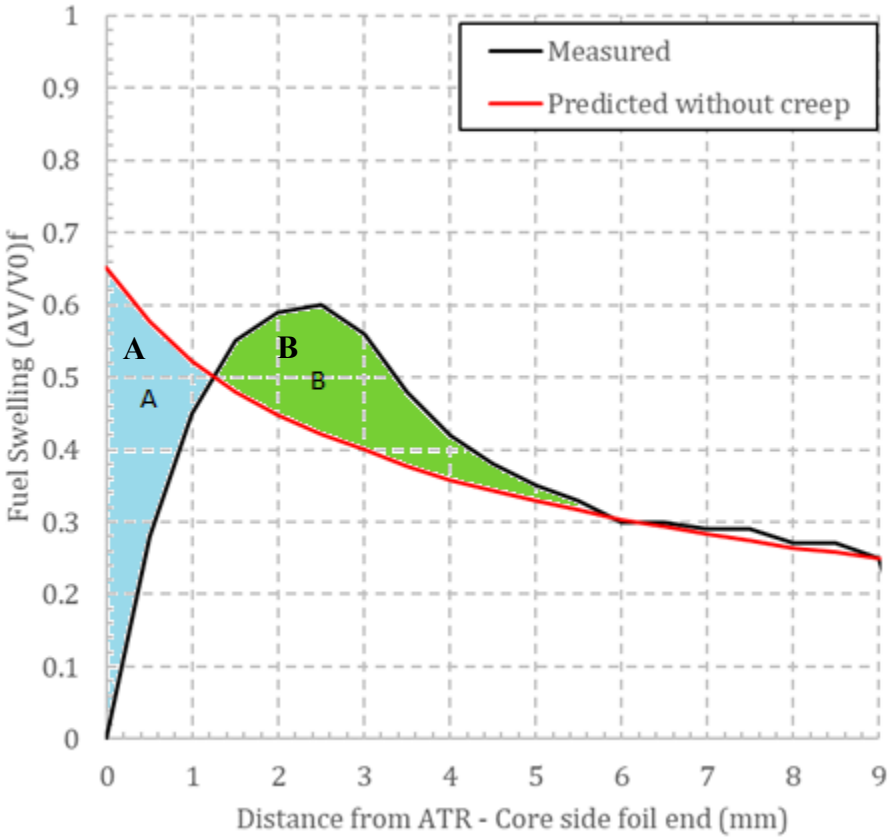

Figure 4.3. Mass relocation by creep of U-10Mo (based on L1F140 from RERTR-7 test).

Table 4.2. Comparison of areas A and B marked in Figure 4.3.

Plate ID	Test ID	Area A	Area B	Difference
B1-L1T34T	RERTR9	130	99	31
B7-L1F140	RERTR7	53.7	60.9	-7.2
B3-L1P05A	RERTR9	115.5	106.4	9.1
C6-L1P04A	RERTR9	74.2	90.5	-16.3
C1-L1F26C	RERTR-9	97.7	126.4	-28.7

If it is desired to reduce the node size, requiring creep to be incorporated, a linear relationship with stress and fission rate was recommended by Kim [92], and is shown in equation 4.7.

$$\dot{\varepsilon_c} = A\sigma\dot{f} \tag{4.7}$$

where $\dot{\varepsilon_c}$ is the equivalent creep strain rate (s^{-1}), A is the creep rate coefficient (cm^3/MPa-fission), σ is the equivalent stress (MPa), and $\dot{f}$ is the fission rate (fissions/cm^3 s). Finite Element Analysis (FEA) was utilized to determine that the creep rate coefficient, based on the data available at the time and the swelling correlation shown in equation 4.2, is 500 × 10^{-25} cm^3/MPa fission. If a different swelling correlation is used, the FEA would need to be repeated to determine if the aforementioned creep rate coefficient (500 × 10^{-25} cm^3/MPa-fission) should be revised. The Preliminary UMo Report [1] recommends the same value for A, as does HFIR [3], although it highlights the need to reevaluate this value. A report for MURR [4] references an older report by Kim [93], which determined A for U-10Mo to be 2.5 × 10^{-25} cm^3/MPa fission. Until the (500 × 10^{-25} cm^3/MPa-fission) value of the U-10Mo creep rate coefficient is revised based on recent swelling correlations, it is recommended to perform a sensitivity study for a range of values (from 2.5 to 750 x 10^{-25} cm^3/MPa fission), or use the 500 × 10^{-25} cm^3/MPa fission value, as it is based on more recent analysis.

4.3 Blister Anneal Temperature

Data have been collected on fuel performance at elevated temperatures after irradiation. This post-irradiation testing is performed by annealing plates. Inspection follows to determine whether blistering has occurred. Hence, this process is known as a 'blister anneal test'. Historically this test has been established as a basis for retention of fission products [94,95]. Consequently, blister temperature data have been used to establish fuel temperature safety limits for fuel being used in reactors in order to maintain fuel integrity [96,97].

4.3.1 Blister Anneal Temperature of UAl_x-Al Dispersion Fuel

Blister temperature data for irradiated HEU U-Al_x fuel samples were collected and reported by Beeston, *et al* [98] and is presented here for comparison to the LEU U-10Mo fuel data. Additional data measurements of the blister temperature are provided in Figure 10 in Reference [99]. Figure 4.4 presents a summary of these measured data values. All data points are for U-Al_x without any B_4C burnable poison in the fuel matrix. Beeston, *et al.* observed blisters in the range of 482 to 598 °C when irradiated fuel plates with fission densities from 0.3x10^{21} to 2.7x10^{21} fissions/cm^3 were placed in a furnace. The data collected by Gahlert and Nazaré [99] demonstrated blisters in the range of 551 to 638 °C in irradiated fuel plates at fission densities from 0.1 to 1.6x10^{21} fissions/cm^3. It is observed from Figure 4.4 that for a given fuel burnup, the blister temperature data measured by Beeston are about 40 °C lower than those reported by Gahlert and Nazaré. Thus, the data by Beeston, *et al.* are considered to be conservative.

Beeston, *et al* provided a least squares regression fit of their measured data as a second-order polynomial of the form:

$$T_{blister} = 905 - 139.9f_d + 44.8{f_d}^2 \tag{4.8}$$

where $T_{blister}$ is the blister threshold temperature in K and f_d is the fission density in units of 10^{21} fissions/cm^3. The data fit is shown in Figure 4.4 along with the -2σ value (lower bound of the 95% CI), which is conservatively extended as a constant value after reaching a minimum of 480°C

(896 °F) at a fission density of around 1.5x10^{21} fissions/cm^3. In references such as Beeston *et al.*, it can be seen that where there is increased gas production during irradiation due to fission product gas the blister temperature threshold decreases. If additional sources of gas are added to the fuel, such as boron, the blister threshold will be further decreased.

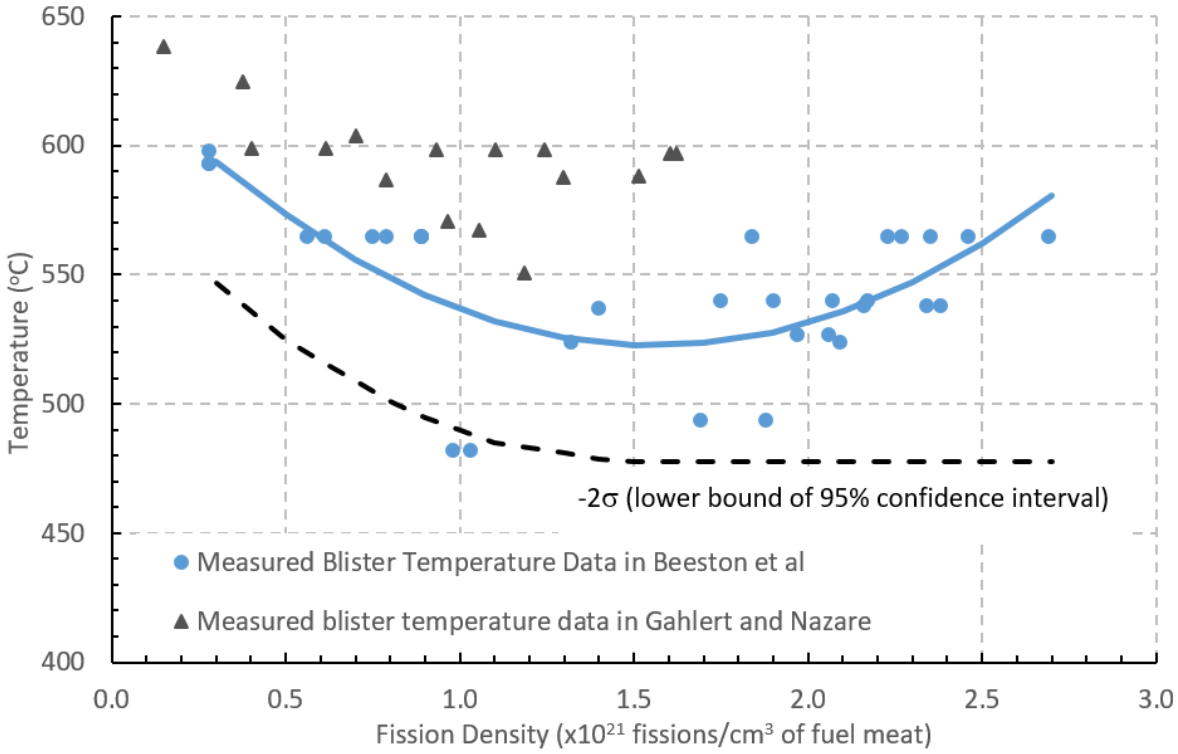

Figure 4.4. U-Al$_x$ Fuel Blister Temperature Data [98,99]. The blue line is the data fit by Beeston [98], equation 4.8**.**

4.3.2 Blister Temperature of U-10Mo Monolithic Fuel

For the monolithic fuel under development, substantial testing has been performed to collect data on blister temperatures. This work is described in reports by Rice, et al. [100,101]. Blister threshold temperatures are presented as a function of blister average and blister peak (local) fission density in Table A-1 of both reports by Rice. The peak (local) fission density is most relevant since the regions of peak local fission density were observed to correspond to the regions that blistered. The blister temperature data in References [100] and [101] were evaluated for irradiated U-10Mo samples up to a local fission density of 12.1x10^{21} fissions/cm^3, but most of the data were in the range of 2.5x10^{21} to 7.5x10^{21} fissions/cm^3. Data from these references are plotted in Figure 4.5.

The references do not formulate a best-fit equation for the blister threshold temperature as a function of the peak local fission density in the blister, although a correlation based on the plate average fission density was included. The nominal blister threshold temperature ($T_{blister,nom}$) has been formulated below as a function of peak fission density, as reported in [4]:

$$T_{blister,nom} = \begin{cases} 5.20 \times 10^{6} f_d^{-0.1889} & \text{for } f_d \geq 1.5 \times 10^{21} \\ 550 & \text{for } f_d < 1.5 \times 10^{21} \end{cases} \quad (4.9)$$

where $T_{blister,nom}$ is the temperature in °C and f_d is the peak fission density in fissions/cm³ in the fuel foil. There were three plates tested that had a maximum local fission density in the range of 0.6×10^{21} to 2.2×10^{21} fissions/cm³. These did not blister when annealed for 20 minutes at temperatures up to 550 °C, which was the temperature limit of the furnace. Thus, it is conservatively assumed that for plates with peak fission densities less than 1.5×10^{21} fissions/cm³, $T_{blister, nom}$ of 550 °C should be used. The fit of the blister threshold temperature with fission density is shown in Figure 4.5.

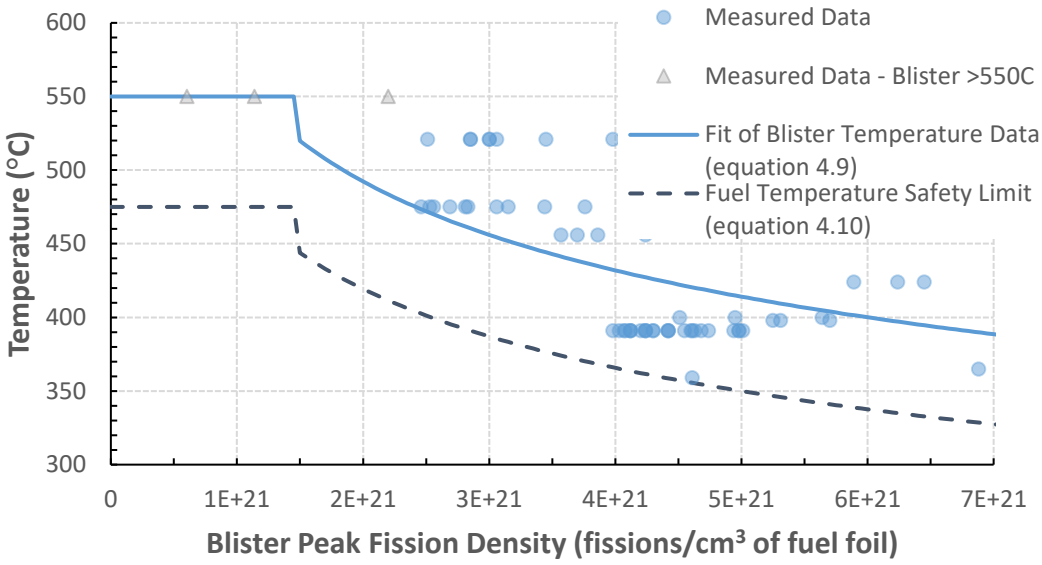

Figure 4.5. U-10Mo Monolithic Alloy Fuel Blister Temperature vs. Burnup.

The U-10Mo fuel temperature safety limit as a function of the peak fission density has been formulated for MURR [4] at the lower bound of the 95% CI (-2σ) of the blister threshold temperature in the present work as $T_{blister, 95\%CI, lower}$:

$$T_{blister,95\%\,CI,lower} = \begin{cases} 6.72 \times 10^{6} f_d^{-0.1974} & \text{for } f_d \geq 1.5 \times 10^{21} \\ 450 & \text{for } f_d < 1.5 \times 10^{21} \end{cases} \quad (4.10)$$

As described above, there were three plates tested with peak fission densities in the range of 0.6×10^{21} to 2.2×10^{21} fissions/cm³ that did not blister at temperatures up to 550 °C. It is conservatively assumed here that a $T_{blister, 95\%CI, lower}$ of 450 °C be used for plates with peak local fission densities less than 1.5×10^{21} fissions/cm³. The fit for the lower bound of the 95% CI is also shown in Figure 4.5. It appears that at less than $1.5x10^{21}$ fission/cm³ this lower 95% CI limit could be increased to approximately 475 °C based on the offset from the plates that were heated to 550 °C but did not blister. A 95% CI equation was proposed during initial evaluations, and is reproduced here as equation 4.11.

$$T_{blister,95\%\,CI,lower} = \begin{cases} 6.72 \times 10^{6} f_d^{-0.1974} & \text{for } f_d \geq 1.5 \times 10^{21} \\ 475 & \text{for } f_d < 1.5 \times 10^{21} \end{cases} \quad (4.11)$$

As a note, blister threshold temperatures have been measured using an isothermal furnace annealing procedure. Although some reactors have indicated that the blister threshold temperatures relates to

the cladding, the entire fuel plate, including the fuel and the cladding, are tested. For typical HEU dispersion fuels, the temperature differences between the cladding and the fuel were minimal. However, for the U-10Mo monolithic fuel there is a larger difference and so the maximum fuel temperatures are conservatively used in comparison to the fuel temperature safety limit.

4.3.2.1 Blister Temperature Correlation Comparison to the Preliminary UMo Report

The Preliminary UMo Report [1] recommends equation for the lower 95% prediction bound, which is reproduced as equation 4.12.

$$T_{blister}(Lower\ 95\%\ Prediction\ Bound) = \begin{cases} 3.25 \times 10^{7} f_d^{-0.2282} & \text{for } f_d > 1.5 \times 10^{21} \\ 478 & \text{for } f_d \leq 1.5 \times 10^{21} \end{cases} \quad (4.12)$$

This correlation was developed based on a data set limited to what are considered to be the most representative plates, as was discussed in section 9.2.4 of the Preliminary UMo Report [1]. Equation 4.12 is in close agreement with equation 4.11, as shown in Figure 4.6. For all fission densities, equation 4.11 is conservative relative to the correlation recommended by the Preliminary UMo Report [1]. However, because equation 4.12 is based on the most representative plates, and bounds the collected data, it is recommended to use equation 4.12 for any future analyses.

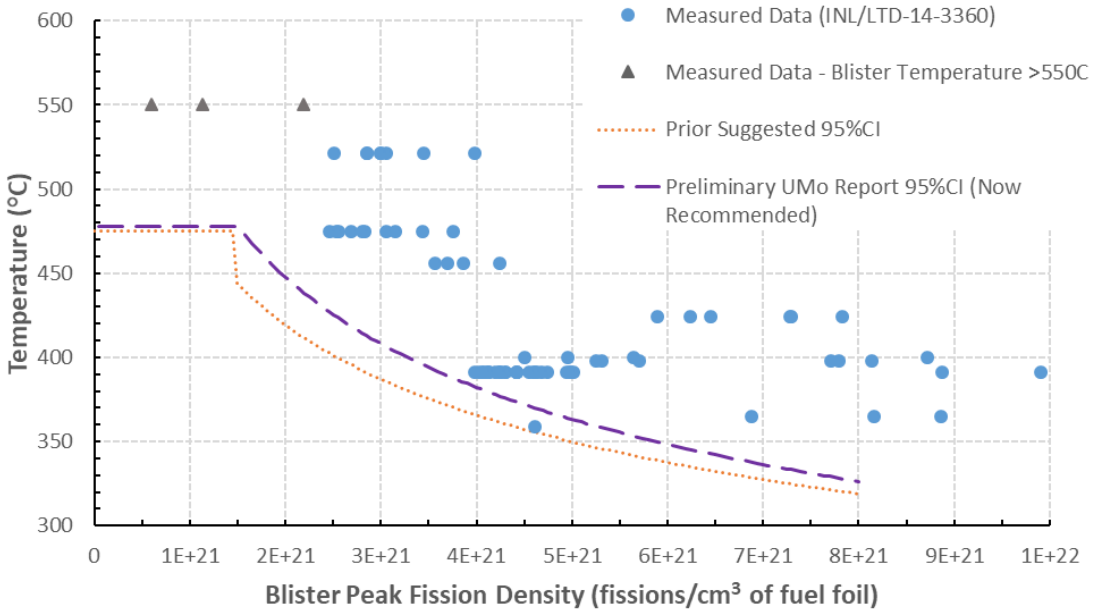

Figure 4.6. Comparison of the lower 95% prediction bounds recommended by the Preliminary UMo Report (equation 4.12) and suggested here (equation 4.11).

4.3.2.2 Comparison of the Correlations Used for the Fuel Temperature Limit for Analyses of the USHPRR

A comparison of measured blister threshold temperature data, the lower 95% CI recommended by the Preliminary UMo Report, and the fuel temperature safety limits used in analyses of the USHPRR is presented in Figure 4.7. Analyses for ATR [7] used a correlation for the lower 95% CI blister temperature shown in equation 4.13, valid for fission densities greater than or equal to 1.5×10^{21} fissions/cm³, and applied up to a fission density of 4.9×10^{21} fissions/cm³ (the current maximum burnup from neutronics analysis of a prototypic cycle).

$$T_{95\%\,CI} = 1.94 \times 10^{6} \times f_d^{-0.172} \quad (4.13)$$

where $T_{95\%\,CI}$ is in °C and f_d is the fission density in fissions/cm³. It should be noted that the correlation used for the ATR analysis was from a draft version of Revision 0 of the Preliminary UMo Report. Analyses for MURR [4] utilized equation 4.10, as discussed above, and applied it to fission densities up to 3.4x10²¹ fissions/cm³, which is the maximum fission density of the MURR LEU design for prototypic operations. Analyses for MITR [6] and NBSR [24] both utilized a constant (not dependent upon burnup) fuel temperature safety limit. The fuel temperature limit was set to 350°C up to a fission density of 5.0x10²¹ fissions/cm³ for MITR analyses and 380°C up to a fission density of 7.2x10²¹ fissions/cm³ for NBSR analyses. There was no explicit mention of the blister temperature in the report for HFIR [3].

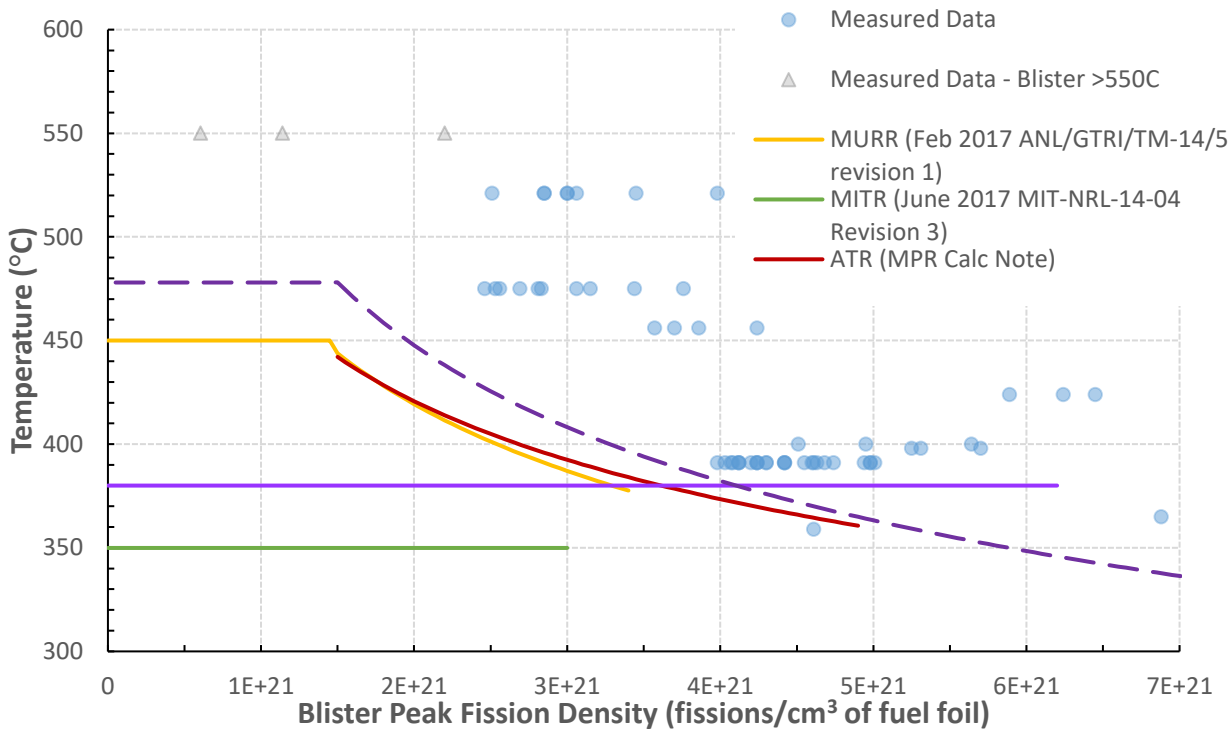

Figure 4.7. Comparison of the fuel temperature limits of analyses for the USHPRR, the Preliminary UMo Report, and the measured blister temperature [100].

All reactor assumptions are in reasonable agreement with the Preliminary UMo Report [1], or are more conservative. An exception is noted for the value assumed for analyses of the NBSR [5,35] for fission densities greater than 4.1x10²¹ fissions/cm³. However, the assumed temperature limit is still lower than all but two measured blister temperature data points, so it is still a valid assumption for the 95% CI temperature limit. Although all safety analyses that address the temperature limit are reasonably conservative, additional data is required. In particular, data for fresh fuel and burnups greater than 5×10²¹ fissions/cm³ are limited. This data is necessary to develop a correlation for the fuel temperature safety limit from fresh fuel through full burnup of 6.2×10²¹ fissions/cm³ for the USHPRR for each type of potentially limiting plate geometry.

5 Conclusions

This report has reviewed the materials properties and fuel performance correlations important for modeling the LEU U-10Mo monolithic fuel proposed to convert high performance RTR currently operating with HEU and which cannot be converted with currently qualified LEU fuel forms. Collection and comparison of the data available in the open literature for the LEU properties reviewed was conducted to determine consistency between those available sources, and to identify any knowledge gaps.

The collected literature data was used to assess the reasonableness of the documented data inputs and property assumptions used in the conversion analysis of each of the USHPRR that have been performed to date. Reactor-specific application of available data is expected due to the different operating regimes and the fuel-dependent safety basis requirements. However, even with a range of input data parameters, this report presents a significantly consistent, and what is acknowledged as conservative, use of the available data among the USHPRR and within the literature.

It is particularly important to note that all LEU data presented herein requires confirmation by the Fuel Qualification (FQ) Pillar with the prototypic fuel that has been selected and that is scheduled to begin qualification irradiation tests. There remain several important areas where it is recommended that FQ should gather additional data on fuel plates made with the prototypic fabrication process that is currently being used to qualify the fuel.

- It is imperative to collect a set of density values for U-10Mo as a function of temperature and irradiation on samples considered to be prototypic of the monolithic fuel foil to establish accurate values and a clear understanding of the uncertainties.
- Data for fuel homogeneity from prototypic foils is needed so that the correct tolerances for the fuel surface density can be used for analysis.
- Limited data on the effect of irradiation on thermal conductivity of the fuel is available, and it is considered to be of great importance that additional data is collected, as discussed in detail in Section 2.6.1.
- Another key area of additional experimental measurements necessary for qualification is measurements of the blister anneal temperature on a statistically significant number of plates prototypic of each USHPRR fuel element design. The bounds of this data should cover the range from fresh fuel up to the anticipated maximum fission densities and beyond the anticipated maximum fuel temperatures for postulated accidents in the USHPRRs.
- The irradiation test "target" conditions for the fuel qualification tests need to allow for various uncertainties. These uncertainties include:
    - Uncertainties in the best-estimate plate-level calculations for each USHPRR design parameter for maximum local fission density and power density
    - Uncertainties in the calculations performed during the irradiation test planning and design
    - Uncertainties in the irradiation test operating cycle duration, reactor power, and local experiment power which will impact the data (e.g. fixed duration cycles provide discrete steps in fission density if irradiated for another cycle)
    - Uncertainties in measured data and correlations generated from post-irradiation examination (PIE).

  Since irradiation test targets will never be precisely achieved, it is important to note that the first three sources of uncertainties are part of the planning process, and the final uncertainty is on the data gathered and correlations generated from the irradiation test measurements. Still, all these uncertainties are critical to allow that the experiment reach

appropriate levels for each design parameter. This emphasizes the importance of accounting for these appropriately to establish exit criteria for irradiation tests, such as continuing the irradiation until 50% of plates reach target values with an expected distribution of data above and below the best-estimate values plus some additional margin. Also of note is that while the plate-level data is targeting these bounding values to gather fuel qualification data, there are subsequent reactor-specific demonstration tests of full elements planned that are intended to test to prototypic parameters.

- Lastly, when performing reactor safety analyses, it is important to consider the uncertainties in experimental data for fuel properties and performance. For this reason, experimental uncertainties for measured data and/or correlations should be consistently reported and, when the uncertainties are reported, the level of the uncertainty value must be documented (i.e.: 1 σ, 95% CI, etc.). Whereas the above work is under the FQ Pillar, when the Reactor Conversion Pillar finds that uncertainty values are not available, a sensitivity study must be conducted to properly understand the impact of any variation on the safety margins.

Acknowledgements

This work was sponsored by the U.S. Department of Energy, Office of Material Management and Minimization in the U.S. National Nuclear Security Administration Office of Defense Nuclear Nonproliferation under Contract DE-AC02-06CH11357.

The authors would like to acknowledge that this work could not have been possible without the prior work produced by the staff from each of the organizations within the US High Performance Research Reactor Project's Reactor Conversion Pillar. The staff members at the Massachusetts Institute of Technology Nuclear Reactor Laboratory, University of Missouri Research Reactor (MURR), Department of Commerce National Institute of Standards and Technology National Center for Neutron Research, as well as Brookhaven, Idaho, Oak Ridge and Argonne National Laboratories are recognized for their contributions. The authors would like to acknowledge, in particular, the efforts of Barry Rabin and James Cole, Fuel Qualification Pillars, and their entire staff for dedication in developing the experimental results and interpretations from Idaho, Pacific Northwest, and Argonne National Laboratories that have been cited. The authors are also thankful for the helpful suggestions provided by Jim Snelgrove and Gerard Hofman of Argonne National Laboratory during the preparation of this work.

References

1. Rabin, B, et al. Preliminary Report on U-Mo Monolithic Fuel for Research Reactors, revision 1. Idaho Falls, ID: Idaho National Laboratory, 2017. INL/EXT-17-40975 Revision 1.
2. Massalski, T. Binary alloy phase diagrams, 2nd edition. Materials Park, OH: ASM International, 1990.
3. Popov, E, et al. Interim Basis for Analysis of the Performance and Safety of the High Flux Isotope Reactor for Conversion to LEU Fuel. Oak Ridge, TN: Oak Ridge National Laboratory, 2017.
4. Stillman, J, et al. Accident Analyses for Conversion of the University of Missouri Research Reactor (MURR) from Highly-Enriched to Low-Enriched Uranium. Lemont, IL: Argonne National Laboratory, 2017. ANL/GTRI/TM-14/5, rev.1.
5. Baek, J-S. NBSR Calculation Notebook RELAP5 Models for Non-LOCA Events. Upton, NY: Brookhaven National Laboratory, 2015.
6. Sun, K, et al. Accident Analysis for Conversion of the MIT Research Reactor (MITR) from Highly Enriched Uranium to Low Enriched Uranium using an Unfinned Fuel Element. Cambridge, MA: Massachusetts Institute of Technology, 2017. MIT-NRL-14-04 Rev 3.
7. Rashid, R. Mark 1A ELF Thermal Hydraulic Inputs. Washington, DC: MPR, 2017. 1129-0076-CALC-003 Revision 1.
8. McGeary (ed.), R K, et al. Development and Properties of Uranium-Base Alloys Corrosion Resistant in High Temperature Water. Atomic Power Division. Pittsburgh, PA: Westinghouse Electric Corporation, 1955. WAPD-127.
9. Meyer, M K and Woolstenhulme, N E. Density of U-Mo Alloys. Idaho Falls: Idaho National Laboratory, 2011. TEV-1338.
10. Burkes, Douglas E, et al. Thermo-physical properties of DU–10 wt.% Mo alloys. Journal of Nuclear Materials, 2010, Vol. 403 (1-3), pp. 160-166.
11. Wilson, A S and Rundle, R E. The structures of uranium metal. Acta Crystallographica, 1949, Vol. 2 (1), pp. 126-127.
12. Lee, S-H, et al. An Investigation on Thermophysical Properties of U-Mo Dispersion Fuel Meats. Las Vegas, NV, USA: 2000 International Meeting on Reduced Enrichment for Research and Test Reactors, 2000. pp. 261-272.
13. Del Grosso, A. Technical Memorandum No. 3: Compilation of U-10 w/o Mo Fuel Alloy Properties. Detroit, MI: Atomic Power Development Associates, Inc., 1957. AECU-3679.
14. Burkes, D E, Mickum, G S and Wachs, D M. Thermophysical Properties of U-10Mo Alloy. Idaho Falls, ID: Idaho National Laboratory, 2010. INL/EXT-10-19373.
15. Gates, John E, et al. Irradiation Studies of Uranium-10 w/o Molybdenum Fuel Alloy. Columbus, Ohio: Battelle Memorial Institute, 1961. BMI-APDA-660.
16. Dwight, Austin E. The uranium-molybdenum equilibrium diagram below 900° C. Journal of Nuclear Materials, 1960, Vol. 2 (1), pp. 81-87.
17. Bridge, J R, Schwartz, C M and Vaughan, D A. X-Ray Diffraction Determination of the Coefficients of Expansion of Alpha Uranium. Journal of Metals, 1956, Vol. 8(10), pp. 1282-1285.

18. Kim, C K, et al. Fabrication of Atomized U-Mo Dispersion Rod Type Fuel for Irradiation Test Related to Qualification Program. Las Vegas, NV: 2000 International Meeting on Reduced Enrichment for Research and Test Reactors, 2000.

19. Specification for Low Enriched Uranium Monolithic Fuel Plates. Idaho Falls, ID: Idaho National Laboratory, 2019. SPC-1635, Rev. 11.

20. Betzler, B R and Chandler, D. Modeling and depletion simulations for a HFIR cycle with LEU interim fuel design. Oak Ridge, TN: Oak Ridge National Laboratory, 2016. C-HFIR-2016-004.

21. Ilas, G and Primm III, R T. Low enriched uranium fuel design with two-dimensional grading for the High Flux Isotope Reactor. Oak Ridge, TN: Oak Ridge National Laboratory, 2011. ORNL/TM-2010/318.

22. Joshi, V, Tegtmeier, E and Prabhakaran, R. USHPRR/FF Pillar Technical Bulletin: Density of Bare LEU-10wt%Mo. Richland, WA: Pacific Northwest National Laboratory, 2018. PNNL-SA-138487.

23. Klein, J L. Nuclear Reactor Fuel Elements: Metallurgy and Fabrication. [ed.] A R Kaufmann. New York: Interscience Publishers, 1962. pp. 69-72.

24. Diamond, D J, Baek, J-S and Hanson, A L. Conversion preliminary safety analysis report for the NIST research reactor. Upton, NY: Brookhaven National Laboratory, 2014. BNL-107265-2015-IR.

25. Bergeron, A, et al. Low Enriched Uranium Core Design for the Massachusetts Institute of Technology Reactor (MITR) with Un-finned 12 mil-thick Clad Monolithic Fuel. Lemont, IL: Argonne National Laboratory, 2013. ANL/GTRI/TM-13/15.

26. Chemistry, Royal Society of. Periodic Table - Molybdenum. Chemistry RSo. [Online] 2017.

27. Kim, Yeon Soo and Hofman, Gerard L. Fission product induced swelling of U–Mo alloy fuel. Journal of Nuclear Materials, 2011, Vol. 419 (1-3), pp. 291-301.

28. Burkes, D E, et al. Fuel Thermo-physical Characterization Project: Fiscal Year 2013 Final Report. Richland, WA: Pacific Northwest National Laboratory, 2013. PNNL-22981.

29. Burkes, D E, et al. Fuel Thermo-physical Characterization Project: Fiscal Year 2014 Final Report. Richland, WA: Pacific Northwest National Laboratory, 2015. PNNL-24135.

30. Robinson, A., Burkes, D., Adkins, C. Qualification of U-Mo thermal properties data. Idaho Falls, ID; Idaho National Laboratory, 2020. TEV-3464

31. Burkes, D E, et al. Thermal properties of U–Mo alloys irradiated to moderate burnup and power. Journal of Nuclear Materials, 2015, Vol. 464, pp. 331-341.

32. Farkas, M S. Mechanical and Physical Properties of Fuels and Cladding Materials with Potential for use in Brookhaven's Pulsed Fast Reactor. Columbus, OH: Battelle Memorial Institute, 1967. BMI-X-455.

33. Fackelmann, J M, Bauer, A A and Moak, D P. Literature Survey on Dilute Uranium Alloys for Sandia Booster Concept to Sandia Corporation. Columbus, OH: Battelle Memorial Institute, 1969. BMI-X-10264.

34. Wachs, D M, et al. Draft Report on Information Relevant to U-Mo Fuel Design, rev 3. Idaho Falls, ID: Idaho National Laboratory, 2013. INL/LTD-12-25703.

35. Baek, J-S. NBSR Calculation Notebook Thermal-Hydraulic Models for LOCA. Upton, NY: Brookhaven National Laboratory, 2015.

36. Progress Report on Metallurgy of Tuballoy to University of Chicago from Battelle Memorial Institute. Columbus, OH: Battelle Memorial Institute, 1945. CT-2632.

37. Westphal, R C. Thermal conductivity of reactor fuel element materials. Pittsburgh, PA: Westinghouse Electric Corporation, Atomic Power Division, 1954. AECD-3864.

38. Hengstler, R M, et al. Physical properties of monolithic U8 wt.%-Mo. Journal of Nuclear Materials, 2010, Vol. 402(1), pp. 74-80.

39. Konobeevsky, S T, et al. Some Physical Properties of Uranium, Plutonium and their Alloys. Geneva, Switzerland: United Nations International Conference on the Peaceful Uses of Atomic Energy, 1958. Vol. 6, pp. 194-203.

40. Matsui, T, Natsume, T and Naito, K. Heat Capacity Measurements of U0.80Zr0.20 and U0.80Mo0.20 Alloys from Room Temperature to 1300K. Journal of Nuclear Materials, 1989, Vol. 167, pp. 152-159.

41. Roy, C, Radenac, A and Cado, F. Conductivite Thermique d'un Alliage D'Uranium A 10% en Poids de Molybdene Entre 320K et 680K. Journal of Nuclear Materials, 1973, Vol. 48 (3), pp. 369-371.

42. Saller, H A, et al. Properties of a Fissium-Type Alloy. Columbus, Ohio: Battelle Memorial Institute, 1956. BMI-1123.

43. Rest, J, et al. U-Mo Fuels Handbook. Lemont, IL: Argonne National Laboratory, 2009. ANL-09/31.

44. Touloukian, Y S. Thermophysical properties of matter. Lafayette, IN: Purdue University, 1970-1979.

45. Kim, Y. S., Cho, Tae Won and Sohn, Dong-Seong. Thermal conductivities of actinides (U, Pu, Np, Cm, Am) and uranium-alloys (U–Zr, U–Pu–Zr and U–Pu–TRU–Zr). Journal of Nuclear Materials, 2014, Vol. 445 (1-3), pp. 272-280.

46. Kim, Y S and Hofman, G. AAA Fuels Handbook. Lemont, IL: Argonne National Laboratory, 2003. ANL-AAA-068.

47. Bruggeman, D.A.G. Berechnung verschiedener physikalischer Konstanten von heterogenen Substanzen: I-Dielektrizitatskonstanten und Leitfahigkeiten der Mischkorprt aus isotropen Substanzen. Annalen der Physik, 1935, Vol. 416(7), pp. 636-664.

48. Peddicord, K L, Cunningham, M E and Tripathi, A. Porosity correction to thermal conductivity based on analytical temperature solutions. San Diego, CA: ANS Annual Meeting, 1978. Vol. 28, pp. 548-549.

49. Huber, T K, et al. First results of scanning thermal diffusivity microscope (STDM) measurements on irradiated monolithic and disperse fuel. Warsaw, Poland: International Meeting on Reduced Enrichment for Research and Test Reactors, 2012.

50. Gan, J, et al. Irradiated microstructure of U-10Mo monolithic fuel plate at very high fission density. Journal of Nuclear Materials, 2017, Vol. 492, pp. 195-203.

51. Rabin, B. irradiated U-Mo thermal conductivity data. Personal Communication to E. Woolstenhulme. 2017.

52. Dunn, F E, et al. Preliminary Accident Analysis for Conversion of the Massachusetts Institute of Technology Reactor (MITR) from Highly Enriched to Low Enriched Uranium. Lemont, IL: Argonne National Laboratory, 2017. ANL/GTRI/TM-13/5.

53. Metzroth, K. Thermal Conductivity of U-10Mo Fuel. MPR, 2017. 1129-0078-LTR-001 Rev 0.

54. Nomine, A M, Collogue sur la rupture des materiaux. Grenoble, France: Societe Francaise de Metallurgie, January 19-21, 1972.

55. Hoge, K G. Some mechanical properties of uranium-10 molybdenum alloy under dynamic tension loads. Journal of Basic Engineering, 1966, Vol. 88(2), pp. 509-517.

56. Waldron, M B, Burnett, R C and Pugh, S F. The Mechanical Properties of Uranium-Molybdenum Alloys. Harwell, UK: Atomic Energy Research Establishment (AERE), 1958. AERE-M/B-2554.

57. Burkes, D E, et al. Mechanical Properties of DU-xMo Alloys with x=7 to 12 Weight Percent. Metallurgical and Materials Transactions A, 2009, Vol. 40(5), pp. 1069-1079.

58. Schulthess, J. Elevated Temperature Tensile Tests on DU-10Mo Rolled Foils. Idaho Falls, ID: Idaho National Laboratory, 2015. INL/EXT-14-33639.

59. Lloyd, W R, et al. Mechanical Properties Characterization of Irradiated U–10Mo Fuel. Idaho Falls, ID: Idaho National Laboratory, 2015. INL/LTD-15-34764.

60. Rabin, B H, et al. Four-point bend testing of irradiated monolithic U-10Mo fuel. Bucharest, Romania: European Research Reactor Conference (RRFM), 2015. pp. 126-141.

61. Tentner, A, et al. Evaluation of thin plate hydrodynamic stability through a combined numerical modeling and experimental effort. Lemont, IL: Argonne National Laboratory, 2017. ANL/RTR/TM-16/9.

62. Ozaltun, H, Herman Shen, M H and Medvedev, P. Assessment of residual stresses on U10Mo alloy based monolithic mini-plates during Hot Isostatic Pressing. Journal of Nuclear Materials, 2011, Vol. 419(1-3), pp. 76-84.

63. Reese. Evaluation of Young's Modulus and Anisotropy in Cold Rolled DU-10Mo Foils Using Laser Ultrasonic Methods, Rev. 0. Idaho Falls: Idaho National Laboratory, 2013. TEV-1799.

64. Davis, J R, et al., [ed.]. ASM Handbook Formerly Tenth Edition, Metals Handbook. 1990. Vols. Volume 2 Properties and Selection: Nonferrous Alloys and Special-Purpose Materials.

65. Lloyd, R, et al. Evaluation of 6061 Al Alloy Mechanical Properties of Fuel Plate Cladding: HIP-Bonded Fuel Plates. Idaho Falls, ID: Idaho National Laboratory, 2013. TEV-1758.

66. Davis, J R. ASM Specialty Handbook- Aluminum and Aluminum Alloys. ASM International, 1993.

67. Cheon, J S and Kim, Y S. Material Properties of Aluminum Alloys and Pure Zirconium for Use in High-Density Fuel Development for Research Reactors. Lemont, IL: Argonne National Laboratory, 2012. ANL/RERTR/TM-12-6.

68. Metallic Materials and Elements for Aerospace Vehicle Structures. Department of Defense, 2003. MIL-HDBK-5J.

69. Polkinghorne, S T and lacy, J M. Thermo-physical and mechanical properties of ATR core materials. Idaho Falls, ID: EG&G Idaho, Inc., Idaho National Engineering Laboratory, 1991. PG-T-91-031.

70. Metallic Materials and Elements for Aerospace Vehicle Structures. Department of Defense, 1998. MIL-HDBK-5H.

71. Kaufman, J.G., [ed.]. Properties of Aluminum Alloys: Tensile, Creep and Fatigue Data at High and Low Temperatures. ASM International, 1999.

72. Martin, W.R.; Weir, J.R. Mechanical Properties of X8001 and 6061 Aluminum Alloys and Aluminum-Base Fuel Dispersion at Elevated Temperatures. Oak Ridge, TN: Oak Ridge National Laboratory. ORNL-3557.

73. Alexander, D J, et al. Tensile Properties of 6061 Aluminum Alloy Materials. Los Alamos, NM: Los Alamos National Laboratory. LA-UR-11-06707.

74. Farrell, K and King, R T. Tensile Properties of Neutron-Irradiated 6061 Aluminum Alloy in Annealed and Precipitation-Hardened Conditions. Oak Ridge, TN: Oak Ridge National Laboratory, 1979. conf-780722--9.

75. Jeong, Gwan Yoon, Kim, Yeon Soo and Sohn, Dong-Seong. Mechanical analysis of UMo/Al dispersion fuel. Journal of Nuclear Materials, 2015, Vol. 466, pp. 509-521.

76. Matzke, H J. Radiation enhanced diffusion in UO2 and (U, Pu)O2. Radiation Effects, 1983, Vol. 75(1-4), pp. 317-325.

77. Farrell, K. Performance of Aluminum in Research Reactors. [ed.] Rudy J. M. Konings. Comprehensive Nuclear Materials. Elsevier, 2012, Vol. 5, pp. 143-175.

78. Farrell, K. Assessment of Aluminum Structural Materials for Service Within the ANS Reflector Vessel. Oak Ridge, T: Oak Ridge National Laboratory, 1995. ORNL/TM-13049.

79. Kim, Yeon Soo, et al. Oxidation of aluminum alloy cladding for research and test reactor fuel. Journal of Nuclear Materials, 2008, Vol. 378(2), pp. 220-228.

80. Ervine, G and Osborn, E F. The System Al2O3-H2O. The Journal of Geology, 1951, Vol. 59(4), pp. 381-394.

81. Griess, J C, Savage, H C and English, J L. Effect of heat flux on the corrosion of aluminum by water, part IV. Tests relative to the advanced test reactor and correlation with previous results. Oak Ridge, TN: Oak Ridge National Laboratory, 1964. ORNL-3541.

82. Anthony, J W, et al. Handbook of Mineralogy. Chantilly, VA: Mineralogical Society of America, 1997. Vol. III.

83. Wefers, K and Misra, C. Oxides and Hydroxides of Aluminum. Alcoa Laboratories, 1987. Technical Paper 19, revised.

84. Fricke, R and Severin, H., Uber die Zersetzungsdrucke kristallisierter Hydroxyde insbesondere von Aluminum und Beryllium. Zeitschrift für anorganische und allgemeine Chemie, Vol. 205(3), pp. 287-308, 1932.

85. Hemingway, B S, Robie, R A and Apps, J A. Revised values for the thermodynamic properties of boehmite, AlO(OH), and related species and phases in the system Al-H-O. American Mineralogist, 1991, Vol. 76, pp. 445-457.

86. Griess, J C, et al. Effect of Heat Flux on the Corrosion of Aluminum by Water Part III: Final Report on Tests Relative to the High-Flux Isotope Reactor. Oak Ridge, TN: Oak Ridge National Laboratory, 1961. ORNL-3230.

87. Miller, G L. Zirconium. Academic Press, 1957.

88. Fink, J K and Leibowitz, L. Thermal conductivity of zirconium. Journal of Nuclear Materials, 1995, Vol. 226(1-2), pp. 44-50.

89. Mohamed, W, Ozaltun, H, and Roh, H S. Effect of Zr Diffusion Barrier Properties on the Irradiation Performance of U-10Mo Monolithic Fuel Plate. Snowbird, UT. Proceedings of the ASME 2019 Power Conference July 14-18, 2019.

90. Feldman, E E, et al. Preliminary Accident Analysis for Conversion of the University of Missouri Research Reactor (MURR) from Highly-Enriched to Low-Enriched Uranium. Lemont, IL: Argonne National Laboratory, 2013. ANL/GTRI/TM-13/7.

91. Diamond, D J. Variations in NBSR LEU Fuel Plate Loading and Dimensions. Upton, NY: Brookhaven National Laboratory, 2017.

92. Kim, Yeon Soo, et al. Fission induced swelling and creep of U–Mo alloy fuel. Journal of Nuclear Materials, 2013, Vol. 437(1-3), pp. 37-46.

93. Hofman, G, Kim, Y S and Robinson, A. Fission Induced Swelling and Creep of Uranium-Molybdenum Alloy Fuel. Vienna, Austria: International Topical Meeting on Research Reactor Fuel Management, 2009. pp. 161-165.

94. Posey, J C. Release of Fission Products from Miniature Fuel Plates at Elevated Temperature. Lemont, IL: Argonne National Laboratory, 1982. Proceedings of the International Meeting on Research and Test Reactor Core Conversions from HEU to LEU Fuel. ANL/RERTR/TM-4.

95. Shibata, T, et al. Release of Fission Products from Irradiated Aluminide Fuel at High Temperatures. Nuclear Science and Engineering, 1984, Vol. 87(4).

96. Guidelines for Preparing and Reviewing Applications for the Licensing of Non-Power Reactors, Standard Format and Content. United States Nuclear Regulatory Commission, 1996. NUREG-1537, Part 1.

97. Guidelines for Preparing and Reviewing Applications for the Licensing of Non-Power Reactors, Standard Format and Content. United States Nuclear Regulatory Commission, 1996. NUREG-1537, Part 2.

98. Beeston, J M, et al. Development and Irradiation of Uranium Aluminide Fuels in Test Reactors. Nuclear Technology, 1980, Vol. 49(1), pp. 136-149.

99. Gahlert, S and Nazare, S. Bestrahlungsverhalten von UAlx-Al Dispersionbrennstoffen auf HEU-Basis; ein Literaturstudie. Institut für Material und Festkörperforschung, Kernforschungszentrum Karlshrue GmbH, 1983. 15-01-o2P01A.

100. Rice, F, et al. Preliminary Blister Anneal Testing Results for U-Mo Monolithic Fuel Plates. Idaho Falls, ID: Idaho National Laboratory, 2015. INL/LTD-14-33608 Revision 1.

101. Rice, F, et al. Preliminary Blister Anneal Testing Results for U-Mo Monolithic Fuel Plates. Idaho Falls, ID: Idaho National Laboratory, 2015. INL/LTD-14-33608, Revision 2.

Appendix A: Tabulated Density Values

Density variation with Mo content

Weight % Mo	Density (g/cm³)	Source	Notes
6.2	17.7	McGeary [8]	Data points on plot digitized by Argonne National Laboratory
11.9	16.8		
15.0	16.6		
15.9	16.5		
18.4	16.2		
24.9	15.4		
10.34	16.9	Meyer-TEV-1338 [9]	
8.08	16.98		
6.08	17.60		
3.95	17.96		
11.15	17.08	Meyer-TEV-1338 [9]	Data points averaged for linear fit
11.15	17.14		
10	16.48	Lee [12]	Data points averaged for linear fit
10	16.65		

Linear fit from [9]:

$$\rho_{U-Mo} = -0.0763X_{Mo} + 17.763 \quad \text{(A.1)}$$

New linear fit:

$$\rho_{U-Mo} = -0.110X_{Mo} + 18.16 \quad \text{(A.2)}$$

where X_{Mo} is the weight percent of molybdenum and $\rho_{U\text{-}Mo}$ is the density of the U-Mo alloy in g/cm³.

Density variation with Temperature

Temperature (°C)	Density (g/cm³)	Source	Notes
29.0	17.1	McGeary [8]	Crossed-out data points were those that were discarded as outliers. Data points on plot digitized by Argonne National Laboratory
175.5	17.1		
185.6	17.0		
~~196.7~~	~~16.7~~		
256.0	16.9		
285.5	16.9		
~~301.5~~	~~16.6~~		
351.2	17.0		
376.9	16.9		
406.7	16.8		
437.5	16.7		
464.6	16.9		
478.6	16.7		
489.2	16.7		
555.6	16.7		
572.8	16.8		
100	16.38	Burkes [10]	Although the density values are well below the expected value (due to as-fabricated porosity), the slope of the data fit of this
200	16.31		
300	16.23		
400	16.14		
500	16.06		

550	16.02		data is still accepted, as that does not depend on porosity.
600	15.98		
700	15.9		
25	17.13	Klein [23]	This data set is not independent. The source for the data was cited as an APDA contact, McGeary worked for APDA, and the data lies along the recommended data fit line from McGeary's report.
100	17.06		
200	16.97		
300	16.88		
400	16.8		
500	16.71		
550	16.66		

Appendix B: Tabulated Thermal Conductivity Values

Mo content and temperature dependence of the thermal conductivity of U-Mo alloy fuel

Weight % Mo	Temperature (°C)	Thermal Conductivity (W/m-K)	Source	Notes
5	125	16	(a) Curve 3 Touloukian [44]	In Touloukian [44] curves 3 and 5 are designated as gamma phase, while curve 4 is alpha phase. Comparison with source data [36] revealed that curves 3 and 4 are gamma, and 5 is alpha.
	190	18		
	255	20.5		
	312	22	Data from BMI [36]	
	120	16	(b) Curve 4 Touloukian [44]	
	188	18		
	250	20.5		
	310	22	Data from BMI [36]	
8	50	14.4	McGeary [8] Data from Westphal [37]	Incorrectly cited as from Lee in UMo Handbook [43]
12	50	13.8		
8	51.7	14.2	Hengstler [38]	
	74.6	14.8		
	99.2	16.0		
	122.7	16.7		
	143.8	17.2		
	181.2	19.5		
	232.3	20.6		
9	100	16.7	Konobeevsky [39]	Data set not included in correlation development, as the data trend is in disagreement with all other data sets.
	200	20.9		
	300	26.8		
	400	32.6		
	500	38.5		
9.2	20	14.3	Matsui [40]	
	100	16.6		
	200	19.4		
	300	22.3		
	400	25.1		
	500	27.9		
	600	31.1		
10	25	12.1	Klein [23]	There is an error in the thermal conductivity values reproduced in the UMo Handbook [43]
	100	14.4		
	200	17.1		
	300	20.1		
	400	23.2		
	500	26.7		
	550	28.4		
	600	30.3		
	700	33.9		
10	25	9.7	Lee [12]	This data set was discarded, as the density is atypically low, leading to a decreased thermal conductivity. Incorrectly cited as McGeary in UMo Handbook [43].
	100	11.7		
	200	14		
	300	17.2		
	400	21.6		
	500	25.7		
10	50	12.97 ± 1.26	Roy [41]	

	212	17.99 ± 2.52		
	308	21.34 ± 2.52		
	404	25.94 ± 4.18		
10	20	11.9	Saller [42]	Listed twice in the UMo Handbook [43]. Once as Touloukian [44], and once as Saller [42], but with the incorrect Mo content (10.7 instead of 10).
	100	14.4		
	200	17.5		
	300	20.6		
	400	23.7		
	500	26.9		
	600	29.9		

Irradiation dependence of the thermal conductivity of U-10Mo fuel

Fission Density ($x10^{21}$ f/cm^3)	Thermal Conductivity (W/m-K)	Source	Notes
0	17	Farkas [32] Data from Del Grosso [13]	Collected at 200°C
0.100	17		
0.138	15		
0.268	15		
0.332	15		
0.016	18.09	Burkes [28]	Collected at 150°C Digitized from figure
2.903	12.29		
2.914	12.87		
3.225	10.96		
3.226	13.35		
4.127	10.37		

Appendix C: U-10Mo Elastic Modulus Irradiation Dependence

Lloyd INL-LTD-15-34764 [59]		
Sample ID	Average Fission Density (f/cm^{3}x10^{21})	E (GPa)
L1P461-15	2.1	94
L1P461-21	2.1	96
L1P461-27	2	103
L1P773-15	3.7	82
L1P773-21	3.5	86
L1P773-27	3.4	81
L1P786-15	6.2	63
L1P786-21	5.8	69
L1P786-27	5.6	63
L2P481-15	2.4	77
L2P481-21	2.3	85
L2P481-27	2.2	79
L2P482-15	2.8	80
L2P482-21	2.7	77
L2P482-27	2.7	84
L5P1B0-15	0.38	89
L5P1B0-21	0.36	87
L5P1B0-27	0.34	93
L5P3B1-15	3.8	77
L5P3B1-21	3.7	78
L5P3B1-27	3.7	75
L5P3B3-15	2.7	80
L5P3B3-21	2.5	86
L5P3B3-27	2.4	82
L5P3C2-15	2	76
L5P3C2-21	2	71
L5P3C2-27	2	69

Rabin RRFM 2015 [60]			
Sample ID	Average Fission Density (f/cm^3 x10^{21})	Flexural Stiffness (MPa/%)	Modulus (GPa)
L1P461-15	2.1	867	86.7
L1P461-21	2.1	909	90.9
L1P461-27	2	1011	101.1
L1P773-15	3.7	746	74.6
L1P773-21	3.5	770	77
L1P773-27	3.4	718	71.8
L1P786-15	6.2	566	56.6
L1P786-21	5.8	616	61.6
L1P786-27	5.6	551	55.1
L2P481-15	2.4	678	67.8
L2P481-21	2.3	794	79.4
L2P481-27	2.2	714	71.4
L2P482-15	2.8	719	71.9
L2P482-21	2.7	671	67.1
L2P482-27	2.7	769	76.9

L5P1B0-15	0.38	865	86.5
L5P1B0-21	0.36	871	87.1
L5P1B0-27	0.34	916	91.6
L5P3B1-15	3.8	729	72.9
L5P3B1-21	3.7	746	74.6
L5P3B1-27	3.7	715	71.5
L5P3B3-15	2.7	751	75.1
L5P3B3-21	2.5	838	83.8
L5P3B3-27	2.4	775	77.5
L5P3C2-15	2	707	70.7
L5P3C2-21	2	700	70
L5P3C2-27	2	625	62.5

Appendix D: Summary of Material Properties

This section is a summary of the equations and values recommended by this report and used for analyses of the USHPRR. The recommendation is based on the best data available at the time of this report, and will be updated as new data becomes available. For a detailed discussion of these correlations and values, see the section number referenced to under the Property header.

Property (section)	Reactor	Equation/Value	Reference
Melting Temperature U-10Mo (°C) (2.1)	ATR	555	[7]
	HFIR	-	
	MITR	1135	[6]
	MURR	-	
	NBSR	-	
	Recommendation	1165	[2]
Density of U-10Mo Fuel (g/cm³) (2.2.1)	ATR	17.0	[7]
	HFIR	17.02	[20, 21]
	MITR	17.02	[6]
	MURR	17.02	[4]
	NBSR	17.2	[5]
	Recommendation	17.13	[1]
Temperature Dependence of Density (g/cm³) (2.2.2)	ATR	$\rho_{U-10Mo} = \left(17.0 - 8.63 \times 10^{-4} \times \left(\left(\frac{T-32}{1.8}\right) - 20.0\right) \times (2.54^3)\right) \times \left(\frac{0.00220462}{\left(\frac{t_{swell}}{t_0}\right)+1}\right) \frac{lbm}{in^3}$	[7]
	HFIR	$\rho_{U10Mo} = 17.14 - 8.68x10^{-4}(T)$	[3]
	MITR	-	
	MURR	-	
	NBSR	-	
	Recommendation	$\rho_{U10Mo} = 17.15 - 8.766 \times 10^{-4}$	[13]
Irradiation Dependence of Density (g/cm³) (2.2.4)	ATR	$\rho_{U-10Mo} = \left(17.0 - 8.63x10^{-4} \times \left(\left(\frac{T-32}{1.8}\right) - 20.0\right) \times (2.54^3)\right) \times \left(\frac{0.00220462}{\frac{(t_{swell})}{t_0}+1}\right) \frac{lbm}{in^3}$ $t_{swell} = \frac{(5.9957x10^{-43} \times (F_d \times 10^{21})^2 + 4.30015 \times 10^{-21} \times F_d \times 10^{21})}{100 \times t_0} in$	[7]
	HFIR	see swelling correlation	
	MITR	see swelling correlation	
	MURR	see swelling correlation	
	NBSR	see swelling correlation	
	Recommendation	Use swelling correlation	

<table>
<tr><td rowspan="6">Heat Capacity of U-10Mo Monolithic Fuel J/(g K) (2.3)</td><td>ATR</td><td>$c_{U-10Mo} = \left(113 + \left(\frac{T + 459.67}{1.8}\right) \times 0.0705\right) \times 5.266 \times \frac{10^{-7}}{0.00220462} \frac{BTU}{lbm°\mathrm{F}}$</td><td>[7]</td></tr>
<tr><td>HFIR</td><td>$c_p = 0.114 + 7.23 \times 10^{-5} T$</td><td>[3]</td></tr>
<tr><td>MITR
MURR</td><td>$c_p = 0.113 + 7.05 \times 10^{-5} (T + 273.15)$</td><td>[4]</td></tr>
<tr><td>NBSR (J/mol K)</td><td>$c_p^{UMo} = 29.84 - 8.9 \times 10^{-3} T + 4.32 \times 10^{-5} T^2 - 2.06 \times 10^{-8} T^3$</td><td>[5, 35]</td></tr>
<tr><td>Recommendation</td><td>$c_p(U - 10Mo) = (0.113 \times 10^3 \pm 4.28) + (7.05 \times 10^{-2} \pm 5.20 \times 10^{-3}) \times T$</td><td>[1]</td></tr>
<tr><td>Unirradiated Thermal Conductivity (W/ (m K)) (2.5.1)</td><td>ATR</td><td>$k_{U-10Mo} = \left(0.8087 + 0.03487 \times \left(\frac{T + 459.67}{1.8}\right) + 0.6718 \times F_d - 0.0046 \times \left(\frac{T + 459.67}{1.8}\right) \times F_d\right) \times \frac{0.57779}{12 \times (60 \times 60)} \frac{BTU}{s - in - °F}$</td><td>[7]</td></tr>
<tr><td>HFIR</td><td>$k = 13.07 + 0.033 \times T$</td><td>[3]</td></tr>
<tr><td>MITR</td><td>$k = 12.57 + 0.04T - F_d \times (1.322 + 0.00278T) - T^2(2.351x10^{-5} + 4.996 \times 10^{-6} F_d)$</td><td>[6]</td></tr>
<tr><td>MURR</td><td>$k = 14.821 + 0.0309 \times T$</td><td>[4]</td></tr>
<tr><td>NBSR</td><td>Equations 2.19 to 2.22</td><td>[5, 35]</td></tr>
<tr><td>Recommendation</td><td>Combined correlation in the following section</td><td></td></tr>
<tr><td rowspan="6">Irradiated Thermal Conductivity (W/ (m K)) (2.5.2)</td><td>ATR</td><td>$k_{U-10Mo} = \left(0.8087 + 0.03487 \times \left(\frac{T + 459.67}{1.8}\right) + 0.6718 \times F_d - 0.0046 \times \left(\frac{T + 459.67}{1.8}\right) \times F_d\right) \times \frac{0.57779}{12 \times (60 \times 60)} \frac{BTU}{s - in - °F}$</td><td>[7]</td></tr>
<tr><td>HFIR</td><td>$k = 8.83 + 0.022T, for\ fd = 2.9 \times 10^{21} f/cm^2$
$k = 8.02 + 0.0127T, for\ fd = 4.11 \times 10^{21} f/cm^3$</td><td>[3]</td></tr>
<tr><td>MITR</td><td><table><tr><th>Fission Density (x10^{21} fissions/cm^3)</th><th>Ratio</th><th>Thermal Conductivity (W/m°C)</th></tr><tr><td>5.00</td><td>0.434</td><td>8.676</td></tr><tr><td>4.40</td><td>0.487</td><td>9.735</td></tr><tr><td>3.60</td><td>0.559</td><td>11.174</td></tr><tr><td>0.00</td><td>1</td><td>19.99</td></tr></table></td><td>[6]</td></tr>
<tr><td>MURR</td><td>$k = 12.57 + 0.04T - f_d(1.322 + 0.00278T) - T^2(2.351 \times 10^{-5} + 4.996 \times 10^{-6} f_d)$</td><td>[4]</td></tr>
<tr><td>NBSR</td><td>Fresh fuel values</td><td>[5]</td></tr>
<tr><td>Recommendation</td><td>$k = 11.33 + T \times 0.04175 - F_d \times (0.7908 + 0.00611 \times T)$</td><td></td></tr>
<tr><td rowspan="2">Heat Capacity AA6061 J/(g K) (3.1.3)</td><td>ATR</td><td><table><tr><th>Temperature (°F)</th><th>Volumetric Heat Capacity (BTU/in^3 °F)</th><th>Specific Heat Capacity* (J/ (g K))</th></tr><tr><td>62</td><td>0.02089</td><td>0.9146</td></tr><tr><td>260</td><td>0.02196</td><td>0.9614</td></tr><tr><td>440</td><td>0.02303</td><td>1.008</td></tr><tr><td>620</td><td>0.02411</td><td>1.056</td></tr><tr><td>800</td><td>0.02518</td><td>1.102</td></tr><tr><td>980</td><td>0.02625</td><td>1.149</td></tr><tr><td>1079</td><td>0.02684</td><td>1.175</td></tr><tr><td>1205</td><td>0.02527</td><td>1.106</td></tr><tr><td colspan="3">*calculated, density of 0.095629 lb/in^3 used</td></tr></table></td><td>[4]</td></tr>
<tr><td>HFIR</td><td>$c_p = 0.324 + 2.93 \times 10^{-3} T - 4.34 \times 10^{-6} T^2 + 2.42 \times 10^{-9} T^3$</td><td>[3]</td></tr>
</table>

<table>
<tr><td></td><td>MITR</td><td>MURR correlation</td><td>[6]</td></tr>
<tr><td></td><td>MURR</td><td>$\rho c_p = 4.252 \times 10^6 - 2.685 \times 10^3 (T + 273.15) + 2.214 (T + 273.15)^2 - 3.774 \times 10^8 (T + 273.15)^{-1}$</td><td>[4]</td></tr>
<tr><td></td><td>NBSR</td><td>0.896</td><td>[35]</td></tr>
<tr><td></td><td>Recommendation</td><td>$c_p = 0.324 + 2.93 \times 10^{-3} T - 4.34 \times 10^{-6} T^2 + 2.42 \times 10^{-9} T^3$</td><td>[67]</td></tr>
<tr><td rowspan="15">Thermal Conductivity AA6061 (W/ (m K)) (3.1.4)</td><td rowspan="2">ATR</td><td><table><tr><td>Temperature (°F)</td><td>Thermal Conductivity (BTU/ (s-in-°F)</td></tr><tr><td>80</td><td>0.00223</td></tr><tr><td>170</td><td>0.00231</td></tr><tr><td>260</td><td>0.00237</td></tr><tr><td>350</td><td>0.00239</td></tr><tr><td>440</td><td>0.00251</td></tr><tr><td>530</td><td>0.00255</td></tr><tr><td>620</td><td>0.00254</td></tr><tr><td>710</td><td>0.00251</td></tr><tr><td>800</td><td>0.00247</td></tr><tr><td>890</td><td>0.00243</td></tr><tr><td>980</td><td>0.00239</td></tr><tr><td>1079</td><td>0.00234</td></tr><tr><td>1205</td><td>0.00116</td></tr><tr><td>1340</td><td>0.00119</td></tr><tr><td>1520</td><td>0.00122</td></tr><tr><td>1700</td><td>0.00126</td></tr></table></td><td>[7]</td></tr>
<tr><td>HFIR</td><td>$k = 106 + 0.149T + 8.47 \times 10^{-5} T^2 - 2.14 \times 10^{-7} T^3$</td><td>[3]</td></tr>
<tr><td>MITR</td><td>MURR Correlation</td><td>[6]</td></tr>
<tr><td>MURR</td><td>$k = 147.8 + 0.1792T - 2.616 \times 10^{-4} T^2$</td><td>[4]</td></tr>
<tr><td>NBSR</td><td>180 (AA6061-O)</td><td>[5, 35]</td></tr>
<tr><td>Recommendation</td><td>$k = 106 + 0.149T + 8.47 \times 10^{-5} T^2 - 2.14 \times 10^{-7} T^3$</td><td>[67]</td></tr>
<tr><td rowspan="6">Heat Capacity Boehmite (J/(g K)) (3.2.2)</td><td>ATR</td><td>-</td><td>[7]</td></tr>
<tr><td>HFIR</td><td>-</td><td>[3]</td></tr>
<tr><td>MITR</td><td>MURR Assumption</td><td>[6]</td></tr>
<tr><td>MURR</td><td>0.33x10^{-6} (1 J/m^3°C assumed, converted with density= 3.03 g/cm^3)</td><td>[4]</td></tr>
<tr><td>NBSR</td><td>-</td><td>[5, 35]</td></tr>
<tr><td>Recommendation</td><td>$c_p = 3.4043 \times 10^{-3} + 3.83 \times 10^{-3} T - 2.694 \times 10^{-6} T^2$ (0.905 at 25°C)</td><td>[85]</td></tr>
<tr><td></td><td>Note</td><td>Assumptions by reactors conservative, but reasonable due to the minimal effect of oxide presence on the safety analysis.</td><td></td></tr>
<tr><td rowspan="5">Thermal Conductivity Oxide (W/(m K) (3.2.3)</td><td>ATR</td><td>2.25</td><td>[7]</td></tr>
<tr><td>HFIR</td><td>$k_{oxide} = 2.25$ x < 0.001” (25μm)
$k_{oxide} = 2.25 - 0.016(x - 25)$ 0.001” ≤ x ≤0.004”</td><td>[3]</td></tr>
<tr><td>MITR</td><td>2.25</td><td>[6]</td></tr>
<tr><td>MURR</td><td>2.25</td><td>[4]</td></tr>
<tr><td>NBSR</td><td>-</td><td>[5, 35]</td></tr>
</table>

	Recommendation	2.25	[86]
Density of Zr (g/cm^3) (3.3.1)	ATR	0.237356 (lbm/in^3) = 6.57 g/cm^3	[7]
	HFIR	$\rho_{Zr} = 6.518 - 0.0827 \times 10^{-3}T - 4.803 \times 10^{-8}T^2 + 7.322 \times 10^{-12}T^3$	[3]
		6.52	[20]
	MITR	MURR Assumption	[6]
	MURR	6.57	[4]
	NBSR	6.52	[5, 35]
	Recommendation	$\rho = \frac{1}{(1+\Delta T\,\bar{\alpha}_l)^3}\rho_0$	
Thermal Expansion of Zr ($x10^{-6}\ K^{-1}$) (3.3.1)	ATR	-	[7]
	HFIR	$LTE = -1.11 \times 10^{-3} + 2.325 \times 10^{-6}T + 5.595 \times 10^{-9}T^2 - 1.768 \times 10^{-12}T^3$	[3]
	MITR	-	[6]
	MURR	-	[4]
	NBSR	-	[5, 35]
	Recommendation	$\bar{\alpha}_l = 3.4556 + 0.00400435 \times (T + T_0) - 1.07437 \times 10^{-6} \times (T^2 + T \times T_0 + {T_0}^2)$	
Heat Capacity Zr (J/(g K)) (3.3.2)	ATR	$c_{Zr} = \left[24.1618 + 8.7558 \times 10^{-3} \times \frac{(T+459.67)}{1.8} - 6.9942 \times \frac{10^4}{\left(\frac{(T+459.67)}{1.8}\right)^2}\right] \times 5.266 \times 10^{-4} \times \frac{1}{91.224 \times 0.00220462}$	[7]
	HFIR (J/(kg K))	$c_{Zr} = 187.38 + 0.583T - 0.001258T^2 + 1.0155 \times 10^{-6}T^3$	[3]
	MITR	MURR Assumption	[6]
	MURR	$\rho c_p = 1.859 \times 10^6 + 739.2\ T$	[4]
	NBSR	0.27 (assuming density of 6.52 g/cm^3)	[5
	Recommendation	$c_p = 0.2476 + 1.023 \times 10^{-4}T$ (if linear relationship required) $c_p = 22.839 + 9.091 \times 10^{-3}T - 2.132 \times 10^4 T^{-2}$ (if inverse relationship allowed)	[46, 67]
Thermal Conductivity Zr (W/(m K)) (3.3.3)	ATR	$k_{Zr} = \left(8.8527 + 7.0820 \times 10^{-3} \times \frac{T+459.67}{1.8} + 2.5329 \times 10^{-6} \times \left(\frac{T+459.67}{1.8}\right)^2 + 2.9918 \times 10^3 \times \left(\frac{T+459.67}{1.8}\right)^{-1}\right) \times \frac{0.57779}{12 \times (60 \times 60)}\ \frac{BTU}{s\ in\ °F}$	[7]
	HFIR	$k_{Zr} = 36.84 - 0.077T + 1.259 \times 10^{-4}T^2 - 8.966 \times 10^{-8}T^3 + 3.168 \times 10^{-11}T^4 - 4.413 \times 10^{-15}T^5$	[3]
	MITR	MURR Recommendation	[6]
	MURR	$k_{Zr}(T) = 8.8527 + 7.0820 \times 10^{-3}T + 2.5329 \times 10^{-6}T^2 + 2.9918 \times 10^3 T^{-1}$	[4]
	NBSR	22.7	[5]
	Recommendation	$k_{Zr}(T) = 8.8527 + 7.0820 \times 10^{-3}T + 2.5329 \times 10^{-6}T^2 + 2.9918 \times 10^3 T^{-1}$	[88]
Swelling Correlation (%) (4.1)	ATR	$t_{swell} = \frac{(5.69957 \times 10^{-43}(f_d \times 10^{21})^2 + 4.30015 \times 10^{-21} \times f_d \times 10^{21})t_0}{100}\ in$	[7]
	HFIR	Recommended Correlation	[3]
	MITR	Recommended Correlation	[6]
	MURR	Channel closure of 8mil after fabrication	[4, 90]
	NBSR	$\frac{\Delta t}{t_0}(\%) = 0.5700{f_d}^2 + 4.300 f_d$	[91]

	Recommendation	$\left(\frac{\Delta V}{V_0}\right)_f = 0.05\, f_d, \quad for\ f_d \le 3\times10^{21}\ fissions/cm^3$ $\left(\frac{\Delta V}{V_0}\right)_f = 0.15 + 0.063(f_d - 3) + 0.0033(f_d - 3)^2, \quad for\ 3\times10^{21} < f_d\ fissions/cm^3$	
95% CI Blister Temperature (4.3)	ATR	$T_b = 1.94 \times 10^6 \times {f_d}^{-0.172}$	[7]
	HFIR	-	
	MITR	350°C up to a fission density of 5.0x10^{21} fissions/cm^3	[6]
	MURR	$T_{blister,95\%\ CI,lower} = \begin{cases} 6.72 \times 10^6 f_d^{-0.1974} & \text{for } f_d \ge 1.5\times10^{21} \\ 450 & \text{for } f_d < 1.5\times10^{21} \end{cases}$	[4]
	NBSR	380°C up to a fission density of 7.2x10^{21} fissions/cm^3	[24]
	Recommendation	$T_{blister}(Lower\ 95\%\ Prediction\ Bound) = \begin{cases} 3.25 \times 10^7 f_d^{-0.2282} & \text{for } f_d > 1.5\times10^{21} \\ 478 & \text{for } f_d \le 1.5\times10^{21} \end{cases}$	[1]

Nuclear Science & Engineering Division
Argonne National Laboratory
9700 South Cass Avenue, Bldg. 208
Argonne, IL 60439

www.anl.gov

Argonne National Laboratory is a U.S. Department of Energy
laboratory managed by UChicago Argonne, LLC